MAGNETIC PROPERTIES OF SEDIMENTARY GREIGITE (Fe_3S_4): AN UPDATE

Andrew P. Roberts,[1,2] Liao Chang,[1] Christopher J. Rowan,[1,3] Chorng-Shern Horng,[4] and Fabio Florindo[5]

Received 6 April 2010; revised 3 August 2010; accepted 28 September 2010; published 29 January 2011.

[1] Greigite (Fe_3S_4) is an authigenic ferrimagnetic mineral that grows as a precursor to pyrite during early diagenetic sedimentary sulfate reduction. It can also grow at any time when dissolved iron and sulfide are available during diagenesis. Greigite is important in paleomagnetic, environmental, biological, biogeochemical, tectonic, and industrial processes. Much recent progress has been made in understanding its magnetic properties. Greigite is an inverse spinel and a collinear ferrimagnet with antiferromagnetic coupling between iron in octahedral and tetrahedral sites. The crystallographic *c* axis is the easy axis of magnetization, with magnetic properties dominated by magnetocrystalline anisotropy. Robust empirical estimates of the saturation magnetization, anisotropy constant, and exchange constant for greigite have been obtained recently for the first time, and the first robust estimate of the low-field magnetic susceptibility is reported here. The Curie temperature of greigite remains unknown but must exceed 350°C. Greigite lacks a low-temperature magnetic transition. On the basis of preliminary micromagnetic modeling, the size range for stable single domain behavior is 17–200 nm for cubic crystals and 17–500 nm for octahedral crystals. Gradual variation in magnetic properties is observed through the pseudo-single-domain size range. We systematically document the known magnetic properties of greigite (at high, ambient, and low temperatures and with alternating and direct fields) and illustrate how grain size variations affect magnetic properties. Recognition of this range of magnetic properties will aid identification and constrain interpretation of magnetic signals carried by greigite, which is increasingly proving to be environmentally important and responsible for complex paleomagnetic records, including widespread remagnetizations.

Citation: Roberts, A. P., L. Chang, C. J. Rowan, C.-S. Horng, and F. Florindo (2011), Magnetic properties of sedimentary greigite (Fe_3S_4): An update, *Rev. Geophys.*, *49*, RG1002, doi:10.1029/2010RG000336.

1. INTRODUCTION

[2] Greigite (Fe_3S_4) is a thiospinel (i.e., a sulfide with inverse spinel crystal structure (Figure 1)) that, like its iron oxide counterpart, magnetite (Fe_3O_4), is strongly ferrimagnetic. Unlike magnetite, which has been known to humans for millennia (as lodestone) because of its magnetic properties, greigite was not formally reported until 1964, when it was discovered in Miocene lake sediments in San Bernardino County, California [*Skinner et al.*, 1964]. The existence of a black, magnetic iron sulfide different from pyrrhotite was postulated and named melnikovite in the era prior to the use of X-ray crystallography in mineralogy [*Doss*, 1912a, 1912b], but its precise composition was not demonstrated until 1964. Indiscriminate use of the term melnikovite to describe a range of minerals led to adoption of the name greigite for Fe_3S_4 by *Skinner et al.* [1964] after the mineralogist and physical chemist J. W. Greig (1895–1977) of the Pennsylvania State University. There are many motivations for systematically reviewing the magnetic properties of sedimentary greigite, as outlined below.

[3] Greigite is now well known to form as a precursor to pyrite (FeS_2) in anoxic sulfate-reducing sedimentary environments [e.g., *Berner*, 1970, 1984; *Wilkin and Barnes*, 1996; *Benning et al.*, 2000]. It is expected to be thermodynamically metastable under sedimentary conditions and has therefore been considered unlikely to persist in the geological record [*Berner*, 1970, 1984]. However, modern superconducting rock magnetometers can detect magnetic particles at the parts per billion concentration level, which, contrary to geochemical expectation, has led to increasing reports of sedimentary greigite in the geological record over the last 30 years [e.g., *Giovanoli*, 1979; *Snowball and Thompson*, 1988, 1990a, 1990b; *Hilton*, 1990; *Krs et al.*, 1990, 1992; *Snowball*, 1991;

[1]National Oceanography Centre, Southampton, University of Southampton, Southampton, UK.
[2]Now at Research School of Earth Sciences, Australian National University, Canberra, ACT, Australia.
[3]Now at School of GeoSciences, University of Edinburgh, Edinburgh, UK.
[4]Institute of Earth Sciences, Academia Sinica, Taipei, Taiwan.
[5]Istituto Nazionale di Geofisica e Vulcanologia, Rome, Italy.

8755-1209/11/2010RG000336
Paper number 2010RG000336

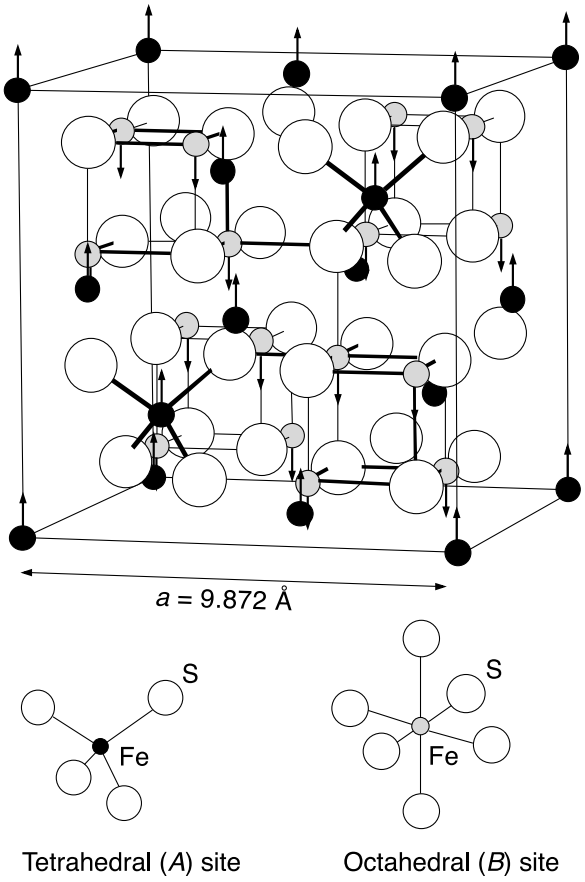

Figure 1. Crystallographic and magnetic structure for greigite (Fe_3S_4). Greigite has an inverse spinel structure with cubic close-packed sulfur array (space group $Fd\bar{3}m$ and $Z = 8$). Fe^{3+} occupies tetrahedral (*A*) sites; both Fe^{2+} and Fe^{3+} occupy octahedral (*B*) sites. Greigite has a collinear ferrimagnetic spin arrangement with antiferromagnetic coupling between octahedral and tetrahedral ions [*Chang et al.*, 2009a]. The unit cell (lattice parameter *a*) is shown, with arrows representing magnetic moment directions for each Fe ion, which are aligned along the easy axis of magnetization (the [100] or *c* crystallographic axis). See Table 1 for relevant parameters. After *Chang et al.* [2009a] and adapted from *García and Subías* [2004], copyright Institute of Physics.

Tric et al., 1991; *Horng et al.*, 1992a, 1992b, 1998; *Roberts and Turner*, 1993; *van Velzen et al.*, 1993; *Hallam and Maher*, 1994; *Reynolds et al.*, 1994, 1999; *Florindo and Sagnotti*, 1995; *Roberts et al.*, 1996, 2010; *Sagnotti and Winkler*, 1999; *Jiang et al.*, 2001; *Sagnotti et al.*, 2005, 2010; *Rey et al.*, 2005; *Rowan and Roberts*, 2005, 2006; *Horng and Chen*, 2006; *Babinszki et al.*, 2007; *Florindo et al.*, 2007; *Frank et al.*, 2007a, 2007b; *Ron et al.*, 2007; *Vasiliev et al.*, 2007, 2008; *Blanchet et al.*, 2009; *Hüsing et al.*, 2009; *Porreca et al.*, 2009; *Porreca and Mattei*, 2010]. Sedimentary greigite forms through a series of microbially mediated reactions that can be reproduced inorganically in the laboratory [*Berner*, 1984; *Wilkin and Barnes*, 1996; *Benning et al.*, 2000]. *Magnetotactic bacteria* can also produce sedimentary greigite through biomineralization of *magnetosomes* in anoxic aqueous environments [e.g., *Bazylinski et al.*, 1990, 1993, 1995; *Heywood et al.*, 1990, 1991; *Mann et al.*, 1990; *Moskowitz et al.*, 2008], including waterlogged soils [*Stanjek et al.*, 1994]. (Italicized terms are defined in the glossary, after the main text.) The importance of fossil greigite magnetosomes as recorders of paleomagnetic signals remains largely unknown, but initial reports of greigite magnetosome preservation in sedimentary rocks in addition to "nonbiogenic" greigite indicate that it is potentially important [*Pósfai et al.*, 2001; *Vasiliev et al.*, 2008]. A snail from a deep-sea hydrothermal vent also has a dense coat of mineralized scales consisting of pyrite, mackinawite (FeS), and greigite on its foot, a feature that is inferred to provide mechanical protection and that has not been observed in any other living metazoan [*Wáren et al.*, 2003; *Goffredi et al.*, 2004; *Suzuki et al.*, 2006]. The greigite is likely to have formed via hydrothermal reactions that are important for mineralization in ore deposits and other hydrothermal environments [e.g., *Radusinovic*, 1966; *Williams*, 1968; *Krupp*, 1991, 1994; *Oles and Houben*, 1998].

[4] Independent of its possible geological importance as a carrier of paleomagnetic signals, occasional reports of various magnetic properties of greigite have been published in the solid state physics literature [*Yamaguchi and Wada*, 1970; *Spender et al.*, 1972; *Vandenberghe et al.*, 1991] as well as in paleomagnetic and rock magnetic studies [e.g., *Snowball and Thompson*, 1988, 1990a, 1990b; *Krs et al.*, 1990, 1992; *Snowball*, 1991, 1997a, 1997b; *Tric et al.*, 1991; *Horng et al.*, 1992b; *Roberts and Turner*, 1993; *Moskowitz et al.*, 1993; *Reynolds et al.*, 1994; *Torii et al.*, 1996; *Snowball and Torii*, 1999; *Sagnotti and Winkler*, 1999; *Frank et al.*, 2007b]. *Roberts* [1995] made the first systematic attempt to describe the magnetic properties of greigite. By analyzing the most diverse collection of greigite samples then available, *Roberts* [1995] concluded that greigite commonly occurs in a stable *single-domain (SD)*-like state, that its magnetic properties are controlled by *magnetocrystalline anisotropy*, that it is thermally unstable at elevated temperatures (thermal instability precluded determination of the *Curie temperature* (T_C), which must lie above 322°C), and that, unlike magnetite, it undergoes no crystallographic or magnetic transition when cooled to low temperatures (i.e., from room temperature down to 20–4 K).

[5] Over the past 15 years, greigite has been reported from globally distributed localities, which demonstrates that it is a far more important magnetic mineral than has been assumed in the geochemical literature [e.g., *Berner*, 1970, 1984]. Greigite has been demonstrated to be the dominant magnetic mineral over stratigraphic thicknesses of hundreds to thousands of meters and is present in sedimentary rocks that often crop out over hundreds to thousands of km^2 in Taiwan, Italy, New Zealand, Hungary, Romania, and Israel [e.g., *Horng et al.*, 1992a, 1998; *Sagnotti and Winkler*, 1999; *Rowan and Roberts*, 2006; *Babinszki et al.*, 2007; *Vasiliev et al.*, 2007, 2008; *Frank et al.*, 2007a, 2007b; *Ron et al.*, 2007]. These occurrences represent the tip of the iceberg in terms of greigite preservation in the geological record. Pyrite is ubiquitous in sediments and rocks that have undergone

reductive diagenesis under sulfate-reducing conditions [*Berner*, 1984]. Greigite, as a common precursor to pyrite [*Pósfai et al.*, 1998; *Benning et al.*, 2000], will therefore have been present at some point in time within the majority of the world's muds and mudstones. *Kao et al.* [2004] demonstrated that widespread greigite preservation is likely if abundant reactive iron is available to react with sulfide during pyritization reactions. If organic carbon supply is diluted by terrigenous sediment and abundant reactive iron exhausts available sulfide supplied by anaerobic decomposition of organic matter, pyritization will be arrested, and the intermediate product, greigite, will be preserved. Preservation of greigite therefore depends on the balance between organic carbon supply, sulfide production, and reactive iron concentration. Greigite will not always be preserved in significant concentrations, but it occurs frequently enough in anoxic sulfidic environments that it is now recognized as a common terrestrial magnetic mineral.

[6] Many assemblages of natural greigite tend to have grain size distributions that span the ideal stable SD state [*Roberts*, 1995] and the ultrafine-grained *superparamagnetic (SP)* state [*Rowan and Roberts*, 2006; *Rowan et al.*, 2009] (where thermal vibrations cause the magnetization to fluctuate so that no stable magnetization can be retained at room temperature). Until recently, we have only had a reasonable knowledge of the magnetic properties of SD and SP greigite. A new hydrothermal technique for producing uniquely pure crystalline greigite samples [*Tang et al.*, 2007] has enabled determination of a spectrum of magnetic properties from SP through to *multidomain (MD)* behavior (from sizes of tens of nanometers to tens of micrometers) [*Chang et al.*, 2007]. Documentation of the full range of magnetic properties of greigite, in addition to the more restricted range of properties described by *Roberts* [1995], should lead to better understanding of the real distribution of greigite in sediments and therefore of its true paleomagnetic significance.

[7] Paleomagnetic studies of sedimentary rocks usually rely on acquisition of the *natural remanent magnetization (NRM)* during or shortly after deposition. This requirement could hold true in many cases involving greigite because it can grow rapidly as a precursor to pyrite in the laboratory at <80°C [e.g., *Sweeney and Kaplan*, 1973; *Schoonen and Barnes*, 1991; *Wilkin and Barnes*, 1996; *Benning et al.*, 2000; *Hunger and Benning*, 2007; *Tang et al.*, 2007], in the water column of euxinic marine waters [e.g., *Cutter and Kluckhohn*, 1999], or in anoxic natural sediments within decades or less of deposition [e.g., *Pye*, 1981; *Reynolds et al.*, 1999]. In contrast, however, it has been repeatedly demonstrated that greigite can grow during later diagenesis, which can lead to remagnetization of the host sediment. Multiple mechanisms for late diagenetic remagnetizations involving greigite have been documented [*Roberts and Weaver*, 2005]. Greigite can grow as long as there are appropriate Eh-pH conditions with sufficient dissolved pore water sulfide and iron for sulfidization reactions to proceed. Greigite can therefore be a problematic mineral from a paleomagnetic perspective [e.g., *Florindo and Sagnotti*, 1995; *Thompson and Cameron*, 1995; *Horng et al.*, 1998; *Jiang et al.*, 2001; *Liu et al.*, 2004; *Roberts et al.*, 2005, 2010; *Rowan and Roberts*, 2005, 2006; *Sagnotti et al.*, 2005, 2010; *Fu et al.*, 2008; *Porreca et al.*, 2009; *Rowan et al.*, 2009]. Identifying its presence and deciphering evidence for the timing of its growth are crucial to avoid misinterpretation of paleomagnetic records in geomagnetic, tectonic, or environmental investigations. Having a detailed knowledge of the magnetic properties of greigite is therefore fundamental to paleomagnetic studies of greigite-bearing sediments.

[8] Greigite is also demonstrably or potentially important in a range of other contexts, including evolutionary, extraterrestrial, industrial, and environmental. The magnetic properties of greigite are incidental to some of these contexts but are directly important to others. For example, greigite is inferred to have formed as part of an iron monosulfide membrane that served as a catalyst between fluids in a submarine hydrothermal redox front that may have enabled emergence of life on Earth [e.g., *Russell et al.*, 1994; *Russell and Hall*, 1997]. Greigite of postulated biogenic origin has also been suggested to be present in Martian meteorite ALH84001 [*McKay et al.*, 1996]. In industrial processes, anoxic sulfidic fluids can result in iron sulfide formation and undesirable corrosion of steel structures [e.g., *Zapponi et al.*, 2005] or archeological artifacts [e.g., *Fell and Ward*, 1998]. Disseminated nanoparticulate sulfides, including greigite, mackinawite, and pyrite that result from steel corrosion, can result in spontaneous combustion when exposed to air. This pyrophoric property is suspected of causing explosions when crude oil is pumped off ships without inert gas equipment [*Walker et al.*, 1996, 1997]. In a more constructive possibility, disseminated iron sulfide nanoparticles have high surface area to volume ratios [*Watson et al.*, 2000], which makes them good absorbers of toxic heavy metals and radionuclides [e.g., *Watson et al.*, 1995, 2001]. The magnetic, optical, and electronic properties of greigite have also attracted interest in solid-state physics and chemistry [e.g., *Coey et al.*, 1970; *Yamaguchi and Wada*, 1970; *Spender et al.*, 1972; *Goodenough and Fatseas*, 1982; *Braga et al.*, 1988; *Chen et al.*, 2005; *Letard et al.*, 2005; *He et al.*, 2006; *Pearce et al.*, 2006; *Han and Gao*, 2008]. The semimetallic and ferrimagnetic nature of greigite [*Devey et al.*, 2009] places it in a select group of materials with potential applications in spintronics [cf. *Wolf et al.*, 2001].

[9] Largely independent of its importance in the above mentioned applications and as a carrier of paleomagnetic signals, greigite also has considerable potential as a paleoenvironmental indicator. Greigite can be a sensitive indicator of lake chemistry [e.g., *Snowball and Thompson*, 1988, 1990a, 1990b; *Hilton*, 1990; *Snowball*, 1991; *Roberts et al.*, 1996; *Reynolds et al.*, 1999; *Frank et al.*, 2007b; *Ron et al.*, 2007] or marine environment [e.g., *Blanchet et al.*, 2009; *Mohamed et al.*, 2011]. Greigite also commonly grows in association with the anaerobic oxidation of methane [e.g., *Kasten et al.*, 1998; *Neretin et al.*, 2004; *Horng and Chen*, 2006; *Larrasoaña et al.*, 2007; *van Dongen et al.*, 2007; *Fu et al.*, 2008], which confirms earlier reports of the usefulness of rock magnetism in identifying the former presence of methane hydrates in sediments [*Housen and*

Musgrave, 1996]. Gas hydrates released from sediments have been implicated as a major source of greenhouse gases and global warming during past warm paleoclimatic intervals [e.g., *Dickens et al.*, 1997; *Kennett et al.*, 2000]. Identifying the past position and extent of gas hydrate reservoirs using sediment magnetic properties [e.g., *Horng and Chen*, 2006; *Musgrave et al.*, 2006; *Enkin et al.*, 2007; *Larrasoaña et al.*, 2007] could therefore be important in paleoclimate studies. Greigite therefore has importance far beyond the normal range of paleomagnetic and geochemical studies, which justifies a comprehensive review of its magnetic properties, as presented here.

[10] In this paper, we provide a detailed account of the known magnetic properties of sedimentary greigite. This synthesis is based on a review of the literature, as well as on new results that are presented here for the first time. In some cases, our new data provide completely new insights; in other cases, syntheses of old and new data provide new insights into old problems; while in yet other cases, we present previously unpublished data to illustrate different aspects of the magnetic properties of greigite. We also describe the magnetic properties of greigite using techniques that have become more popular in the last decade and that have not been systematically described elsewhere. Finally, after summarizing the known magnetic properties of greigite, we discuss some remaining unknown properties of greigite and suggest areas where future work is needed to bring knowledge of greigite to the same level as for other common magnetic minerals.

[11] The language of rock magnetism used throughout this paper contains technical terminology that might need additional explanation to nonexpert readers. We provide a concise explanation of technical terms used in this paper in a glossary to help readers to better understand important concepts.

2. METHODS

[12] New results presented here were obtained using a range of methods. *Alternating field (AF) demagnetization* and *thermal demagnetization* experiments were made on conventional 2.5 cm diameter paleomagnetic samples that were drilled from outcrops. Remanence measurements were made using a 2-G Enterprises superconducting rock magnetometer that is housed in a magnetically shielded laboratory at the National Oceanography Centre, Southampton (NOCS), U.K. AF demagnetization was performed using both static and tumbling treatments. Static AF demagnetization was achieved by progressively demagnetizing the three sample axes in coils arranged in-line with the 2-G Enterprises magnetometer. Tumbling AF demagnetization was achieved using a Molspin AF demagnetization unit in which the sample is tumbled so that its axes are presented to the field in a random manner. Progressively increasing peak fields of 5, 10, 15, 20, 25, 30, 35, 40, 45, 50, and 60 mT were used for both sets of treatments. Peak fields of 70 and 80 mT were also used for static AF demagnetization. Thermal demagnetization was performed at NOCS using a Magnetic Measurements MM-60 oven at temperatures of 80°C, 120°C, 160°C, 200°C, 240°C, 280°C, 320°C, 350°C, 380°C, and 410°C. High-field measurements were made at NOCS using a Princeton Measurements Corporation vibrating sample magnetometer (VSM) up to peak fields of 1.4 T on 1 cm^3 subsamples (lower fields were used where appropriate). High-field measurements made with the VSM include stepwise acquisition of a *saturation remanent magnetization (M_r)* (sometimes referred to as saturation isothermal remanent magnetization), DC demagnetization of M_r, hysteresis loops, and *first-order reversal curves (FORCs)* [cf. *Pike et al.*, 1999; *Roberts et al.*, 2000]. M_r acquisition and DC demagnetization measurements were made using logarithmically spaced field steps. One hundred forty FORCs were measured for each sample, using regular field steps of 1.85 mT, an averaging time of 250 ms, and a 0.5 T saturating field. FORC distributions were generally calculated using a smoothing factor (SF) of 5, but SF = 3 was used where possible. Hysteresis loops and backfield demagnetization curves were used to determine the standard hysteresis parameters, including M_r, the *saturation magnetization (M_s)*, the *coercive force (B_c)*, and the *coercivity of remanence (B_{cr})*. High-temperature analyses were made at NOCS using a variable field translation balance up to 700°C in air with an applied field of 27 mT. *Anisotropy of magnetic susceptibility (AMS)* was measured for greigite-bearing bulk sediments using a Kappabridge KLY-3 magnetic susceptibility bridge at the Institute of Earth Sciences, Academia Sinica, Taipei, Taiwan, or with a Kappabridge KLY-4S system at NOCS. M_r, imparted at 5 K with an applied field of 2.5 T, was repeatedly measured during warming from 5 K to room temperature using a Magnetic Properties Measurement System (MPMS) either at the Institute for Rock Magnetism (IRM), University of Minnesota, U.S.A., or in the School of Physics and Astronomy, University of Southampton, U.K. *Low-temperature cycling (LTC)* of a room temperature M_r was carried out by measuring M_r from room temperature to 10 K and back to room temperature in zero field with an MPMS at the IRM. Low-temperature FORC measurements were also made with an MPMS at the IRM. Scanning electron microscope (SEM) observations were made on resin-impregnated polished sections from sediment samples using a LEO 1450VP SEM at NOCS, which was operated at 10–20 keV with an acceleration voltage of 17–20 pA. A Princeton Gamma Tech (IMIX-PTS) X-ray energy dispersive spectrometer, calibrated with a pyrite standard, was used for elemental analyses of iron sulfide phases.

3. SAMPLES

[13] All new analyses presented in this paper were conducted on fresh samples. Some data represent unpublished results from previous studies conducted by different coauthors of this paper, while other data are from samples that were collected for this study. For each data set discussed, references for the respective sampling locations are cited in the appropriate figure captions. Some of the data presented here are more than 15 years old but are from

samples that were fresh at the time of measurement. The one exception involves samples from the collection of *Roberts* [1992] from Marlborough, New Zealand, which were used for this study. *Rowan and Roberts* [2006] undertook detailed SEM investigations of polished sections from these samples and demonstrated that greigite is present. This confirms the work of *Reynolds et al.* [1994] and *Roberts et al.* [1996], who demonstrated that greigite can remain stable in storage for many years, which should not be surprising since it is often preserved for millions of years in the geological record. We attribute reported cases of instabilities associated with storage diagenesis [e.g., *Snowball and Thompson*, 1988; *Oldfield et al.*, 1992] to be similar to the degradation that has been observed in the field or laboratory when greigite is wet [cf. *Crockford and Willett*, 1995; *Kasama et al.*, 2006]. When greigite is dry, we have not observed significant storage diagenesis apart from slight surficial oxidation. In each case presented, extensive work (including magnetic analyses, SEM observations, and X-ray diffraction (XRD) analysis of magnetic extracts) has been conducted to be sure that greigite is the only magnetic mineral present (even traces of magnetite will be evident in low-temperature and other magnetic analyses). In some cases, it is useful to examine how the additional presence of other magnetic minerals affects various analyses, so we occasionally show such results. If other magnetic minerals are present, we explicitly state this.

4. MAGNETIC CONSTANTS AND MAGNETIC AND ELECTRONIC STRUCTURE OF GREIGITE

[14] Before considering in detail the magnetic properties of greigite, we present what is known of the fundamental magnetic constants; the crystallographic, magnetic, and electronic structure of greigite; and the domain state threshold sizes for greigite. We then outline the magnetic properties of greigite, starting with the high-field properties, followed by room temperature magnetic properties, *low-temperature magnetic properties*, and high-temperature magnetic properties, followed by discussion of the magnetic fabric of greigite-bearing sediments.

4.1. Fundamental Magnetic Constants for Greigite

[15] Fundamental magnetic parameters, including M_s, the first *anisotropy constant* (K_1), and the *exchange constant* (J_{AB}), control the magnetic properties of a magnetic mineral and dictate how well it records magnetic information. Grain size and shape provide a secondary control on mineral magnetic properties. When a magnetic particle becomes large, it is energetically favorable to subdivide into uniformly magnetized domains, separated by thin *domain walls*. Domain state is related to grain size through the fundamental magnetic parameters. Such parameters have been known for decades for magnetite. In contrast, they have remained unknown until recently for greigite; the principal reason for this is that pure greigite samples have not been available. Natural greigite is fine-grained and commonly occurs as intergrowths, or in close association, with other minerals [e.g., *Jiang et al.*, 2001; *Roberts and Weaver*, 2005]. Pure magnetic extracts have therefore not been obtained from geological samples. Hydrothermal laboratory syntheses of greigite have also been blighted by lack of purity and good crystallinity, with several iron sulfide species being produced during rapid quenching of laboratory reactions along with significant concentrations of amorphous particles [see *Chang et al.*, 2008]. Recently, however, a new hydrothermal technique [*Tang et al.*, 2007] enabled production of uniquely pure crystalline *pseudo-single-domain (PSD)* and MD greigite samples [*Chang et al.*, 2007] that have been analyzed to determine the fundamental magnetic parameters and magnetic structure of greigite [*Chang et al.*, 2008, 2009a], as described in sections 4.1.1–4.1.4 (see summary in Table 1).

4.1.1. Saturation Magnetization, M_s

[16] The first precise determination of room temperature M_s for greigite provides a value of 59 A m^2 kg^{-1} (3.13 μ_B fu^{-1}) (where μ_B is Bohr magneton and fu is formula unit) [*Chang et al.*, 2008]. This value is considerably higher than previous estimates [*Uda*, 1965; *Coey et al.*, 1970; *Spender et al.*, 1972; *Hoffmann*, 1992; *Dekkers and Schoonen*, 1996; *Chen et al.*, 2005; *He et al.*, 2006] because of sample purity. This high value of M_s is supported by neutron powder diffraction results, which yield a slightly lower value of 3.0 μ_B fu^{-1} at room temperature [*Chang et al.*, 2009a]. Even though the value of 59 A m^2 kg^{-1} is substantially higher than previous determinations, M_s for greigite is still lower than for magnetite, which also has an inverse spinel crystal structure. This difference is suggested to result from the increased degree of covalency between iron and sulfur compared to oxygen ligands in magnetite or from greater delocalization of the 3*d* electrons in greigite [*Chang et al.*, 2009a].

4.1.2. Exchange Constant, J_{AB}

[17] Applying the *Bloch spin wave* expansion and fitting low-temperature M_s data to a second-degree polynomial with respect to $T^{3/2}$ (see glossary) enabled the first determination of the effective exchange constant J_{AB} for greigite (2×10^{-12} J m^{-1}) [*Chang et al.*, 2008]. Variable estimates of this parameter have been obtained for magnetite, so additional methods should be used in the future to test the robustness of this determination.

4.1.3. First Anisotropy Constant, K_1

[18] Determination of K_1 for greigite has proved problematical. *Spender et al.* [1972] suggested a K_1 value of 10^5 J m^{-3}, while *Diaz Ricci and Kirschvink* [1992] suggested a value of 10^3 J m^{-3}. These disparate values are both crude estimates and are not based on experimental evidence. The most common method for determining K_1 involves analysis of a single oriented crystal using a torque magnetometer. For many magnetic minerals, it is relatively straightforward to obtain large, pure crystals (>100 μm) to enable use of a torque magnetometer. Even if we could accurately orient the largest known single greigite crystal (~44 μm [*Chang et al.*, 2007]), to the best of our knowledge, there is no instrument sensitive enough to measure the small magnetic signal of such a crystal. Alternative methods are therefore necessary to determine K_1 for greigite.

TABLE 1. Key Magnetic and Crystallographic Information for Greigite

Parameter	Value	Source
Saturation magnetization, M_s (at room temperature)	59 A m^2 kg^{-1}	*Chang et al.* [2008]
	3.13 μ_B formula $unit^{-1}$	*Chang et al.* [2008]
A sublattice magnetization	~3.0 μ_B formula $unit^{-1}$	*Chang et al.* [2009a]
B sublattice magnetization	~3.0 μ_B formula $unit^{-1}$	*Chang et al.* [2009a]
Curie temperature, T_c	unknown, but >322°C	*Roberts* [1995]
	unknown, but >350°C	*Chang et al.* [2008]
First anisotropy constant, K_1	2.1–3.1 × 10^4 J m^{-3}	L. Chang et al. (unpublished data, 2011)
Exchange constant, J_{AB}	2 × 10^{-12} J m^{-1}	*Chang et al.* [2008]
Low-field magnetic susceptibility, χ	3.2 × 10^{-4} m^3 kg^{-1}	this study
Easy axis of magnetization	[100]	*Yamaguchi and Wada* [1970], *Heywood et al.* [1991], and *Bazylinski et al.* [1993]
Magnetic structure	collinear ferrimagnetic	*Chang et al.* [2009a]
Type of ferrimagnet	R type	*Chang et al.* [2009a]
Crystallographic structure	inverse spinel (space group $Fd\bar{3}m$, $Z = 8$)	
Lattice parameter, *a*	9.83–9.90 Å	e.g., *Skinner et al.* [1964], *Uda* [1965], and *Spender et al.* [1972]
	9.872 Å	*Chang et al.* [2008]
Mössbauer hyperfine parameters (at room temperature)		
Octahedral sites		
Isomer shift	0.53 mm s^{-1}	*Vandenberghe et al.* [1991]; *Chang et al.* [2008]
Hyperfine field	31.3–31.5 T	
Tetrahedral sites		
Isomer shift	0.28–0.29 mm s^{-1}	
Hyperfine field	31.2–31.3 T	

[19] *Ferromagnetic resonance*, in the form of electron paramagnetic resonance (EPR), has been used to probe K_1 in bacterial magnetite magnetosomes [*Weiss et al.*, 2004; *Kopp et al.*, 2006]. We recently performed EPR measurements on synthetic and natural greigite samples and obtained K_1 estimates in the ~2.9–3.1 × 10^4 J m^{-3} range (L. Chang et al., Micromagnetic calculation of the critical single domain threshold sizes for greigite, manuscript in preparation, 2011). We also used the hysteresis properties of equidimensional particles to estimate K_1. For equidimensional SD grains with magnetocrystalline anisotropy [*Dunlop and Özdemir*, 1997, p. 138], the relationship between the coercivity and anisotropy is $B_c = \sim\langle B_k\rangle = \langle 4/3 \cdot |K_1|/(3\mu_0 M_s)\rangle$, where B_k is the SD microcoercivity, B_c is the bulk coercivity, and μ_0 is the magnetic constant ($4\pi \times 10^{-7}$ m kg $s^{-2}A^{-2}$). For greigite, M_s = 59 A m^2 kg^{-1} [*Chang et al.*, 2008, 2009a], and B_c is estimated to be ~62 mT for randomly oriented SD grains (a typical high value of B_c from among our greigite samples). With this method, K_1 for greigite has a lower estimate of 2.1 × 10^4 J m^{-3}. This empirical approximation of 2.1–3.1 × 10^4 J m^{-3} represents a considerable improvement on the estimates of *Spender et al.* [1972] and *Diaz Ricci and Kirschvink* [1992].

4.1.4. Micromagnetic Modeling

[20] Determination of the three fundamental magnetic constants for greigite enables micromagnetic modeling of greigite for the first time. Micromagnetic modeling enables numerical determination of the magnetic behavior of materials on short length scales (<1 μm), where macroscopic magnetic models can no longer fully describe the behavior of a magnetic material. Recording of an external field will be affected by strong *magnetostatic interactions* associated with close packing of magnetic grains. Close grain packing is commonly observed in greigite [e.g., *Jiang et al.*, 2001; *Roberts and Weaver*, 2005]; micromagnetic modeling will enable scenario testing of the origins of anomalous magnetizations recorded by greigite [e.g., *Jiang et al.*, 2001]. Furthermore, micromagnetic modeling will enable determination of the grain size dependence of domain state for greigite, the results of which can be compared with empirical estimates (see section 5).

4.2. Magnetic Structure of Greigite

[21] Greigite has an inverse spinel crystallographic structure, with a cubic unit cell with 8 Fe^{3+} ions in tetrahedral (*A* site) coordination and 16 Fe ions (both Fe^{2+} and Fe^{3+}) in octahedral (*B* site) coordination with 32 sulfur anions (Figure 1). Using neutron powder diffraction and polarized neutron diffraction, *Chang et al.* [2009a] demonstrated unambiguously that greigite has a collinear ferrimagnetic structure (magnetic space group F-1) with antiferromagnetic (i.e., antiparallel) coupling between the tetrahedral and octahedral iron sites. Neutron diffraction data [*Chang et al.*, 2009a] and in-field Mössbauer data [*Chang et al.*, 2008] confirm the absence of *spin canting* in greigite, so that the formula for greigite can be written as $[\uparrow Fe^{3+}]^A$ $[\downarrow Fe^{2+}$ $\downarrow Fe^{3+}]^B$ S_4^{2-}. Greigite has been suggested to be *nonstoichiometric* by numerous authors [*Coey et al.*, 1970; *Spender et al.*, 1972; *Letard et al.*, 2005; *Rickard and Luther*, 2007]. Using spec-

trophotometry to analyze nanocrystalline synthetic greigite, *Qian et al.* [1999] obtained a greigite stoichiometry of $Fe_{2.994}S_4$. Likewise, Rietveld refinement of neutron diffraction data from coarse-grained synthetic greigite, which included parameters for partial occupancy of iron sites, indicates no significant *vacancy concentration* for the fitted profiles and no departure from stoichiometry [*Chang et al.*, 2009a]. Neutron powder diffraction data enabled determination of the *sublattice magnetizations* for greigite: the magnetic moments of iron for both the *A* and *B* sublattices at room temperature are ~3.0 μ_B. The average magnetic moment of iron in *B* sites decreases with increasing temperature, whereas the *A* site moments are relatively invariant, which indicates that greigite is an R-type ferrimagnet [*Chang et al.*, 2009a]. The crystallographic and magnetic structures of greigite are summarized in Figure 1, where an *inverse spinel structure* with a cubic close-packed sulfur array (space group $Fd\bar{3}m$, $Z = 8$) is shown as for the ionic model stated above. The arrows in Figure 1 indicate the magnetic moment directions for each Fe ion, which are aligned with the crystallographic *c* axis because the easy axis of magnetization is the [100] *crystallographic axis* [*Yamaguchi and Wada*, 1970; *Heywood et al.*, 1991; *Bazylinski et al.*, 1993; *Moskowitz*, 1995].

4.3. Electronic Structure of Greigite

[22] Various proposals for the electronic structure of greigite [e.g., *Coey et al.*, 1970; *Spender et al.*, 1972; *Braga et al.*, 1988; *Sherman*, 1990] are undermined by inaccurate estimates of the magnetic moment. For example, *Sherman* [1990] concluded that greigite could not have a simple inverse spinel structure that contains high-spin Fe^{2+} and Fe^{3+}, like magnetite, and suggested two alternative electronic structures with intermediate-spin Fe^{3+} because of the lower magnetic moment for greigite. Accurate new determinations of the spontaneous magnetization and sublattice magnetizations for greigite [*Chang et al.*, 2008, 2009a] make possible more meaningful estimation of the electronic structure of greigite. *Devey et al.* [2009] undertook ab initio modeling, using the new constraints of *Chang et al.* [2008], and found that the inverse spinel structure can be simulated, with accurate reproduction of lattice parameters and magnetic moments. The two band schemes of *Spender et al.* [1972] could be tested, and the first, where octahedral sites are occupied by Fe^{2+} and Fe^{3+}, is supported [*Devey et al.*, 2009]. *Band structure* calculations suggest that greigite is a semimetal, which would place it within a select group of materials with potential applications in spintronics [cf. *Wolf et al.*, 2001]. Experimental measurements are needed to confirm this conclusion. A complete understanding of the electronic structure of greigite has yet to be obtained and should be a priority for future work.

5. THRESHOLD SIZES FOR DOMAIN STATE TRANSITIONS IN GREIGITE

[23] Difficulty in obtaining pure natural or synthetic greigite samples has hindered development of a grain size–dependent framework for the magnetic properties of greigite. A first effort was made by *Chang et al.* [2007] and is improved upon here (see sections 6.1.3–6.3), but more work is needed. Regardless of limitations of available magnetic data, measurement of the size and shape of bacterial greigite magnetosomes provides useful constraints on SD grain sizes because magnetotactic bacteria generally produce magnetosomes of ideal SD size to aid navigation along geomagnetic field lines. Uncultured bacteria often produce negatively skewed magnetosome size distributions that sharply cut off at the maximum stable SD size [e.g., *Bazylinski and Frankel*, 2004] (Figure 2a). Gaussian-like magnetosome size distributions (Figure 2b) have also been observed [*Pósfai et al.*, 2001; *Arató et al.*, 2005]. Despite these differences in grain size distributions, a range of observations (Table 2 and Figures 2a and 2b) indicate that ideal SD greigite magnetosomes span the size interval from about 50 to 115 nm [*Farina et al.*, 1990; *Heywood et al.*, 1990, 1991; *Mann et al.*, 1990; *Bazylinski et al.*, 1995; *Pósfai et al.*, 2001], with cubo-octahedral or rectangular prismatic morphologies (Figure 2d). Various analyses suggest that greigite has SP properties below ~30 nm (Table 2); *Hoffmann* [1992] inferred that the SP/SD threshold size lies approximately in the 30–50 nm size range, while *Kasama et al.* [2006] reported that equidimensional ~40 nm greigite still has SD behavior.

[24] Available evidence suggests that nonbiogenic greigite has larger grain size distributions than bacterial greigite magnetosomes (Figure 2c). Our observations of octahedral natural greigite (Figure 2e) are consistent with such broader grain size distributions. Using the *magneto-optical Kerr effect* and *Bitter pattern imaging*, *Hoffmann* [1992] observed greigite particles larger than 5 μm with complicated domain structures that therefore display genuine MD behavior; the SD to two-domain (SD/2D) transition was determined to occur at about 0.7–0.8 μm (Table 2). Our analyses of largely octahedral synthetic PSD/MD samples (Figure 2f) have not yet enabled experimental confirmation of the SD/2D threshold size. Many studies that report greigite grain sizes represent aggregates of grains [e.g., *Snowball*, 1991]; we have avoided such estimates in our collation in Table 2 and Figure 2g. SD threshold sizes for greigite have recently been calculated from micromagnetic models as 17 nm (SP/SD threshold) and 200 nm (SD/2D) (Figure 2g) for greigite cubes (Chang et al., manuscript in preparation, 2011). The SD size range is much broader for cubo-octahedral (and octahedral) greigite, with an upper limit above 500 nm for the SD/2D threshold size. Octahedral morphologies, and a wider grain size range for stable SD behavior, are consistent with SEM observations of sedimentary greigite samples that exhibit stable SD behavior (Figure 2e). Grain elongation and magnetostatic interactions will affect the threshold sizes [e.g., *Muxworthy and Williams*, 2009], but it is unlikely that interactions could extend this transition to the 0.7–0.8 μm size range initially estimated by *Hoffmann* [1992]. Nevertheless, the newly determined SD threshold size range for greigite is broader than for magnetite [*Muxworthy and Williams*, 2006, 2009]. More complete results will be published in due course, but it is encouraging

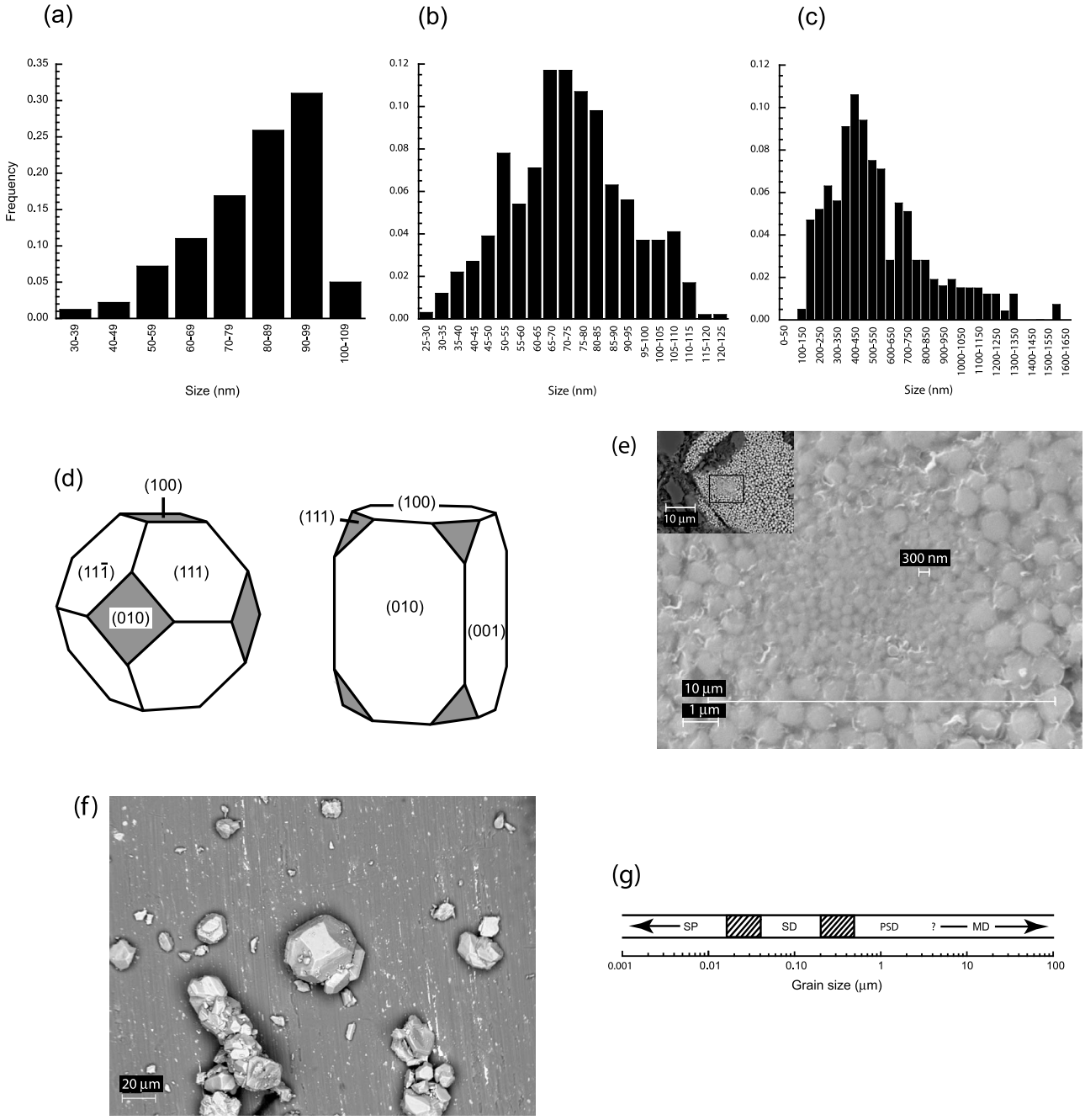

Figure 2. Crystal size, shape, and domain state size thresholds for greigite. (a–c) Grain size distributions for greigite magnetosomes (from *Bazylinski et al.* [1990] (Figure 2a) and *Pósfai et al.* [2001] (Figure 2b)) constrain the grain size distribution for stable SD behavior in greigite. Grain size distributions for nonbiogenic greigite are coarser (from *Pósfai et al.* [2001] (Figure 2c)). (d) Typical cubo-octahedral and rectangular prismatic morphologies for greigite magnetosomes [from *Heywood et al.*, 1990]. (e) Backscattered electron photomicrographs of an aggregate of nonbiogenic greigite particles (fine-grained) within a larger aggregate of coarser pyrite grains. This image is at the limit of scanning electron microscope (SEM) resolution, but individual greigite grains have lengths of several hundred nanometers, which is consistent with the size distribution in Figure 2c. (f) SEM image of coarse, PSD to MD synthetic greigite particles, which have variable (sometimes polyhedral) morphology but with largely equidimensional cubo-octahedral crystals [cf. *Chang et al.*, 2008]. (g) Best current estimates of grain size thresholds for magnetic domain states in greigite (see Table 2 and text for details).

TABLE 2. Grain Size Estimates of Domain State Thresholds for Greigite

Domain State[a]	Length[b] (nm)	Width (nm)	Grain Morphology (Grain Type)	Observation Method[c]	Locality	Reference[d]
SP	9–13		unspecified (synthetic)	XRD	synthetic	*Spender et al.* [1972]
SP	23 ± 2		elongated (magnetosome?)	XRD	soil, Bavaria, Germany	*Stanjek and Murad* [1994] and *Stanjek et al.* [1994]
SP	30–50		unspecified (synthetic)	?	synthetic	*Uda* [1965] and *Hoffmann* [1992]
SP/SD transition	30–50		–	inference	–	*Hoffmann* [1992]
SP/SD transition	<40		equidimensional (magnetosomes)	electron holography	Morro Bay, California	*Kasama et al.* [2006]
SD	75–100		not clearly resolved (magnetosomes)	TEM	Rio de Janeiro, Brazil	*Farina et al.* [1990]
SD	50–90		cubo-octahedra, rectangular prismatic (magnetosomes)	TEM	Woods Hole, Massachusetts; Morro Bay, California	*Heywood et al.* [1990]
SD	75		octohedra, cubo-octahedra (magnetosomes)	TEM	Plum Island, Massachusetts	*Mann et al.* [1990]
SD	69, 67	50	rectangular prismatic, cubo-octahedra (magnetosomes)	TEM	Woods Hole, Massachusetts; Morro Bay, California	*Heywood et al.* [1991]
SD	75.9 ± 1.2, 62.1 ± 13.1	38.4 ± 3.9, 42.7 ± 5.9	rectangular prismatic, rectangular prismatic (magnetosomes)	TEM	Pettaquamscutt Estuary, Rhode Island	*Bazylinski et al.* [1995]
SD	30–115		irregular: elongated to spherical	TEM	Rowley, Massachusetts; Morro Bay, California	*Pósfai et al.* [2001]
SD	17–200		cubes	micromagnetic modeling	–	Chang et al. (manuscript in preparation, 2011)
SD	17–500		cubo-octahedra and octahedra	micromagnetic modeling	–	Chang et al. (manuscript in preparation, 2011)
SD/MD transition	700–800		irregular (natural nonbiogenic)	MOKE/Bitter	coal beds, Czech Republic	*Hoffmann* [1992]
MD	5000		irregular (natural nonbiogenic)	MOKE/Bitter	coal beds, Czech Republic	*Hoffmann* [1992]

[a]SP, superparamagnetic; SD, single domain; MD, multidomain (i.e., greater than two domains).
[b]No grain width is reported for cubo-octohedral grains because they are equidimensional.
[c]Method used to determine grain size of greigite. Indirect determinations use X-ray diffraction (XRD, using widths of X-ray peaks). Direct observations are made using transmission electron microscopy (TEM), magneto-optical Kerr effect (MOKE), or Bitter domain wall patterns with optical imaging (Bitter).
[d]Precise stoichiometry of iron sulfides was often elusive in early studies, and pyrite and pyrrhotite compositions were postulated for magnetosomes in some of these studies [e.g., *Farina et al.*, 1990]. *Pósfai et al.* [1998] later found only greigite, and no pyrite and pyrrhotite, in high-resolution TEM investigations of sulfidic magnetosomes from a wide range of localities including most of those listed above.

that micromagnetic calculations are consistent with expectations from bacterial magnetosome and natural grain size distributions (Table 2 and Figures 2a–2c and 2e).

6. MAGNETIC PROPERTIES OF GREIGITE

6.1. High-Field Magnetic Properties

6.1.1. Hysteresis

[25] *Roberts* [1995] presented magnetic hysteresis data for a wide range of natural samples (Figure 3a). These data supported the inference that natural greigite has dominantly SD-like magnetic properties based on occasional reports of hysteresis [*Snowball*, 1991] and M_r/χ data (where χ is the low-field mass-specific magnetic susceptibility) [*Snowball and Thompson*, 1990a, 1990b; *Horng et al.*, 1992b; *Roberts and Turner*, 1993; *Reynolds et al.*, 1994]. These properties are now well established, and thermally stable greigite with SD-like properties has been widely reported, as demonstrated by the global synthesis of reported results in Figure 3. *Roberts* [1995] observed a power law relationship for hysteresis data (Figure 3a), which he interpreted to represent a mixing relationship between SD and SP end-members. The inferred dominance of SD-like behavior was based on the fact that M_r/M_s for greigite often exceeds 0.5 (the ideal value for SD materials with uniaxial anisotropy), with $B_{cr}/B_c < 1.5$. *Roberts* [1995] extrapolated the SD-SP mixing line to an intercept of $M_r/M_s = 0.75$ at $B_{cr}/B_c = 1$, which suggests that the magnetic properties of greigite are dominated by magnetocrystalline anisotropy rather than uniaxial anisotropy. The [100] crystallographic axis is the easy axis of magnetization for greigite, as indicated by a range of observations [*Yamaguchi and Wada*, 1970; *Heywood et al.*, 1991; *Bazylinski et al.*, 1993; *Moskowitz*, 1995]. For a [100] easy axis of magnetization, if magnetocrystalline anisotropy controls the hysteresis behavior, M_r/M_s should approach 0.83 as B_{cr}/B_c approaches unity [*Chikazumi*, 1964]. The value of 0.75 determined by *Roberts* [1995] is therefore lower than expected. New data measured from a wide range of samples ($n = 46$) for this study (Figure 3b) and data from a global compilation of studies ($n = 104$) published in the last 15 years (Figure 3c) [e.g., *Fassbinder and Stanjek*, 1994; *Mattei et al.*, 1996; *Dekkers and Schoonen*, 1996; *Hall et al.*, 1997; *Jelinowska et al.*, 1998; *Roberts et al.*, 1998; *Sagnotti and Winkler*, 1999; *Frank et al.*, 2007b; *Ron et al.*, 2007; *Fu et al.*, 2008] can be combined with the data of *Roberts* [1995] ($n = 40$) to provide a much larger data set ($n = 190$). The data in our global compilation define a tight power law mixing trend ($R^2 = 0.86$), with $M_r/M_s = 0.81$ at $B_{cr}/B_c = 1$ (Figure 3d). These results resolve questions raised by the less complete data set of *Roberts* [1995] and confirm that magnetocrystalline anisotropy is responsible for the hysteresis behavior of greigite.

[26] Our inference that M_r/M_s versus B_{cr}/B_c trends represent a SD + SP mixing line (Figure 3), rather than a SD + MD trend [e.g., *Day et al.*, 1977], requires justification. *Roberts* [1995] demonstrated that greigite samples undergo variable, but nonnegligible, unblocking during warming of a low-temperature M_r to room temperature, which indicates the presence of SP grains. Furthermore, hysteresis loop shapes provide clues concerning greigite grain size. In Figure 4, we plot from left to right the most open hysteresis loop, followed by an intermediate loop and then the most closed loop for a suite of loops (Figure 4, fourth column) for greigite-bearing samples from four localities. Greigite-bearing samples from Taiwan [*Horng et al.*, 1992a, 1992b] and Butte Valley, California [*Roberts et al.*, 1996], produce consistently open SD-like hysteresis loops. Samples from fluviolacustrine sediments from Rome, Italy [*Florindo et al.*, 2007], produce some open loops, but most samples produce potbellied loops (Figure 4, fourth column), which indicative substantial mixing of SD and SP particles [cf. *Tauxe et al.*, 1996]. Samples from Marlborough, New Zealand [*Roberts*, 1992; *Roberts and Turner*, 1993], are generally even more potbellied than those from Rome. While SP greigite particles were recognized previously [e.g., *Roberts*, 1995], their abundance and the widespread existence of potbellied loops

Figure 3. M_r/M_s versus B_{cr}/B_c plots [cf. *Day et al.*, 1977] for greigite. (a) Data from *Roberts* [1995]. The seven black circles indicate irregularly shaped hysteresis loops that were excluded by *Roberts* [1995] when calculating the power law fit. (b) New data collected for this study for samples from Rome [*Florindo et al.*, 2007]; Taiwan [*Horng et al.*, 1992a, 1992b]; the former Plio-Pleistocene type section at Vrica, Calabria, Italy [*Roberts et al.*, 2010]; Valle Ricca, near Rome [*Florindo and Sagnotti*, 1995; *van Dongen et al.*, 2007]; and Butte Valley, California [*Roberts et al.*, 1996]. Data from New Zealand were excluded and are shown in Figure 5. (c) Data from a global compilation of published hysteresis data for greigite. Many other authors have presented hysteresis data for greigite, but we have used data only where it is possible to differentiate between samples containing greigite and other magnetic minerals or where all four necessary parameters were reported. (d) All data from *Roberts* [1995], this study, and the global compilation in Figure 3c. The intercept of the power law fit at $B_{cr}/B_c = 1$ for 190 data points is 0.81, which is much closer to the expected value for randomly oriented particles with magnetocrystalline anisotropy (0.83) than in Figure 3a. (e) Comparison of hysteresis data for SD greigite samples (from Italy [*Florindo et al.*, 2007] and Taiwan [*Horng et al.*, 1992a, 1992b]) with synthetic PSD/MD samples from *Chang et al.* [2007] and a natural mixture of SD + MD greigite (Czech [*Krs et al.*, 1992]). Samples indicated by "S###" are different batches of synthetic samples with different grain size distributions (see right-hand side for selected samples); samples indicated by "S#" represent aggregations of the S### samples that were sieved to produce restricted grain size ranges (S1 = <1 μm, S2 = 1–5 μm, S3 = 5–15 μm, S4 = 15–25 μm, S5 = 25–35 μm, and S6 = >35 μm). "SD," "PSD," and "MD" fields for titanomagnetite [*Day et al.*, 1977] are plotted following *Dunlop* [2002] along with three of his calculated mixing lines for SD + MD mixtures of magnetite. These "Day plot" regions and mixing lines are not strictly transferrable to other minerals. Nevertheless, the greigite data fall close to the lines calculated by *Dunlop* [2002]. The SD + SP mixing trend in Figure 3d is also consistent with such lines for magnetite [*Dunlop*, 2002] (see Figure 5).

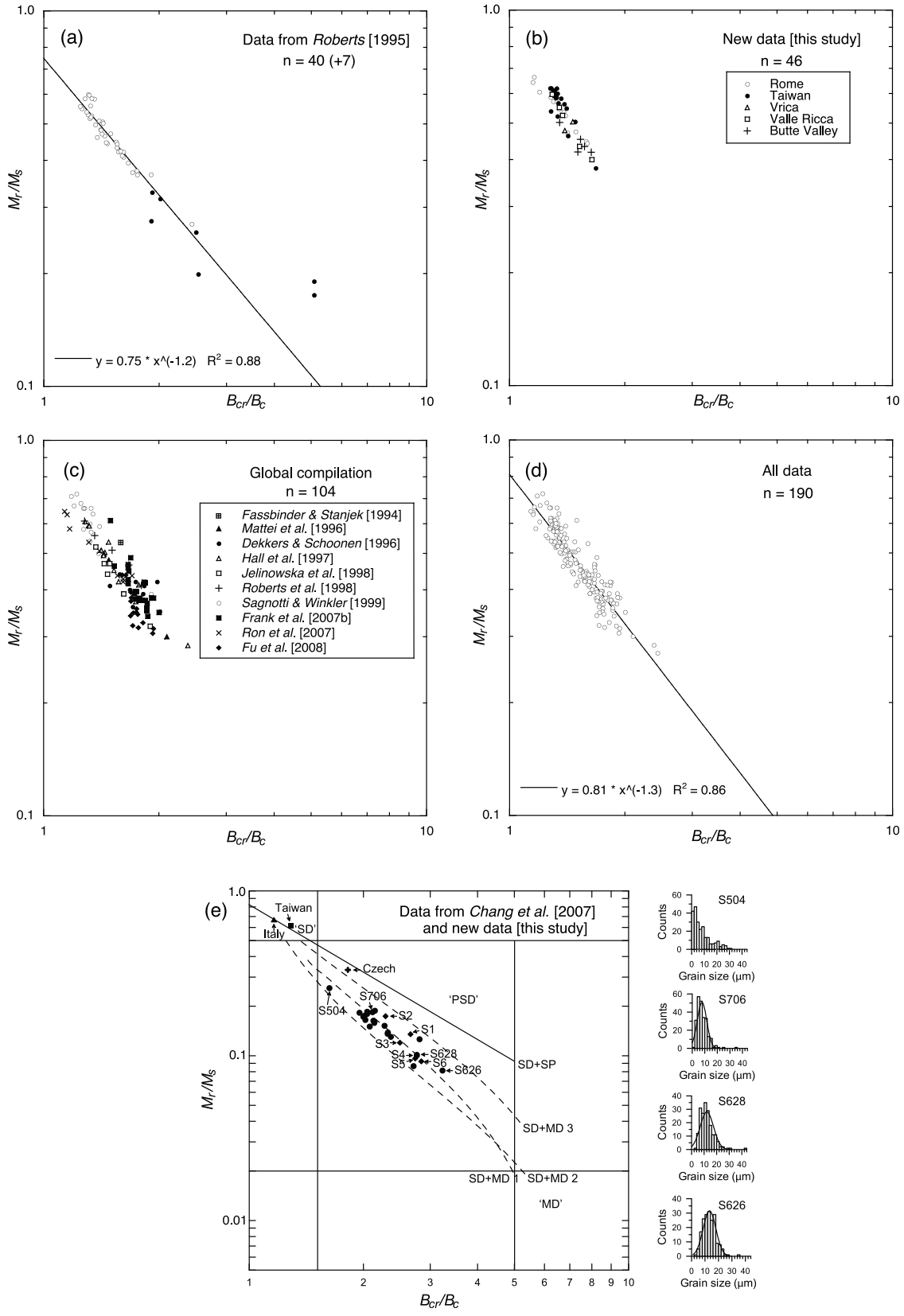
(a)
Data from *Roberts* [1995]
n = 40 (+7)
y = 0.75 * x^(-1.2) R² = 0.88
(b)
New data [this study]
n = 46
Rome
Taiwan
Vrica
Valle Ricca
Butte Valley
(c)
Global compilation
n = 104
Fassbinder & Stanjek [1994]
Mattei et al. [1996]
Dekkers & Schoonen [1996]
Hall et al. [1997]
Jelinowska et al. [1998]
Roberts et al. [1998]
Sagnotti & Winkler [1999]
Frank et al. [2007b]
Ron et al. [2007]
Fu et al. [2008]
(d)
All data
n = 190
y = 0.81 * x^(-1.3) R² = 0.86
M_r/M_s
B_{cr}/B_c
(e)
Data from *Chang et al.* [2007]
and new data [this study]
Taiwan
SD'
Italy
Czech
S706
S504
S2
S1
S3
S4
S628
S5
S6
S626
'PSD'
SD+SP
SD+MD 3
SD+MD 1
SD+MD 2
'MD'
Counts
Grain size (μm)
S504
S706
S628
S626

Figure 3

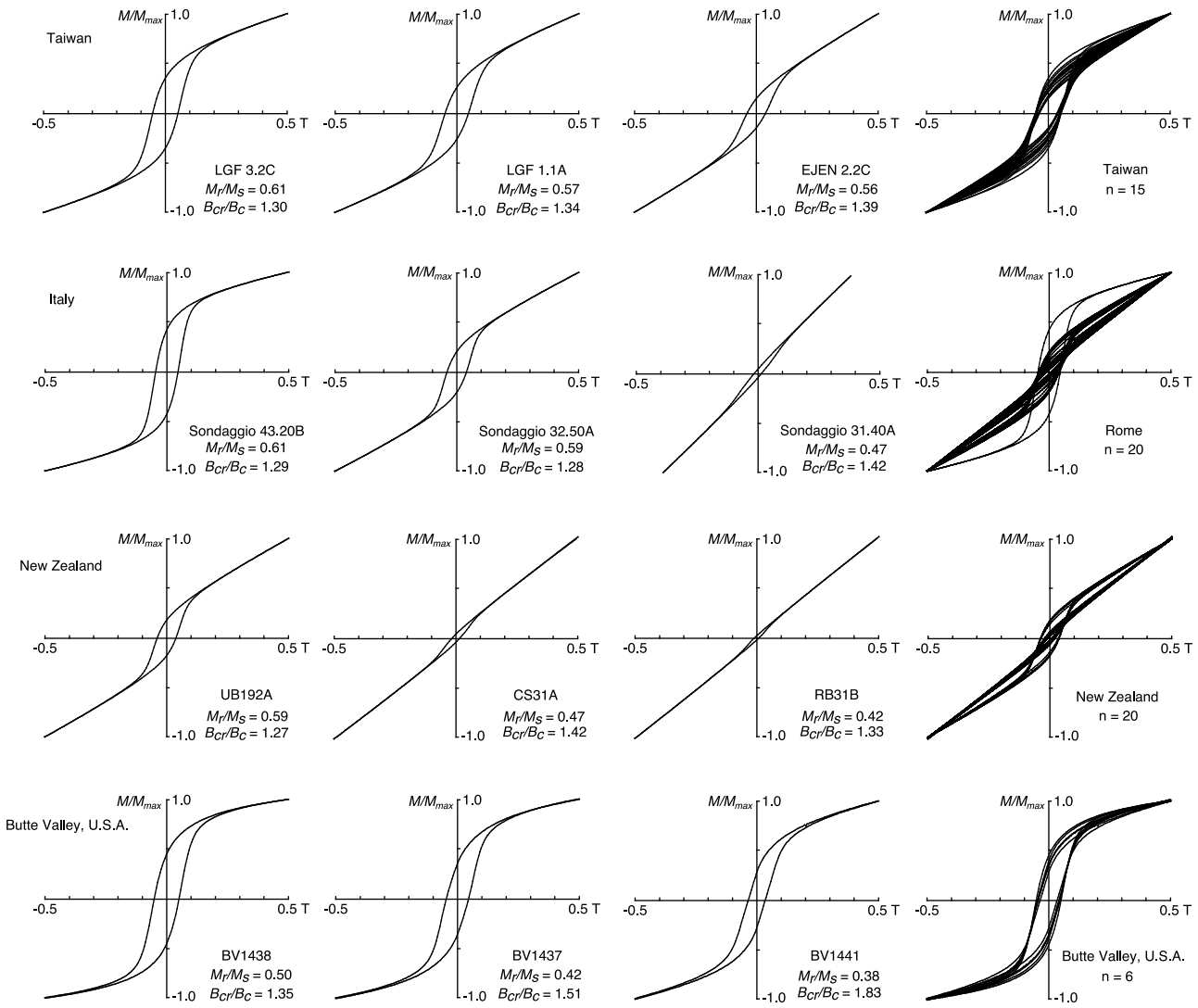

Figure 4. Magnetic hysteresis loops for greigite-bearing samples from southwestern Taiwan [*Horng et al.*, 1992a, 1992b]; Rome, Italy [*Florindo et al.*, 2007]; Marlborough, New Zealand [*Roberts*, 1992; *Roberts and Turner*, 1993]; and Butte Valley, California [*Roberts et al.*, 1996]. The loops in the first, second, and third columns represent the most open, intermediate, and the most closed loops, respectively, for the range of analyzed loops shown in the fourth column. Loops for samples from Taiwan and Butte Valley are consistently open. Some loops for samples from Rome are similar to the open loops from Taiwan, but there is a trend toward increasingly closed and potbellied loops. Loops for samples from New Zealand are even more closed and potbellied. Potbellied loops indicate increased importance of SP particles [*Tauxe et al.*, 1996] in addition to stable SD greigite. While SP particles were recognized previously [e.g., *Roberts*, 1995], the extent of their dominance in samples with potbellied loops was not previously recognized.

[*Tauxe et al.*, 1996] were not recognized. Adding substantial populations of SP grains to a thermally stable SD particle distribution will significantly change the magnetic properties. Failure to recognize the importance of SP greigite in sediments has almost certainly led to underrecognition of greigite in the geological record [*Rowan and Roberts*, 2006; *Rowan et al.*, 2009]. FORC diagrams provide further evidence for significant SP greigite concentrations, as described in section 6.1.2. We will return to the question of discriminating SD + SP from SD + MD mixing trends in section 6.1.3 once this evidence is presented.

6.1.2. FORC Diagrams

[27] FORC diagrams are representations of data from multiple partial hysteresis curves [*Pike et al.*, 1999; *Roberts et al.*, 2000] that provide several important insights concerning magnetization processes in greigite. First, greigite-bearing samples with classic SD-like properties have FORC distributions with concentric distributions (Figure 5a) [see also *Roberts et al.*, 2000, 2006, 2010; *Sagnotti et al.*, 2005, 2010; *Rowan and Roberts*, 2006; *Florindo et al.*, 2007; *Vasiliev et al.*, 2007]. This confirms the interpretation that the observed SD-like properties [cf. *Roberts*, 1995] represent genuine SD magnetic behavior. Second, the FORC distribu-

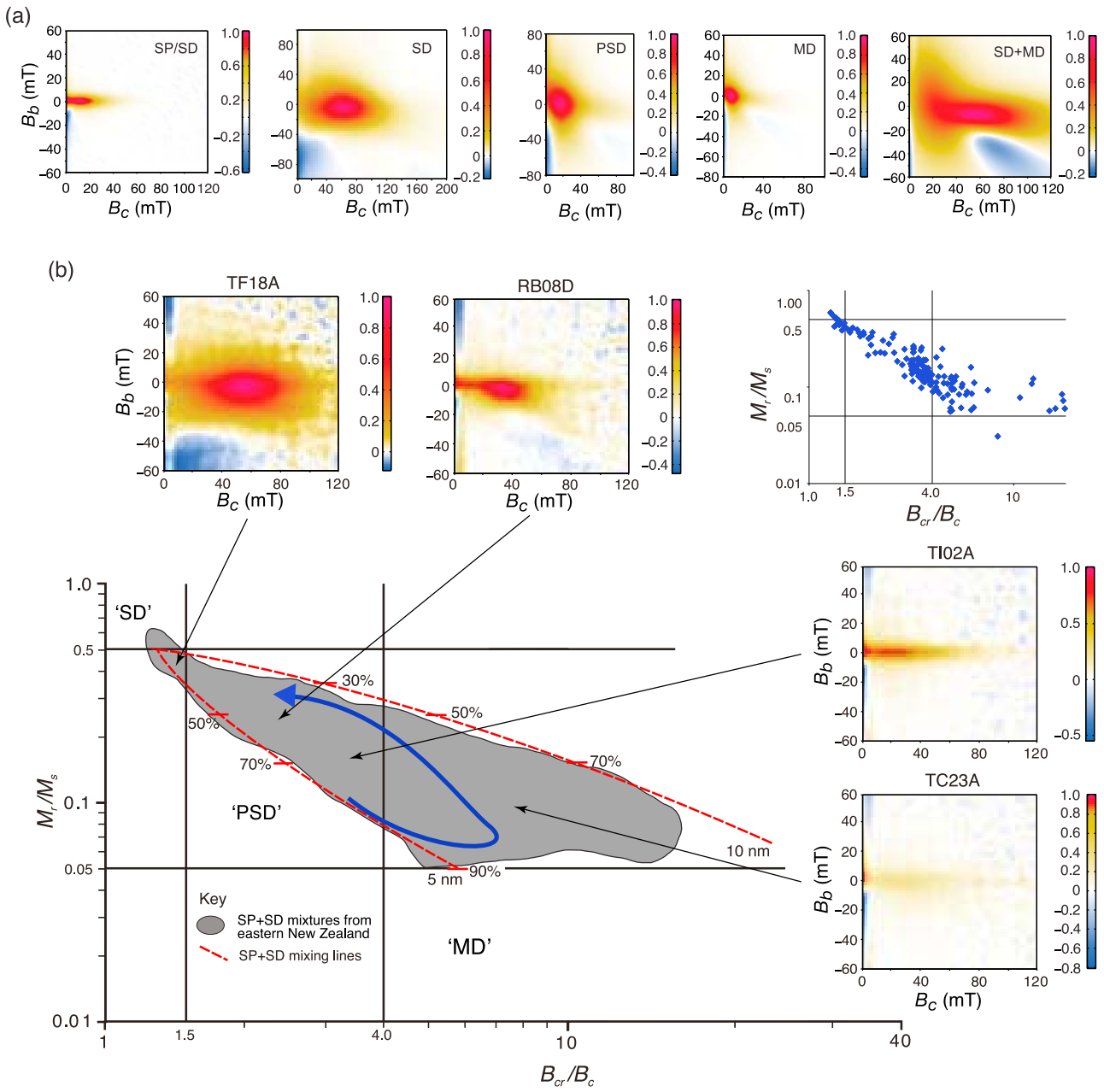

Figure 5. FORC diagrams and hysteresis data for greigite. (a) Representative FORC diagrams for particles near the SP/SD threshold size [*Roberts et al.*, 2006], dominantly stable SD grains [*Roberts et al.*, 2006], PSD grains [*Chang et al.*, 2007], MD grains [*Chang et al.*, 2007], and a mixture of SD + MD grains [*Roberts et al.*, 2006; *Chang et al.*, 2007]. The FORC diagrams are plotted using the software of *Egli et al.* [2010], where blue indicates negative regions that are a fundamental component of the magnetic response of SD particle systems [cf. *Newell*, 2005]. (b) Plot of M_r/M_s versus B_{cr}/B_c [cf. *Day et al.*, 1977] for samples from sedimentary basins of the Hikurangi margin, New Zealand [*Rowan and Roberts*, 2006], with hysteresis parameters and FORC distributions indicated for selected samples. The FORC distribution for sample TF18A indicates dominantly SD greigite grains with strong magnetostatic interactions. Sample RB08D contains SD greigite, with decreased interactions and a coercivity distribution that is shifted toward the origin by thermal relaxation. For samples TI02A and TC23A, the SD peak is proportionally smaller and shifted toward the origin of FORC diagrams because of thermal relaxation of proportionally larger SP populations (smoothing factor (SF) = 5 for all FORC diagrams). The smaller Day plot shown at the top right illustrates individual data that are summarized in the main plot. Theoretical curves for mixtures of SD and SP magnetite [*Dunlop*, 2002] are plotted for 5 nm and 10 nm SP grains (% refers to % SP grains), although the assumption of a constant SP grain size is probably not valid in this case. Compared to sample TF18A, the majority of Hikurangi margin samples contain larger proportions of SP greigite. The arrowed loop indicates the general down-core trend observed by *Rowan et al.* [2009] in diagenetically reduced SP greigite-enhanced sediments worldwide.

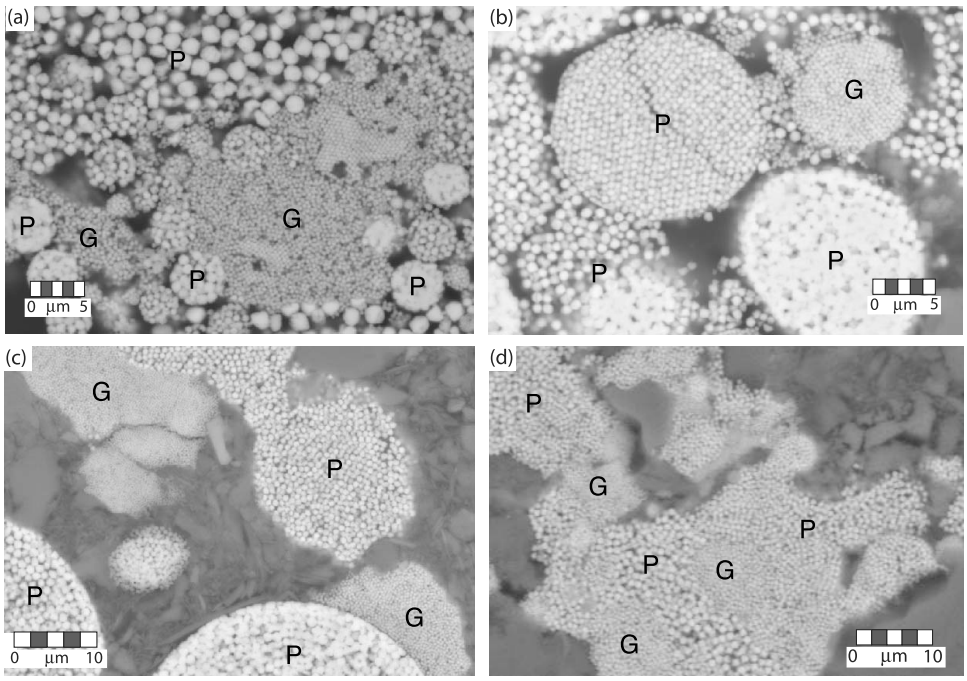

Figure 6. Backscattered electron images illustrating greigite microtextures and occurrence in sediments. (a) Aggregate of fine-grained greigite (G) filling space inside a foraminifer (Crostolo River section, Po Valley, Italy [cf. *Tric et al.*, 1991], sample CR07B, site 2 [*Roberts et al.*, 2005]). (b and c) Spherical framboids of greigite (fine-grained) and pyrite (P; coarser-grained) crystals. (d) Mixed aggregate of fine-grained greigite and coarser pyrite crystals within sediment matrix (sample CR11B, site 3 [*Roberts et al.*, 2005]). The closely packed greigite aggregates are common in diagenetically reduced sediments, which explains why FORC diagrams for sedimentary greigite routinely indicate strong magnetostatic interactions.

tions have a negative region in the bottom left-hand part of the FORC diagram. Many FORC diagrams are scaled such that this part of the distribution is not shown. We show non-truncated FORC diagrams produced using software with a color map [*Egli et al.*, 2010] that illustrates this negative response in blue (Figure 5a). As demonstrated by *Newell* [2005], this negative region is a fundamental component of the magnetic response of a SD particle assemblage (see *Muxworthy and Roberts* [2007] for a more detailed explanation). Third, the concentric FORC distributions have considerable vertical spread (Figures 5a and 5b), which is indicative of magnetostatic interactions [*Pike et al.*, 1999; *Roberts et al.*, 2000]. SEM images of natural greigite consistently indicate that sedimentary greigite grows *authigenically* in clumps (Figure 6), usually with particles close to or in contact with each other [e.g., *Jiang et al.*, 2001; *Roberts and Weaver*, 2005; *Roberts et al.*, 2005, 2010; *Sagnotti et al.*, 2005, 2010; *Rowan and Roberts*, 2005, 2006]. Micromagnetic models confirm that such small interparticle distances will result in substantial magnetostatic interactions and vertical spread of contours on FORC diagrams [*Carvallo et al.*, 2003; *Muxworthy et al.*, 2004].

[28] FORC diagrams for greigite-bearing samples also reveal characteristics of thermally relaxed particles near the SD/SP threshold (samples TI02A and TC23A in Figure 5b) [*Rowan and Roberts*, 2006]. *Pike et al.* [2001] demonstrated that FORC diagrams can indicate the presence of such particles. *Rowan and Roberts* [2006] and *Rowan et al.* [2009] presented FORC diagrams that are characteristic of such grains for sediments of variable age from globally widespread localities. Authigenic minerals grow progressively from solution to a finite size, so it is unsurprising that a substantial volume of sedimentary greigite can be extremely fine grained. Combined interpretation of SEM images and FORC diagrams provided the key insight to demonstrate that this is the case [*Rowan and Roberts*, 2006]. The data shown in Figure 5b are much more scattered along the B_{cr}/B_c axis than the data shown in Figures 3a–3d. *Dunlop* [2002] calculated the SD + SP mixing trends on a Day diagram [*Day et al.*, 1977] for magnetite with different SP grain sizes (5 and 10 nm). While this approach is not rigorously applicable to greigite, which has magnetocrystalline anisotropy rather than uniaxial anisotropy, the mixing lines are shown for reference in Figure 5b. The data scatter between the "5 nm" and "10 nm" mixing lines probably reflects a broad range of SP grain sizes and a larger concentration of SP grains than in the samples in Figure 3d. The potential for dominance of SP greigite, along with small populations of thermally stable SD grains, provides a new view of the magnetic properties of sedimentary greigite and substantially increases the range of magnetic properties, and therefore the range of potential geological occurrences, of greigite.

[29] *Rowan et al.* [2009] confirmed the observation of *Tarduno* [1995] that diagenetically reduced sediments contain enhanced SP particle concentrations and demonstrated that these particles consist of greigite. Diagenetic enhancement of SP greigite is accompanied by counterclockwise looping of data trends on a Day diagram (Figure 5b) away from the end-member mixing trends of *Dunlop* [2002] and into the area for SD + SP mixtures [*Rowan et al.*, 2009]. SP greigite enhancement during anoxic diagenesis therefore appears to be a fundamentally important process.

6.1.3. Grain Size Dependence of Hysteresis Parameters and FORC Diagrams

[30] The SD + SP mixing line in Figure 3d and data for samples containing large proportions of SP particles (Figure 5b) lie well above trends for mixed synthetic SD + MD greigite particles [*Chang et al.*, 2007] or for our sieved synthetic PSD or MD greigite particles (Figure 3e). Trends for synthetic PSD samples fall on the same SD + MD mixing lines calculated for magnetite by *Dunlop* [2002]. Collectively, hysteresis data enable discrimination of SD + SP from SD + MD mixtures for greigite.

[31] The coarse synthetic greigite samples of *Chang et al.* [2007] (Figures 7a and 7b) were sieved in this study to produce mean grain size fractions within a ±5 μm range (Figures 7c–7f). The sieved samples produce a much better indication of the grain size dependence of coercivity (Figures 7c and 7d) because they represent a single grain size fraction rather than the broader size distributions illustrated in Figure 3e. Systematic variation of B_c, B_{cr}, M_r/M_s, and B_{cr}/B_c is observed with grain size (for the S6 = >35 μm, S5 = 35–25 μm, S4 = 25–15 μm, S3 = 15–5 μm, S2 = 5–1 μm, and S1 = <1 μm fractions) in Figures 7c–7f. Data for the <1 μm fraction fall away from the observed trends because this fraction contains SP as well as stable SD samples, which reduces coercivity and M_r. The trend for PSD/MD samples is compared with data for two thermally stable SD natural greigite samples from Taiwan [*Jiang et al.*, 2001] and Italy [*Florindo et al.*, 2007]. It is difficult to make direct grain size observations on natural greigite samples, so the full ranges of grain sizes expected for SD behavior (Table 2) are shown as the error bars for these samples. As expected, there is a major difference in hysteresis properties for SD and PSD/MD particles. While large gaps need to be filled in Figure 7, these data represent the first grain size–dependent representation of hysteresis data for greigite with respect to known size fractions.

6.1.4. Isothermal Remanent Magnetization Acquisition and DC Demagnetization

[32] M_r acquisition curves for fresh greigite-bearing samples (Figure 8a) are typical of ferrimagnets such as magnetite, where M_r is reached at applied fields of <0.3 T. The M_r acquisition curves in Figure 8a have a sigmoidal shape that is typical of SD materials. That is, at low applied fields, the curves have a shallow slope, which steepens at intermediate fields as the peak of the *switching field distribution* is reached and then shallows again at higher applied fields where most particles are magnetically saturated. Coarser-grained greigite has, as expected, contrasting magnetic behavior, with softer magnetizations that saturate more quickly in the direct applied field and without sigmoidal M_r acquisition curves (Figure 8b). The trend of the M_r acquisition curves with increasing grain size mirrors that in Figure 7d (although the Czech sample with mixed SD + MD grains does not saturate as quickly as expected, which probably reflects partial oxidation and the presence of a high-coercivity mineral).

[33] Results of DC demagnetization of M_r are plotted in Figure 9 for the same four sets of samples for which hysteresis data are shown in Figure 4, along with the first derivative of the curves, which is a measure of the switching field distribution. Despite variable hysteresis loop shapes in Figure 4, which vary because of the SP contribution to the in-field magnetization, the SD particle assemblages that contribute to these remanence measurements have a much more uniform range of coercivities. B_{cr} values for these samples from southwestern Taiwan, Italy, and California range between 60 and 86 mT (Figure 9). These values fall within the 45–95 mT range reported for greigite by *Roberts* [1995]. It is worth noting the nature of the samples with the lowest B_{cr} values studied by *Roberts* [1995]. A sample with B_{cr} = 45 mT is from Miocene coal measures from the Czech Republic [cf. *Krs et al.*, 1992]. *Hoffmann* [1992] showed that these samples contain domain walls; they therefore contain the coarsest natural greigite grains reported in the literature. The low coercivity of these samples compared to SD samples reflects the coarser grain size. Two other relatively low B_{cr} values are from synthetic samples for which low-temperature measurements indicate substantial SP contributions [*Roberts*, 1995]. This would not normally be relevant for remanence measurements; however, the samples were analyzed using an alternating gradient magnetometer where measurement time is short compared to the relaxation times of SP particles [*Pike et al.*, 2001]. Grains near the SP/SD threshold size can therefore contribute to the measured remanence, thereby reducing the overall measured value of B_{cr}. The lower coercivities of samples from Marlborough, New Zealand (Figure 9), compared to samples from other localities probably reflects far greater concentrations of SP grains [*Rowan and Roberts*, 2006], as indicated by the more potbellied hysteresis loops for these samples (Figure 4). *Dekkers and Schoonen* [1996] observed a similar range of B_{cr} values (some are as low as 37 mT) for synthetic greigite samples, which also contain substantial concentrations of SP particles. Regardless, B_{cr} values for the natural samples from New Zealand (46–62 mT) and those documented by *Dekkers and Schoonen* [1996] are consistent with the range reported by *Roberts* [1995]. Finally, remanence acquisition above 0.3 T for some samples in Figure 9 probably reflects partial oxidation with small contributions from high-coercivity components (e.g., the New Zealand samples are from *Roberts* [1992] and were stored for 15 years prior to measurement for this study). Overall, however, high-coercivity components like hematite and goethite have low magnetic moments, so they are unlikely to contribute significantly to the B_{cr} values.

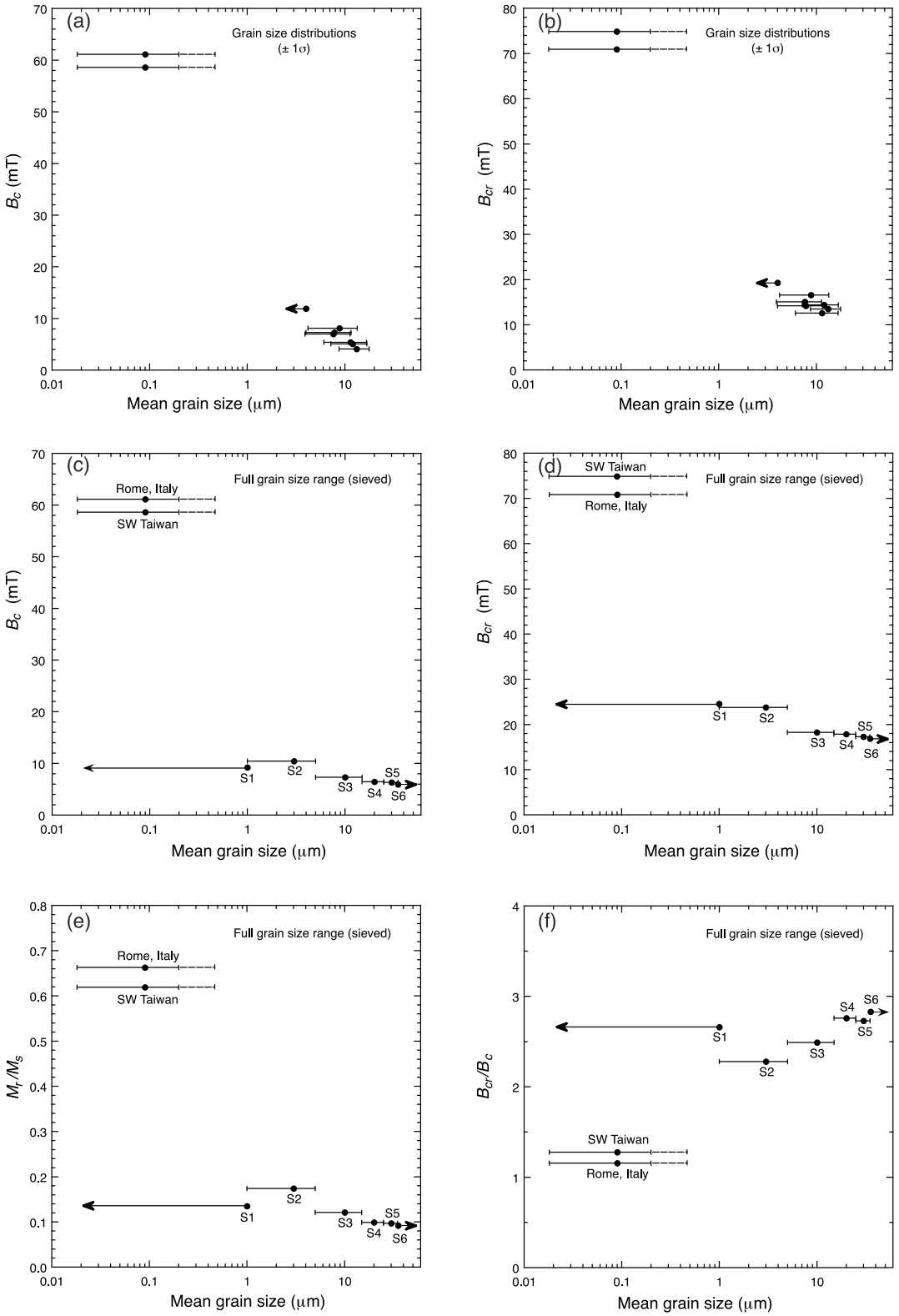

Figure 7. Grain size dependence of magnetic hysteresis properties for greigite. Variations of (a) B_c and (b) B_{cr} for the synthetic greigite samples with grain size distributions reported by *Chang et al.* [2007] (see Figure 3e). Data clustering in the bottom right-hand sides of the plots reflects the broad grain size distributions (uncertainties are indicated by ±1 σ confidence limits about the Gaussian mean). The samples were then sieved into discrete grain size fractions and reanalyzed (samples S6 = >35 μm, S5 = 35–25 μm, S4 = 25–15 μm, S3 = 15–5 μm, S2 = 5–1 μm, and S1 = <1 μm). Much clearer grain size dependence emerges for (c) B_c, (d) B_{cr}, (e) M_r/M_s, and (f) B_{cr}/B_c. The two thermally stable SD samples have unknown sizes, so the error bars reflect the size range reported for SD particles in Table 2.

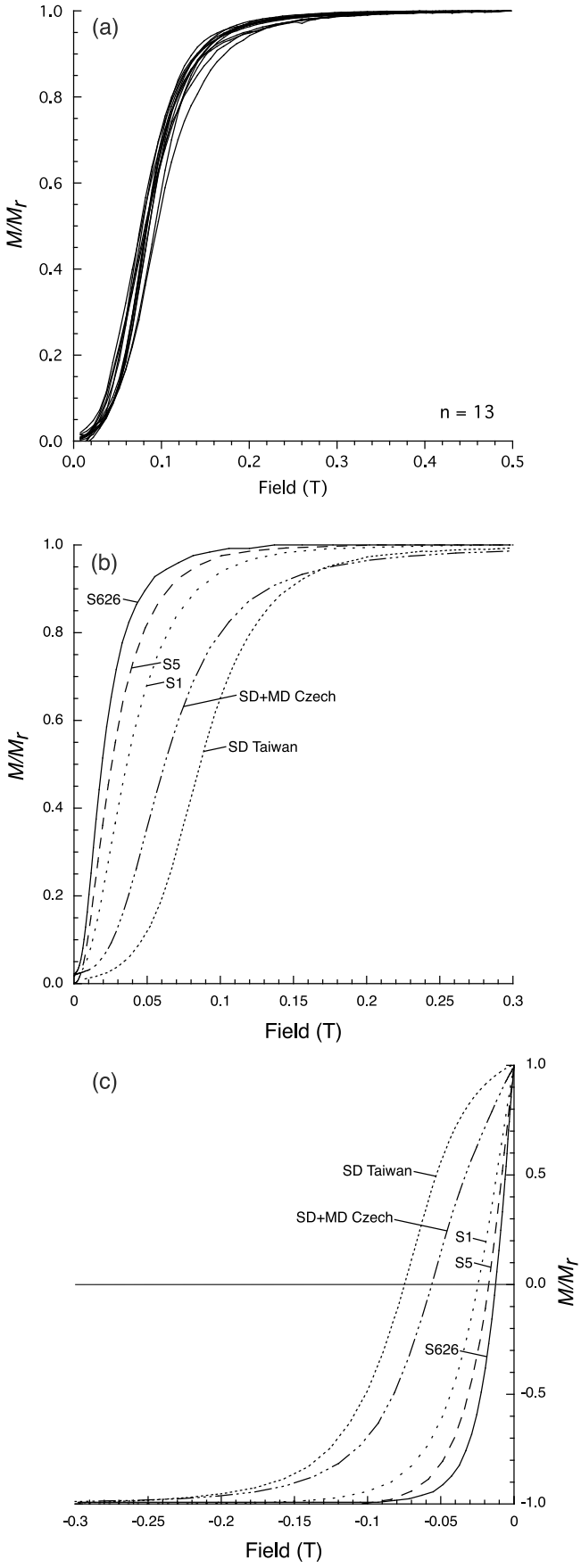

[34] In contrast to backfield demagnetization curves for SD greigite (Figure 9), progressively increasing grain size results in softer magnetizations and lower B_{cr} values (Figure 8c). The illustrated SD greigite has a B_{cr} value of 75 mT, while the Czech sample has high B_{cr} (56 mT) due to the presence of SD grains in addition to MD particles. The MD-dominated samples, however, have much lower B_{cr} values of 24.5 mT (S1), 17.3 mT (S5), and 12.6 mT (S626) (Figure 8c).

[35] When considering domain-state-dependent coercivity variations, one would expect a harder coercivity distribution if remanence measurements are made using a pulse magnetizer with off-line measurement on a separate magnetometer, where the measurement time is long enough to allow magnetic relaxation of grains near the SP/SD threshold size. This is particularly important when fitting components to M_r acquisition spectra [*Kruiver et al.*, 2001; *Heslop et al.*, 2002]. A comparison of curve fits using cumulative log Gaussian functions is shown for two types of data in Figure 10. For data measured online with a VSM, a one-component fit poorly matches the observed coercivity spectrum (compare red line fit (smaller plots on the left) with green and blue line fits (smaller plots in the middle) for the VSM data in Figure 10). In contrast, the observed coercivity spectrum for off-line measurements with a separate magnetometer is modeled satisfactorily by a one-component fit (red line fits (smaller plots on the right) to the pulse magnetizer data in Figure 10). The higher average coercivities indicated by the pulse magnetizer data, particularly for the SP-dominated samples from New Zealand (Figure 10b), provide a clear indication that thermal relaxation of SP particles has affected the VSM measurements. This demonstrates the well-known difference associated with measurement of M_r acquisition and backfield demagnetization on the two different types of systems. We recommend that component fitting for M_r acquisition data should be done with care for data measured with a VSM or equivalent systems because of the greater complexity resulting from SP contributions. If the purpose of such measurements is to determine the coercivity distribution of the remanence carrying magnetic fraction in a sample, off-line measurements, which reflect only the response of these particles, are more useful than those that additionally reflect the response of thermally unstable particles. This conclusion is consistent

Figure 8. M_r acquisition and backfield demagnetization curves for representative greigite samples. (a) M_r acquisition curves for stable SD (EJEM) samples from southwestern Taiwan [*Horng et al.*, 1992a, 1992b]. The curves are sigmoidal in shape, with most of the magnetization acquired below 200 mT and saturation achieved at 300 mT. (b) M_r acquisition curves for a progressive shift from sigmoidal curves for SD Taiwan samples, as plotted in Figure 8a, through to a SD + MD mixture from the Czech Republic [*Roberts et al.*, 2006], to magnetically soft M_r acquisition curves for the synthetic PSD/MD samples (S626) of *Chang et al.* [2007], including sieved samples with discrete grain sizes (S1 and S5). (c) Backfield demagnetization curves for samples in Figure 8b.

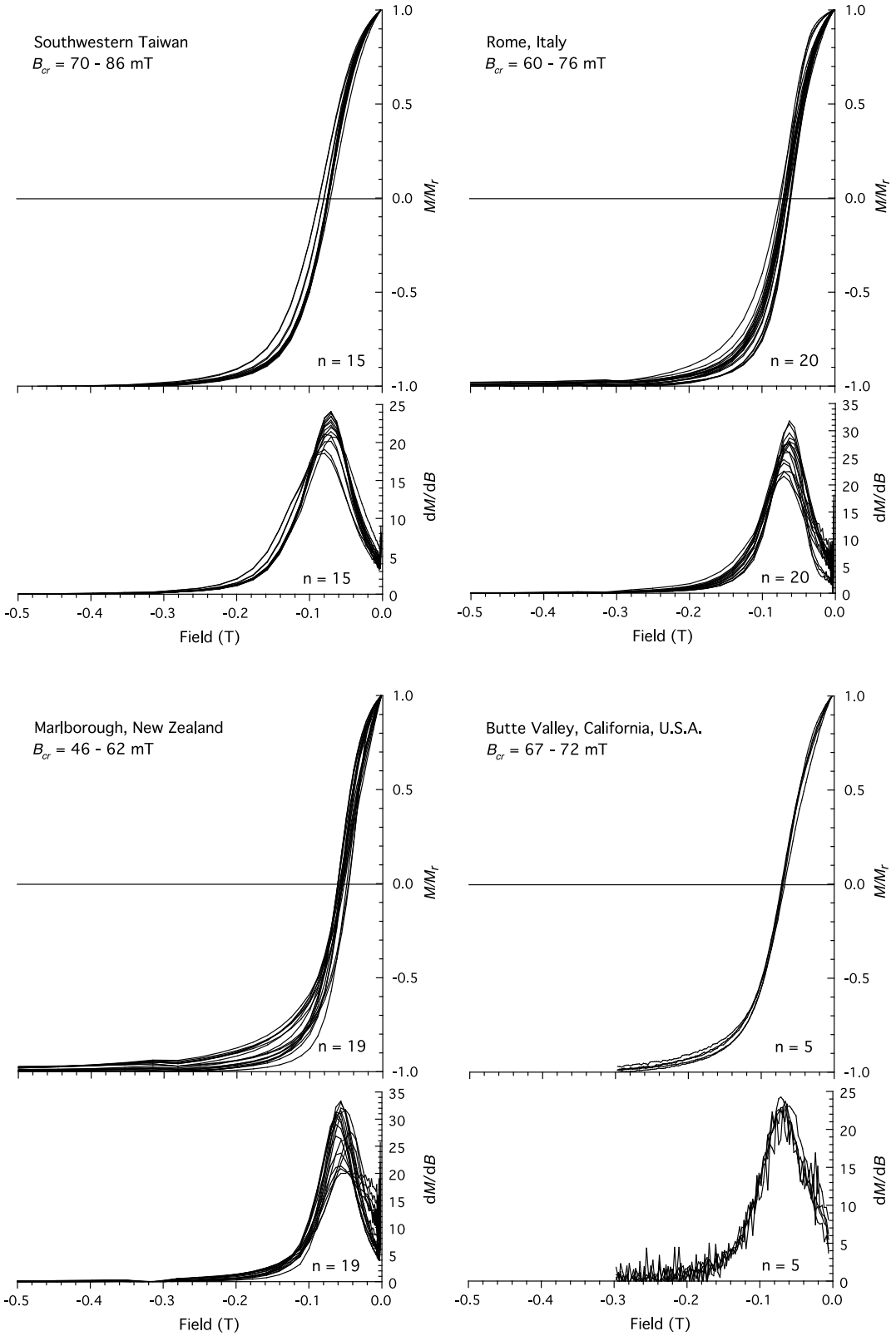

Figure 9. Backfield demagnetization curves for samples that were magnetically saturated in a field of 0.5 T. Samples are from previously described greigite-bearing localities: southwestern Taiwan [*Horng et al.*, 1992a, 1992b]; locations in and around Rome, Italy [*Florindo and Sagnotti*, 1995; *Florindo et al.*, 2007]; Marlborough, New Zealand [*Roberts*, 1992; *Roberts and Turner*, 1993]; and Butte Valley, California [*Roberts et al.*, 1996]. First derivatives of the sigmoidal curves indicate peaks that coincide with the coercivity of remanence value (B_{cr}). B_{cr} values are relatively high compared to magnetite [*Roberts*, 1995].

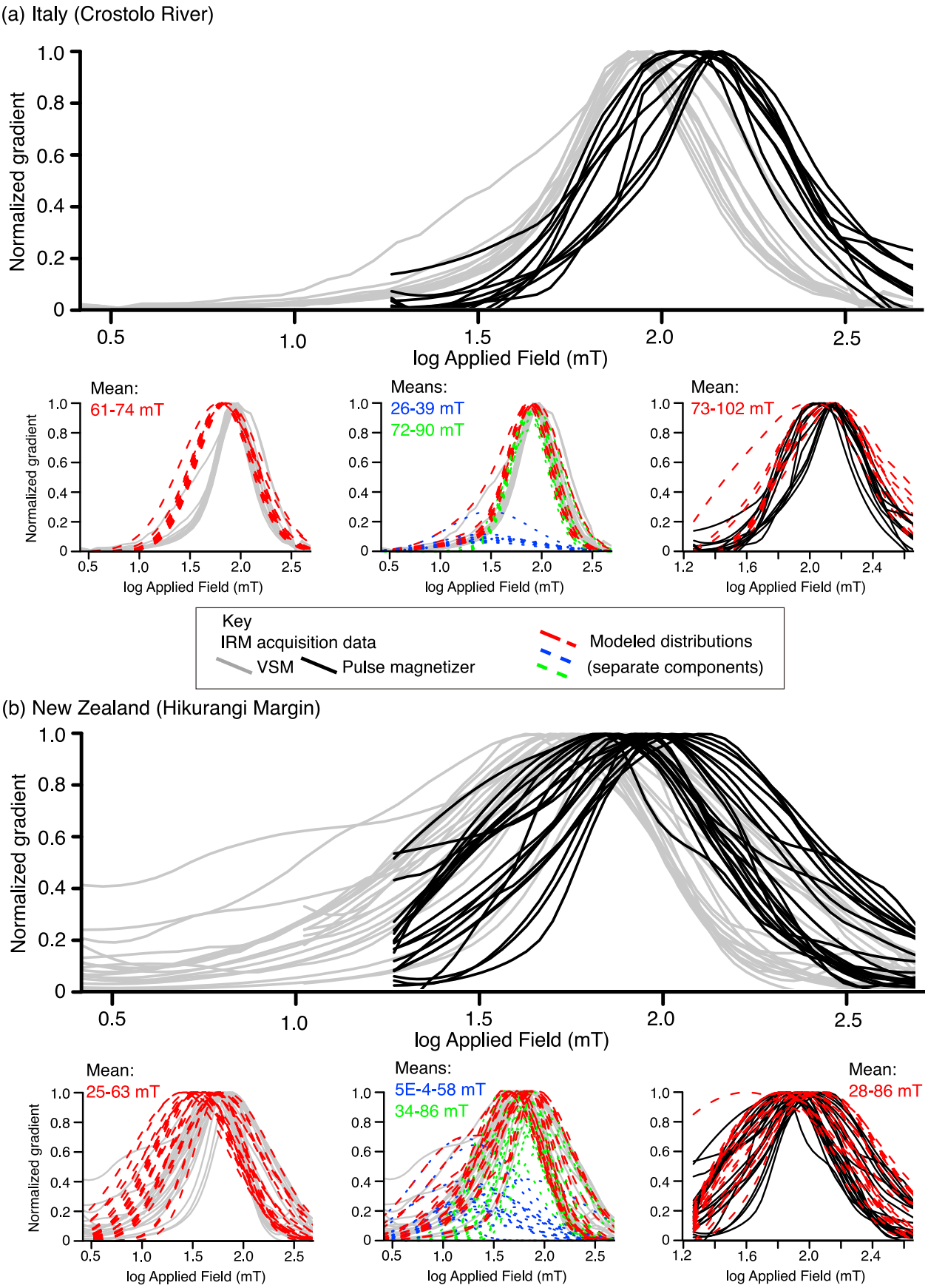
(a) Italy (Crostolo River)
Normalized gradient
log Applied Field (mT)
Mean:
61-74 mT
Means:
26-39 mT
72-90 mT
Mean:
73-102 mT
Key
IRM acquisition data
VSM
Pulse magnetizer
Modeled distributions
(separate components)
(b) New Zealand (Hikurangi Margin)
Mean:
25-63 mT
Means:
5E-4-58 mT
34-86 mT
Mean:
28-86 mT

Figure 10

with the observation of *Heslop et al.* [2004], who state that thermal relaxation can complicate M_r acquisition curve fitting using cumulative log Gaussian functions. It should also be noted that M_r component analysis is only valid for noninteracting magnetic particle assemblages; this assumption does not hold for most natural greigite samples (Figures 5 and 6), so such analyses should be performed with caution when greigite is potentially present. Few detailed M_r acquisition data sets are available for greigite: the comprehensive data set of *Hüsing et al.* [2009] provides a useful basis for comparison.

6.2. Other Room Temperature Magnetic Properties

6.2.1. Low-Field Magnetic Susceptibility

[36] The low-field mass magnetic susceptibility (χ) is the most commonly measured magnetic property of sediments. Despite this, a χ value for greigite is not reported in key compilations of magnetic susceptibility values of rocks and minerals [e.g., *Hunt et al.*, 1995; *Borradaile and Jackson*, 2004]. As is the case for M_s, previously published determinations of χ for greigite are compromised by lack of sample purity. For example, *Dekkers and Schoonen* [1996] obtained values ranging between 0.2 and 1.9×10^{-4} m^3 kg^{-1} for greigite samples with varying purity. *Peters and Dekkers* [2003] used an average value of 1.08×10^{-4} m^3 kg^{-1} in their compilation. Using a synthetic greigite sample studied by *Chang et al.* [2007, 2008, 2009a], we provide here the first report of χ for pure greigite: 3.2×10^{-4} m^3 kg^{-1}. The purity of the studied sample means that this value will be more robust than previous estimations; however, we only analyzed a single sample for which the mass was well determined, and we have not provided an error estimation for this determination. Further measurements could result in refinement of this estimate.

6.2.2. Alternating Field Demagnetization

[37] Several studies have demonstrated that greigite can display nonideal behavior upon AF demagnetization. This is a manifestation of the SD properties exhibited by many natural greigite-bearing samples. SD materials are prone to acquisition of a *rotational remanent magnetization (RRM)* during rotation in a slowly decaying AF. *Stephenson* [1980] explained acquisition of an RRM in terms of a gyroremanent effect associated with a flip of magnetic moments as a sample rotates within a field. This is referred to as a *gyroremanent magnetization (GRM)* and can be acquired during static and tumbling AF demagnetization. The term GRM is used to describe acquisition of spurious magnetizations during either type of AF demagnetization; the term RRM is useful when discussing such magnetizations when either the field or the sample is rotated. A GRM is commonly acquired perpendicular to the last axis along which a static AF was applied. GRM acquisition is common in greigite [e.g., *Snowball*, 1997a, 1997b; *Hu et al.*, 1998, 2002; *Sagnotti and Winkler*, 1999; *Stephenson and Snowball*, 2001; *Florindo et al.*, 2003; *Rowan and Roberts*, 2006; *Frank et al.*, 2007a; *Ron et al.*, 2007; *Fu et al.*, 2008; *Rowan et al.*, 2009; *Sagnotti et al.*, 2010] and probably explains earlier reports of *anhysteretic remanent magnetization (ARM)* acquisition during AF demagnetization at 40–60 mT in greigite-bearing samples [e.g., *Krs et al.*, 1990].

[38] The magnitude of GRM acquisition in greigite is larger than in any other known naturally occurring magnetic mineral, which led *Snowball* [1997b] and *Stephenson and Snowball* [2001] to suggest that the effective gyrofield B_g provides a diagnostic indicator of the presence of greigite. *Sagnotti and Winkler* [1999] also suggested that the propensity of greigite to acquire a field-impressed anisotropy causes the low-field magnetic susceptibility to markedly increase at right angles to the direction of an imparted large field. They therefore suggested a parameter κ_{diff}, which corresponds to the change in volume susceptibility after application of a large DC field, to indicate the concentration of SD greigite within a sample.

[39] GRM acquisition and the usefulness of parameters associated with this phenomenon for identifying greigite are illustrated in Figure 11, where we show results of AF demagnetization of the natural remanent magnetization for greigite-bearing samples. These results demonstrate that a GRM starts to be acquired above 40–70 mT during static AF demagnetization (Figures 11b and 11d–11k). During tumbling AF demagnetization, the magnetization is randomized above 30 mT (Figure 11c), at which point the NRM might only be reduced to about 25% of its original value. *Snowball* [1997a, 1997b] and *Stephenson and Snowball* [2001] observed GRM acquisition during static AF demagnetization above peak fields of 80 mT, while *Oda and Torii* [2004] and *Sagnotti and Winkler* [1999] observed GRM acquisition above peak fields of 60 and 40 mT, respectively. We observe variable peak fields for GRM acquisition (Figures 11b and 11d–11k). For some greigite-bearing samples, no measurable GRM is apparent (Figure 11l), as noted by *Sagnotti et al.* [2005] and *Rowan and Roberts* [2006]. Likewise, *Reynolds et al.* [1994] and *Fassbinder and Stanjek* [1994] observed no GRM acquisition during AF demagnetization of the NRM up to 80 mT for natural greigite from Alaska and for biogenic SD greigite, respectively. Overdependence on parameters such as B_g or κ_{diff} for identifying greigite will therefore result in significant

Figure 10. Representative cumulative log Gaussian representations of M_r acquisition data [cf. *Kruiver et al.*, 2001; *Heslop et al.*, 2002] measured with a VSM (gray lines) compared with those acquired with a pulse magnetizer (black lines). The smaller plots illustrate that data measured online with a VSM cannot be fitted with a one-component coercivity distribution; instead, a two-component fit (blue and green lines) with a substantial low-coercivity component (blue) is required. In contrast, the curves for off-line measurements with a pulse magnetizer can be adequately modeled with a one-component fit (red lines). Data are from (a) Crostolo River, Italy [*Tric et al.*, 1991; *Roberts et al.*, 2005], and (b) the Hikurangi margin, New Zealand [*Rowan and Roberts*, 2006].

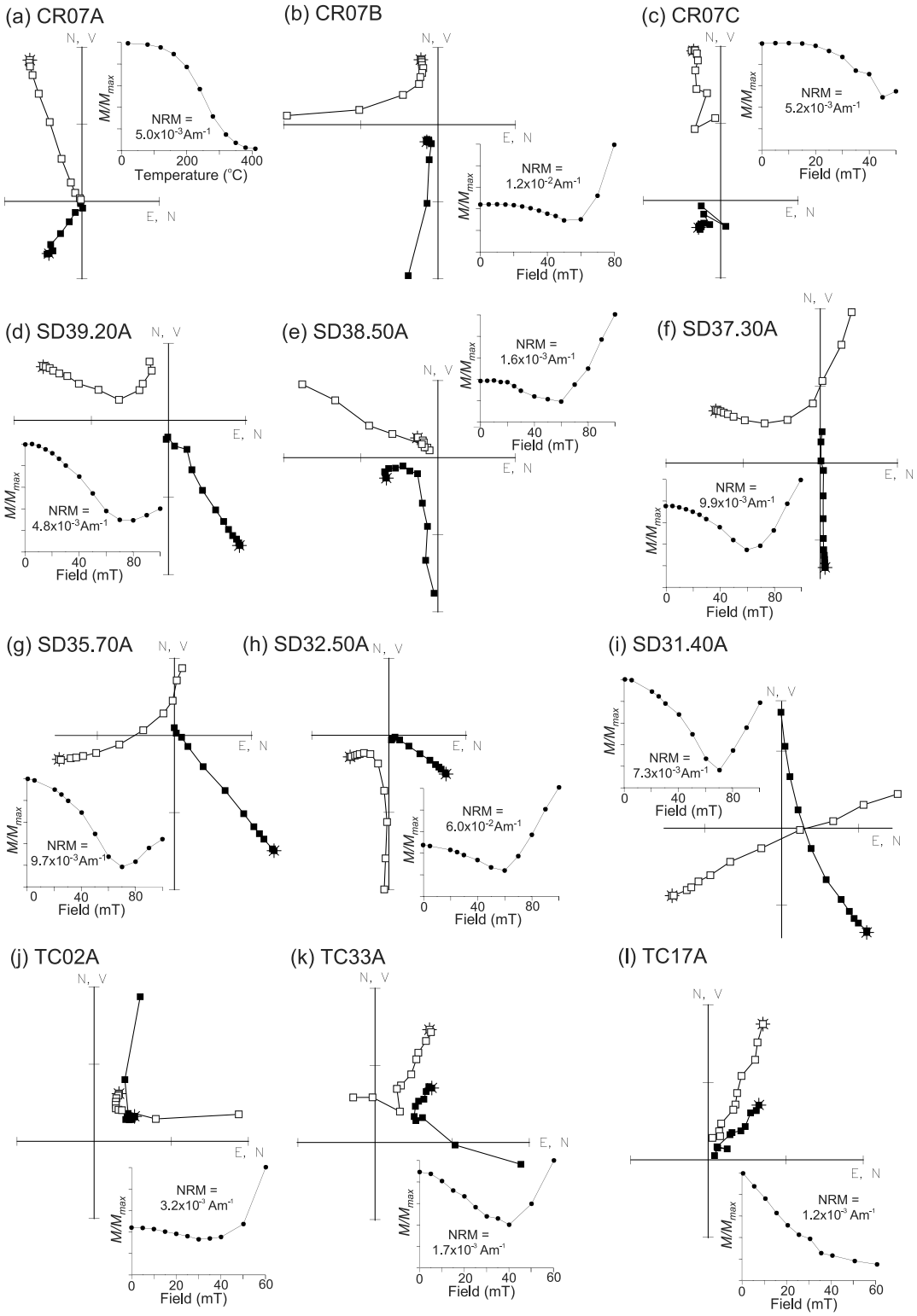

Figure 11. Representative thermal and AF demagnetization results for greigite-bearing sediments. Comparison of (a) thermal, (b) static AF, and (c) tumbling AF demagnetization treatment for three sister samples from the Crostolo River, Italy [*Roberts et al.*, 2005]. Thermal demagnetization yields unambiguous results, static AF demagnetization results in GRM acquisition above ~50 mT, and tumbling AF demagnetization produces random paleomagnetic directions above 35 mT. (d–i) Variable GRM acquisition during static AF demagnetization for samples from fluviolacustrine sediments from the paleo-Tiber Valley, Rome, Italy [*Florindo et al.*, 2007]. (j–l) Variable GRM acquisition for different greigite-bearing samples from Te Waipera Cemetery, Mahia Peninsula, New Zealand [*Rowan and Roberts*, 2006]. Lack of GRM acquisition in SP-dominated samples (e.g., Figure 11l) reduces the usefulness of parameters that rely on GRM acquisition for greigite identification.

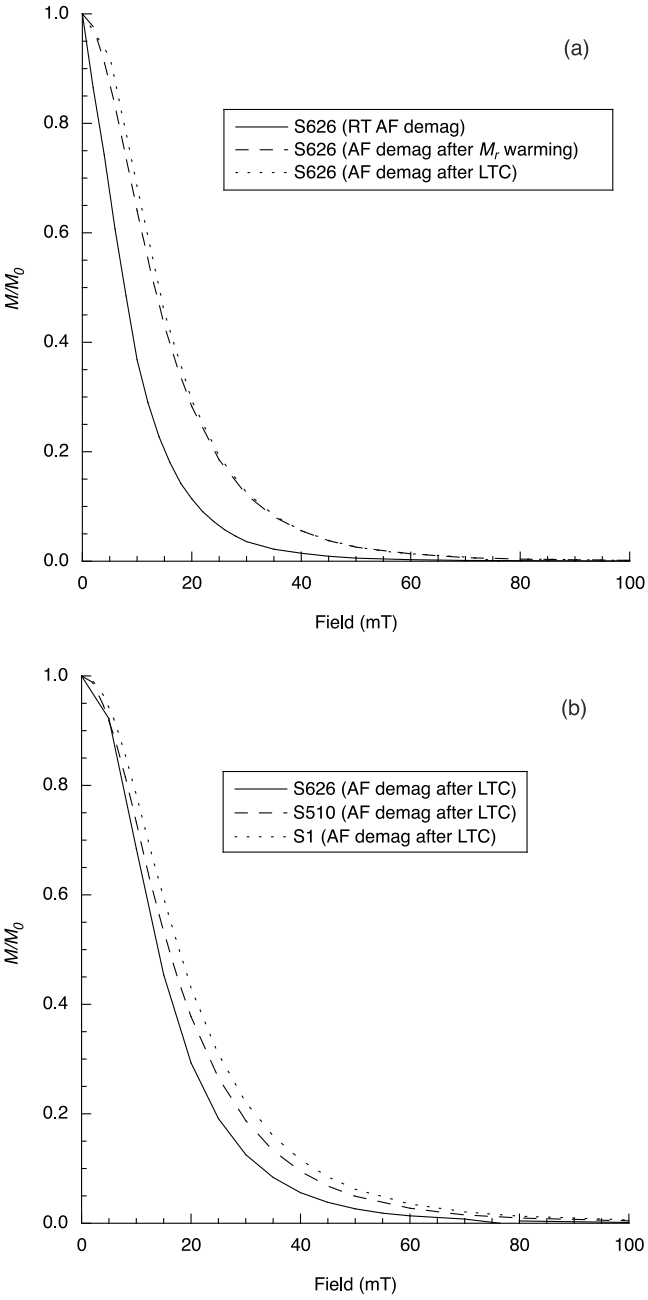

Figure 12. AF demagnetization spectra of M_r for synthetic MD samples. (a) Sample S626 has the softest magnetic properties among our synthetic coarse-grained greigite samples and has a concave-up spectrum during room temperature (RT) AF demagnetization. Upon cooling, either for low-temperature cycling (LTC) experiments or for warming of a low-temperature M_r, the demagnetization spectrum becomes magnetically harder because of low-temperature demagnetization of MD moments. (b) Comparison of AF demagnetization spectra after LTC experiments for three representative samples that reflect grain size differences (see text).

underestimation of its presence and concentration. These parameters are most likely to be large when there is a substantial concentration of thermally stable SD greigite grains, but, as observed in section 6.1.2, this is not the case for all greigite occurrences. Thus, while these properties can be extremely useful indicators of the presence of greigite [e.g., *Fu et al.*, 2008; *Rowan et al.*, 2009], they are not always definitive.

[40] MD greigite, as expected, has strongly contrasting AF demagnetization spectra compared to SD greigite (Figure 12). Classic "concave-up" MD behavior is evident for AF demagnetization of M_r at room temperature for sample S626 (Figure 12a). It has low coercivity and a median destructive field (MDF) < 8 mT, whereas after cooling of a room temperature M_r to 10 K for either M_r warming or LTC experiments, further AF demagnetization reveals a harder coercivity spectrum with MDF = 13 mT. This hardening of coercivity results from irreversible low-temperature demagnetization associated with domain wall unpinning in PSD/MD grains [e.g., *Moskowitz et al.*, 1998]. *Chang et al.* [2007, 2009b] observed that the remanence loss after cooling at low temperatures is grain size dependent. This is supported by variable coercivities in AF demagnetization data after LTC treatment (Figure 12b): the lowest MDF corresponds to the coarsest grain size and vice versa. The data in Figure 12, and the results of *Chang et al.* [2007, 2009b], therefore suggest that magnetic granulometry should be possible for PSD/MD greigite using the classic domain-state-sensitive techniques of low-temperature demagnetization [cf. *Ozima et al.*, 1964] and comparison of AF demagnetization spectra [cf. *Lowrie and Fuller*, 1971].

6.2.3. Interpretation of Demagnetization Results in Paleomagnetic Studies of Greigite

[41] The fact that only ~25%–80% of the NRM is typically removed before a spurious GRM is acquired during static AF demagnetization, or before acquisition of an RRM during tumbling AF demagnetization, means that these treatments are not ideal for identification of *characteristic remanent magnetization (ChRM)* directions in paleomagnetic studies. We therefore routinely prefer thermal demagnetization in paleomagnetic studies of greigite-bearing sediments in our respective laboratories (compare Figure 11a with Figures 11b–11k). In addition to the widely documented GRM acquisition problems associated with static AF demagnetization, randomization of paleomagnetic directions during tumbling AF demagnetization in studies of diagenetically reduced sediments from New Zealand [e.g., *Turner et al.*, 1989] probably resulted from RRM acquisition in greigite. Thermal demagnetization has therefore become the method of choice in paleomagnetic studies of these sediments [e.g., *Turner et al.*, 1989; *Turner and Kamp*, 1990; *Pillans et al.*, 1994; *Roberts et al.*, 1994]. Despite our preference for thermal demagnetization, this approach causes thermal alteration of matrix minerals that can obscure results. Greigite unblocks at intermediate temperatures (usually 230°C–350°C), which can also add interpretational complexities when magnetic minerals with higher *unblocking temperatures* are also present [e.g., *Turner*, 2001]. Many studies have also shown that greigite can be paleomagnetically problematical when it grows significantly later than shallow burial [e.g., *Florindo and Sagnotti*, 1995; *Horng et al.*, 1998; *Jiang et al.*, 2001; *Roberts and Weaver*, 2005; *Rowan and Roberts*, 2005, 2006,

2008; *Sagnotti et al.*, 2005; *Larrasoaña et al.*, 2007; *Fu et al.*, 2008; *Porreca et al.*, 2009; *Roberts et al.*, 2010]. We therefore advocate routine use of paleomagnetic field tests, such as the *fold test*, to ensure that an early magnetization has been identified [*Rowan and Roberts*, 2005, 2006, 2008]. Even identification of a prefolding magnetization might not ensure that the paleomagnetic signal has a syndepositional origin because there could be a considerable time span between deposition and folding. The reversals test is not always diagnostic of an ancient magnetization; patchy remagnetizations and false magnetic polarity records have been recognized [e.g., *Florindo and Sagnotti*, 1995; *Horng et al.*, 1998; *Roberts and Weaver*, 2005; *Sagnotti et al.*, 2005, 2010; *Rowan and Roberts*, 2005, 2006] and could mask results of a reversals test. Greigite can continue to grow several thousand years after deposition in active depositional environments [e.g., *Liu et al.*, 2004; *Rowan et al.*, 2009], so it is not safe to assume that greigite carries a syndepositional paleomagnetic signal, and if it does, the preserved geomagnetic record can be considerably smoothed. Verification of the ancient nature of magnetizations carried by greigite, which is often difficult to achieve with a high degree of confidence, is crucial. We recommend that paleomagnetic records involving greigite should be considered unreliable for studies of geomagnetic field behavior and geochronology unless they can be demonstrated otherwise. Recognition of widespread remagnetizations due to greigite, which makes the magnetization younger than the surrounding rock unit, has resulted in reinterpretation of the tectonic rotation history, with respect to timing and rates of rotation, of the Hikurangi margin, New Zealand [*Rowan and Roberts*, 2008]. Reevaluation of paleomagnetic data from other tectonically active regions in which greigite is widespread could prove to be equally valuable.

6.2.4. Anhysteretic Remanent Magnetization

[42] The κ_{ARM}/κ ratio (i.e., the ratio of susceptibility of ARM to the low-field volume magnetic susceptibility) is a useful proxy for magnetite grain size [*Banerjee et al.*, 1981] and would also be expected to reflect grain size variations in greigite. *Reynolds et al.* [1994] reported κ_{ARM}/κ data for a range of greigite-bearing sediments, as well as for sediments with other magnetic minerals present, but they found that the greigite has rather uniform κ_{ARM}/κ ratios. ARM measurements have not been widely reported for greigite-bearing samples, largely because other parameters (hysteresis and M_r/κ) have been successfully used as magnetic grain size indicators. It therefore remains to be seen whether κ_{ARM}/κ is a useful grain size indicator for greigite. The widespread presence of SD + SP mixtures in natural greigite is likely to complicate interpretation of this parameter because SP grains will contribute to κ but not to κ_{ARM}.

[43] *Peters and Thompson* [1998] and *Peters and Dekkers* [2003] used a range of room temperature magnetic parameters to discriminate among different naturally occurring magnetic minerals. The SD greigite samples used by *Peters and Thompson* [1998] and *Peters and Dekkers* [2003] can be readily discriminated from other minerals on the basis of AF demagnetization characteristics of the ARM combined with other parameters. The fact that the ARM of the studied greigite samples was relatively resistant to AF demagnetization could reflect the countering of demagnetization by simultaneous GRM acquisition. While the parameters proposed by *Peters and Thompson* [1998] and *Peters and Dekkers* [2003] will be useful for identifying SD greigite, their approach will result in significant underestimation of the presence and concentration of greigite if significant concentrations of non-SD greigite are present. Non-SD greigite will produce overlap between the previously recognized magnetic properties of greigite and those of other lower-coercivity minerals. It should be noted that ARM intensity depends strongly on the equipment and settings used to produce the ARM and that this parameter is not well calibrated among different laboratories [*Sagnotti et al.*, 2003]. Caution should therefore be exercised when using κ_{ARM} to compare data acquired in different laboratories. Nevertheless, such analyses carried out within a single laboratory have considerable diagnostic scope. For example, *Frank et al.* [2007b] published a comprehensive rock magnetic data set for lake sediments containing complex, and stratigraphically varying, mixtures of greigite and other magnetic minerals and found significant overlaps in data fields for different parameters. Nevertheless, they demonstrated that careful analysis can provide useful discrimination between components in complex magnetic mineral mixtures.

6.3. Low-Temperature Magnetic Properties

[44] Low-temperature magnetic measurements provide insights into thermal dynamic processes and can provide considerable information in addition to room temperature measurements. They also avoid thermal alteration that affects high-temperature measurements. Detection of low-temperature magnetic transitions can enable identification of magnetic minerals. For example, magnetite undergoes the *Verwey transition* at 110–120 K [e.g., *Verwey*, 1939; *Özdemir et al.*, 1993], hematite undergoes the *Morin transition* at 250–260 K [*Morin*, 1950], and monoclinic pyrrhotite (Fe_7S_8) undergoes a magnetic transition at 30–34 K [*Dekkers et al.*, 1989; *Rochette et al.*, 1990]. Several studies have been made of the low-temperature magnetic properties of greigite [*Spender et al.*, 1972; *Moskowitz et al.*, 1993; *Roberts*, 1995; *Torii et al.*, 1996; *Dekkers et al.*, 2000; *Chang et al.*, 2007]. The most comprehensive analysis, which employed a wide range of low-temperature techniques on samples ranging in size from SP to MD, is that of *Chang et al.* [2009b]. It is not our intention to reproduce their comprehensive analysis here. Key observations are highlighted, but the reader is referred to *Chang et al.* [2009b] for a more in-depth treatment.

6.3.1. Warming of M_r From Low Temperatures

[45] Measurement of M_r, imparted in a 2.5 T field at 5 K, as it is warmed (i.e., thermally demagnetized) to room temperature (Figure 13a) for a wide range of greigite-bearing samples [*Roberts*, 1995; *Torii et al.*, 1996] confirms earlier

suggestions that greigite lacks any characteristic low-temperature magnetic transitions [*Spender et al.*, 1972; *Moskowitz et al.*, 1993]. Of the range of low-temperature M_r warming curves in Figure 13a, dominantly SD and PSD/MD samples undergo minimal magnetic unblocking during warming (e.g., dominantly SD samples EJEM15 and EJEM13-2; synthetic PSD/MD samples S504, S706, and S628 [*Chang et al.*, 2009b]; and a SD + MD sample (Krs) from Czech coal measures [cf. *Krs et al.*, 1992]). This minimal decay is consistent with the theoretically expected decay of saturation magnetization with temperature. Other natural samples undergo highly variable degrees of magnetic unblocking with temperature (EJEM10F and NR27). The largest amounts of unblocking are observed in a synthetic sample that is dominated by SP behavior (SYN93A) [cf. *Roberts*, 1995], in a sample grown in a laboratory chemostat with sulfate-reducing bacteria that produced largely amorphous extracellular hyperfine greigite (DSV0.5T) [*Watson et al.*, 2000], and in diagenetically reduced sediment from northeastern New Zealand (NR27 [*Rowan and Roberts*, 2006]). These data demonstrate that natural greigite can occur with a wide range of hyperfine SP particle distributions in addition to SD particles. The low-temperature data of *Dekkers et al.* [2000] for synthetic samples containing abundant SP as well as SD greigite [*Dekkers and Schoonen*, 1996] confirm this interpretation, although they reported a local M_r maximum at ~10 K, which has since been confirmed to be related to unblocking of fine particles and is not a magnetic transition [*Chang et al.*, 2009b].

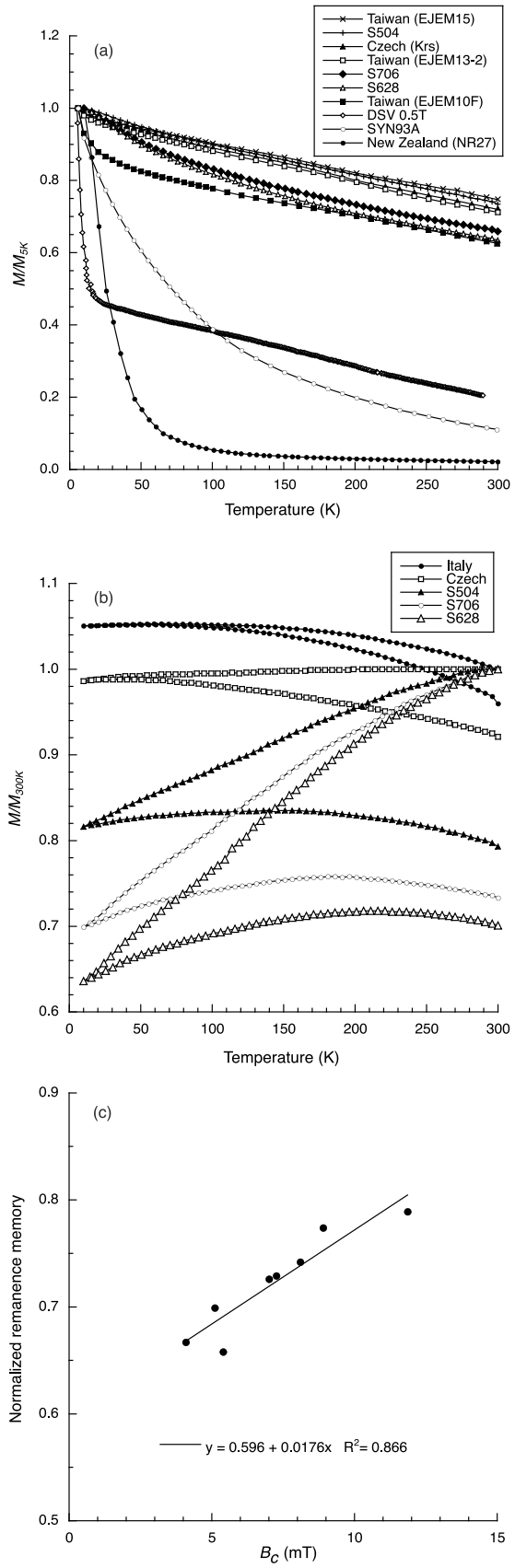

6.3.2. Zero-Field-Cooled and Field-Cooled Low-Temperature Measurements

[46] *Zero-field-cooled (ZFC) and field-cooled (FC) low-temperature measurements* provide a powerful means of

Figure 13. Low-temperature M_r measurements for representative greigite samples. (a) For M_r during warming from low temperatures, no low-temperature transitions are observed. Samples EJEM15, EJEM13-2 [*Horng et al.*, 1992a, 1992b; *Roberts*, 1995], and Czech (Krs) [*Krs et al.*, 1992] do not unblock much at low temperatures, which suggests that they contain thermally stable greigite. Coarse-grained synthetic sample S504 [*Chang et al.*, 2007] also does not unblock much. Sample EJEM10F [*Horng et al.*, 1992a, 1992b; *Roberts*, 1995] unblocks more, as do synthetic samples S706 and S628 [*Chang et al.*, 2007], probably because of minor SP particles [cf. *Chang et al.*, 2008]. Samples SYN93A [*Roberts*, 1995] and DSV0.5T [*Watson et al.*, 2000] both undergo substantial unblocking, which suggests that they contain high concentrations of SP grains. Sample SYN93A is a synthetic sample, while sample DSV0.5T contains largely amorphous greigite that was extracellularly produced by sulfate-reducing bacteria [*Watson et al.*, 2000]. Natural greigite from New Zealand (NR27) [*Rowan and Roberts*, 2006] contains the largest fraction of SP grains of all measured samples. (b) LTC results for a room temperature M_r [from *Chang et al.*, 2009b]. Thermally stable SD samples (Italy) lose little remanence, while a sample containing SD + MD particles (Czech) undergoes minor remanence loss due to the presence of MD particles. (c) Progressively larger remanence losses occur for coarser-grained samples and are proportional to coercivity and grain size. LTC measurements therefore have potential for granulometry of coarse greigite samples.

examining domain state in magnetite, where a major difference in ZFC and FC curves at the Verwey transition has been suggested to be diagnostic of bacterial magnetosomes consisting of SD magnetite [e.g., *Moskowitz et al.*, 1993]. Marked differences between ZFC and FC curves have also been suggested to be diagnostic of pyrrhotite [*Snowball and Torii*, 1999] and goethite [*Liu et al.*, 2006]. Of the few such measurements that have been reported for greigite, *Moskowitz et al.* [1993], *Snowball and Torii* [1999], and *Chang et al.* [2007] observed only a negligible difference between ZFC and FC curves and concluded that such measurements are not diagnostically useful for identifying greigite or for granulometry in greigite.

6.3.3. Low-Temperature Cycling of Room Temperature M_r

[47] As shown in section 6.2.1, low-temperature treatment demagnetizes MD greigite so that M_r has a harder coercivity spectrum when AF-demagnetized after warming to room temperature (Figure 12). The remanence memory after LTC (Figure 13b) strongly correlates with B_c (Figure 13c) and with measured grain size [*Chang et al.*, 2007, 2009b]. LTC measurement of a room temperature M_r therefore enables discrimination between SD grains, which do not demagnetize during cooling (Figure 13b), and MD grains, which undergo significant low-temperature demagnetization. The extent of demagnetization increases with grain size (Figure 13c), which makes LTC measurement of a room temperature M_r useful for magnetic granulometry in greigite [*Chang et al.*, 2009b].

6.3.4. Low-Temperature FORC Diagrams

[48] While room temperature FORC diagrams provide important information concerning coercivity and interaction field distributions [*Pike et al.*, 1999; *Roberts et al.*, 2000], low-temperature FORC diagrams provide additional discrimination between materials that undergo thermal relaxation (i.e., particles near the SP/SD threshold size [*Pike et al.*, 2001]) and those that do not (i.e., PSD/MD particles). A representative group of FORC diagrams that were measured from room temperature down to 10–20 K are shown in Figure 14 [cf. *Chang et al.*, 2009b]. A sample with a stable SD FORC distribution at room temperature has slightly higher coercivities upon cooling (Figures 14a–14d), which indicates a minor contribution from SP grains in addition to the dominant thermally stable SD grains. A synthetic sample that has a large proportion of thermally unstable SP particles has a coercivity distribution peak at ~15 mT at room temperature, which progressively undergoes magnetic blocking with cooling so that the peak occurs at ~40 mT at 10 K (Figures 14e–14h). A dominantly PSD sample has both divergent MD-like contours and concentric SD-like contours [cf. *Roberts et al.*, 2000] that do not vary with cooling (Figures 14i–14l). We do not observe splitting of the FORC distribution at low temperatures in contrast to observations for PSD magnetite [*Carvallo and Muxworthy*, 2006; *Smirnov*, 2006]. The three observed types of behavior are typical of SD, SP, and PSD/MD grains, which demonstrates the value of low-temperature FORC measurements for domain state interpretation.

6.3.5. Other Low-Temperature Magnetic Measurements for Greigite

[49] *Chang et al.* [2009b] reported a comprehensive range of low-temperature magnetic data for greigite particles that range from SP to MD sizes. In addition to the results discussed in sections 6.3.1–6.3.4, their analyses include temperature-dependent measurements of hysteresis parameters, B_{cr}, zero-field magnetization and field-cooled magnetization, and AC susceptibility. Readers are referred to *Chang et al.* [2009b] for details of these analyses. The collective evidence indicates that low-temperature measurements indicate strong domain state dependence of magnetic properties and that they therefore provide a useful tool for granulometry of greigite-bearing samples.

6.4. High-Temperature Magnetic Properties

6.4.1. Thermomagnetic Curves, Thermal Alteration, and the Curie Temperature of Greigite

[50] Thermomagnetic curves (M_s versus T or in some cases nonsaturation values of M) for natural greigite have been published in many studies, and considerable similarities exist among many of the curves. Representative published thermomagnetic curves are presented in Figure 15. When heated in air, most thermomagnetic curves for greigite contain a break in slope between 200°C and 300°C, followed by a marked decrease in magnetization. Minimum magnetizations are often reached between 320°C and 460°C (Figures 15a–15j). This minimum is often followed by a small maximum with variable magnitude. This secondary peak decays at 580°C, which is the Curie temperature of magnetite. The thermomagnetic curves are not reversible, and magnetite is usually the only phase evident during cooling, which indicates that greigite has undergone thermal alteration during heating. The amount of magnetite that forms during these heating cycles is variable, as indicated by the magnitude of the magnetization during cooling. A thermomagnetic curve for a synthetic greigite sample [*Dekkers et al.*, 2000] lacks the secondary peak, but magnetite is still the only magnetic mineral evident during the cooling run (Figure 15k).

[51] Thermomagnetic curves are more complicated when other magnetic minerals are present or for heating in a reducing atmosphere. When magnetite co-occurs with greigite [*Roberts et al.*, 1996; *Oda and Torii*, 2004; *Frank et al.*, 2007b; *Ron et al.*, 2007], an inflection still occurs between 200°C and 300°C, but the marked minimum and secondary maximum are not observed, and there is a more gradual decay to the Curie temperature of magnetite at 580°C (Figures 15l and 15m). Similar behavior is observed for oxidized greigite (Figure 15n) from the Caspian Sea [*Jelinowska et al.*, 1998]. When heated in reducing atmospheres such as nitrogen or argon, thermomagnetic curves can have an entirely different form (Figures 15o and 15p). *Reynolds et al.* [1994] noted that a wide range of thermomagnetic behavior can be obtained by varying the flow rate of gas. The general similarity of thermomagnetic curves for many natural greigite samples when heated in air (Figures 15a–15j) led *Reynolds et al.* [1994], *Roberts*

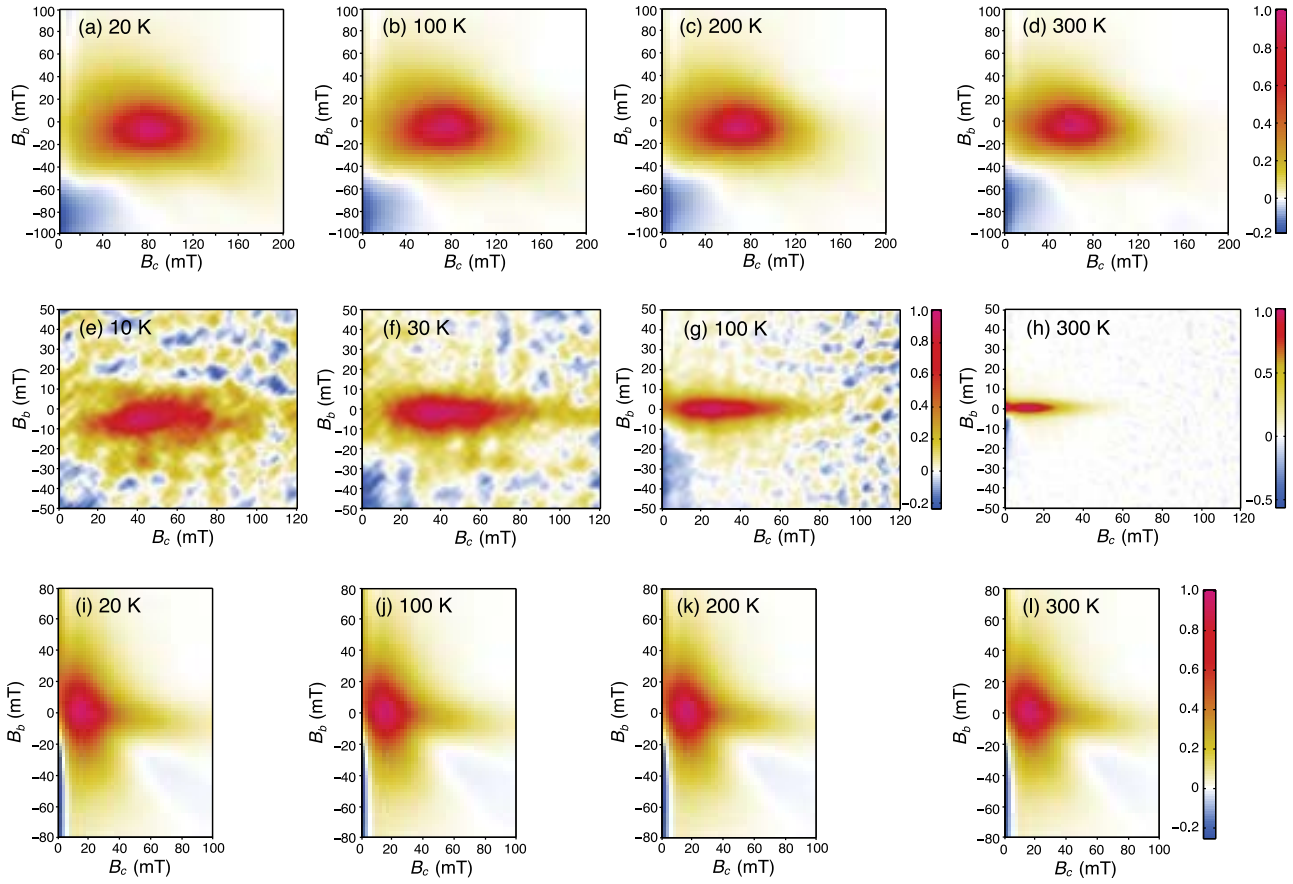

Figure 14. Low-temperature FORC diagrams for representative greigite samples [after *Chang et al.*, 2009b]. Stable SD greigite at (a) 20 K, (b) 100 K, (c) 200 K, and (d) 300 K (note the negative regions (blue) in the bottom left-hand parts of the FORC distributions, produced with the software of *Egli et al.* [2010]); thermally unstable SP/SD greigite at (e) 10 K, (f) 30 K, (g) 100 K, and (h) 300 K; and PSD greigite at (i) 20 K, (j) 100 K, (k) 200 K, and (l) 300 K. Normalized magnetization intensities are shown on color scales on the right-hand side of each relevant set of FORC diagrams. SF = 3 for all diagrams except for Figures 14e and 14f, where SF = 5.

[1995], and *Dekkers et al.* [2000] to conclude that heating in air provides more discriminative behavior than heating in nitrogen or argon atmospheres.

[52] Greigite irreversibly breaks down upon heating above about 280°C [*Skinner et al.*, 1964; *Krs et al.*, 1992; *Reynolds et al.*, 1994; *Roberts*, 1995; *Dekkers et al.*, 2000; *Chang et al.*, 2008]. This thermal decomposition has compromised all attempts to determine the Curie temperature for greigite. *Roberts* [1995] measured hysteresis loops for a greigite sample at discrete temperature steps from 77 to 614 K in an attempt to determine whether any significant changes in trend of hysteresis parameters could be used to identify the thermal blocking point for greigite (Figure 16). The thermal blocking point will be lower than the Curie temperature, but this approach is a useful way of making a minimum estimate of the Curie temperature. *Roberts* [1995] found a break in slope of the trend for all hysteresis parameters (Figure 16) at 595 K (322°C). This break must mark the lower limit of the unblocking temperature range at which thermal energy begins to overcome the magnetocrystalline anisotropy for greigite. This minimum estimate of the maximum unblocking temperature for greigite is lower than two independent estimates of the Curie temperature for greigite. *Spender et al.* [1972] extrapolated a steeply declining portion of a thermomagnetic curve for a synthetic greigite sample to obtain an estimate of 333°C for the Curie temperature, although there can be little doubt that this estimate was affected by thermal alteration. On the basis of Mössbauer measurements made at a range of temperatures up to 480 K (207°C), *Vandenberghe et al.* [1991] extrapolated the hyperfine fields for iron in tetrahedral sites and estimated a Curie temperature of at least 800 K (527°C). No other data are available to indicate whether this is a reasonable inference. The most reasonable conclusion is that the Curie temperature of greigite remains unknown; yet despite the careful language used by *Roberts* [1995] and the clearly stated uncertainty associated with determination of the Curie temperature of greigite, a Curie temperature of ~320°C–330°C is often cited for greigite, even in important books [e.g., *Opdyke and Channell*, 1996; *Dunlop and Özdemir*, 1997; *Snowball and Torii*, 1999].

[53] Although many natural greigite samples yield similar thermomagnetic curves (e.g., Figure 15), such curves are by no means the only type observed. Studies of Italian greigite-bearing sediments have often suggested maximum

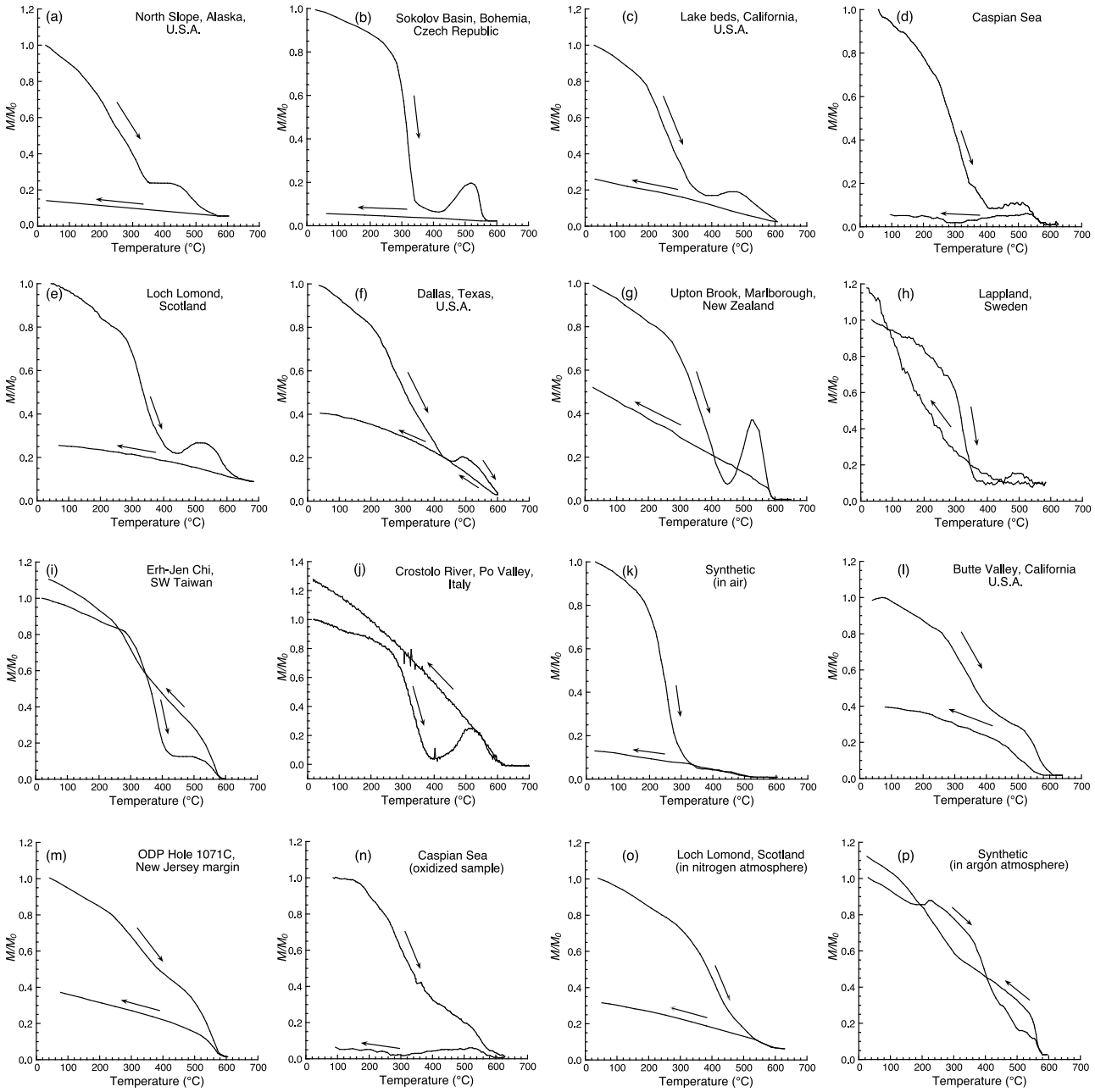

Figure 15. Representative published high-field magnetization versus temperature curves (heated in air unless otherwise stated). Plots are for greigite-bearing samples from (a) North Slope, Alaska (undifferentiated Ninuluk and Seabee formations); (b) Sokolov Basin, South Bohemia, Czech Republic [cf. *Krs et al.*, 1992]; (c) lake beds in California (all from *Reynolds et al.* [1994]); (d) Caspian Sea [*Jelinowska et al.*, 1998]; (e) Loch Lomond, Scotland [*Snowball and Thompson*, 1990a]; (f) White Rock Lake, Dallas, Texas [*Reynolds et al.*, 1999]; (g) Upton Brook, Marlborough, New Zealand [*Roberts and Turner*, 1993]; (h) Gaskkamus Gorsajávri, Swedish Lappland [*Snowball*, 1991]; (i) Erh-Jen Chi, southwestern Taiwan [*Horng et al.*, 1992a, 1992b]; (j) Crostolo River, Po Valley, Italy [*Tric et al.*, 1991]; (k) synthetic greigite (sample G934) [*Dekkers et al.*, 2000]; (l) Butte Valley, California (greigite and titanomagnetite) [*Roberts et al.*, 1996]; (m) Ocean Drilling Program Hole 1071C, New Jersey continental margin (greigite and magnetite) [*Oda and Torii*, 2004]; (n) Caspian Sea (oxidized greigite) [*Jelinowska et al.*, 1998]; (o) Loch Lomond, Scotland (heated in a nitrogen atmosphere) [*Snowball and Thompson*, 1990a]; and (p) synthetic greigite (sample G934; heated in an argon atmosphere) [*Dekkers et al.*, 2000]. Details of apparatus, heating rates, atmospheres, and applied fields are given in the cited studies.

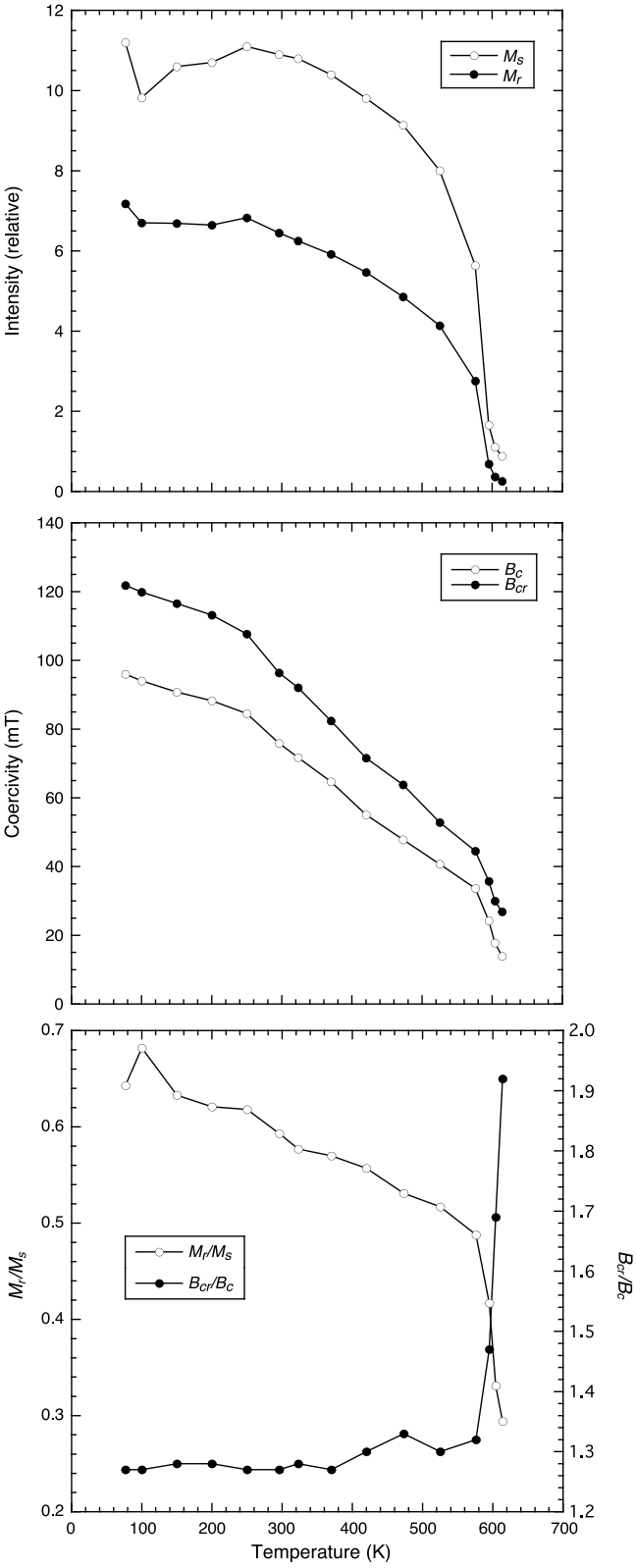

Figure 16. Temperature dependence of magnetic hysteresis parameters for greigite-bearing sample EJEB 380 [from *Roberts*, 1995]. The major break in slope at 322°C indicates that this temperature is close to the maximum unblocking temperature for this sample (note that temperature is in K).

unblocking temperatures for greigite up to 380°C–410°C [e.g., *Florindo and Marra*, 1995; *Mattei et al.*, 1996; *Sagnotti and Winkler*, 1999; *Sagnotti et al.*, 2000]. Greigite from an iron sulfide nodule from the Valle Ricca section near Rome [cf. *Bracci et al.*, 1985; *Florindo and Sagnotti*, 1995] illustrates this behavior, as shown by *Chang et al.* [2008]. The thermomagnetic curve decreases sharply at ~400°C (Figure 17a), which is completely different from the thermomagnetic properties illustrated in Figure 15. The curve eventually decreases to zero at the Curie temperature of magnetite and is irreversible upon cooling. During cooling, a peak occurs at ~290°C between the Curie temperature of monoclinic pyrrhotite at 320°C [*Dekkers*, 1989] and that of hexagonal pyrrhotite (Fe_9S_{10}), which is only ferrimagnetic above ~200°C and which has a Curie temperature of ~265°C [*Schwarz and Vaughan*, 1972]. On the basis of a second heating of this sample, *Chang et al.* [2008] interpreted this peak to represent thermal alteration that eventually resulted in formation of monoclinic pyrrhotite. The fact that the high-temperature behavior of greigite is determined more by thermal alteration than by magnetic unblocking is evident from results for a sister sample that was subjected to successive thermomagnetic cycles at stepwise increasing maximum temperatures (Figures 17b–17d). Thermal cycling indicates progressive increases in magnetization (note the expanded vertical scale) up to about 250°C (Figure 17b). This increase could be similar to the increasing magnetic moments observed by *de Boer and Dekkers* [1998] in non-saturating fields. *de Boer and Dekkers* [1998] stirred their samples between successive thermomagnetic runs to avoid such magnetic changes. We did not stir the sample between thermomagnetic runs, but further increases in magnetization are not observed above 250°C, and the 300°C and 350°C cycles are reversible, which indicates that this sample is particularly stable with no discernible thermal alteration up to 350°C. Thermal alteration is clearly visible in the 400°C cycle, where heating and cooling curves are not reversible. An inflection in the cooling curve at 320°C suggests the formation of monoclinic pyrrhotite (Figure 17b). Pyrrhotite is clearly indicated in the heating and cooling cycle up to 450°C, which is almost reversible (Figure 17c). Further thermal alteration, as indicated by irreversibility and increased magnetizations, is evident in the 500°C and 550°C cycles. The newly formed phase is magnetite, as indicated by the reversible thermomagnetic curves with Curie temperatures of 580°C for cycles up to 600°C, 650°C, and 700°C (Figure 17d). While thermal alteration is a major determinant of the high-temperature magnetic properties of greigite, the fact that this particularly stable sample gives rise to reversible curves up to 350°C indicates that the Curie temperature of greigite must exceed 350°C.

[54] The products of thermal breakdown of greigite can be highly variable (Figures 15 and 17) [*Skinner et al.*, 1964; *Krs et al.*, 1992; *Dekkers et al.*, 2000]. *Dekkers et al.* [2000] concluded that hematite will be the final reaction product when heating in air and that magnetite and pyrrhotite will be the final products when air is excluded. However, the thermomagnetic runs shown in Figure 17 were made in air,

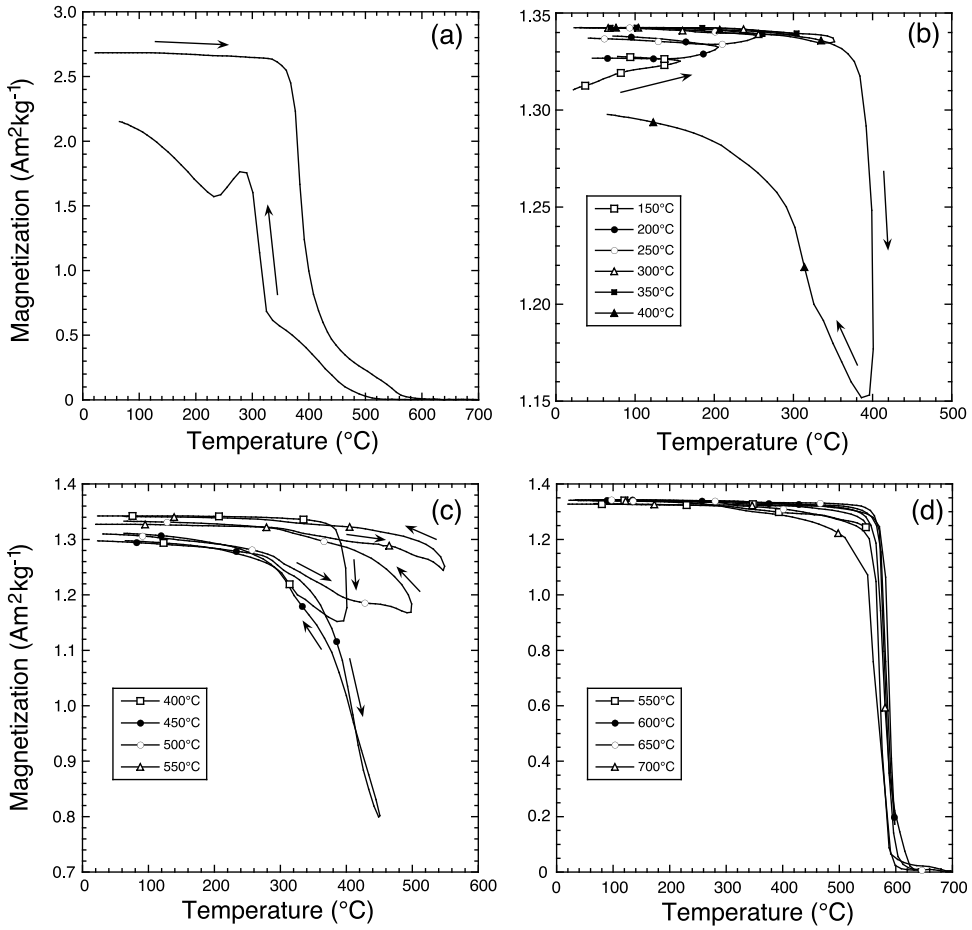

Figure 17. Thermomagnetic cycles for different subsamples from a greigite nodule from the Valle Ricca section [cf. *Bracci et al.*, 1985; *Florindo and Sagnotti*, 1995; *van Dongen et al.*, 2007]. (a) Thermomagnetic cycle up to 700°C and back to room temperature. (b) Repeated cycles for a fresh sample up to progressively increasing maximum temperatures (including maximum temperatures of 150°C, 200°C, 250°C, 300°C, 350°C, and 400°C) and back to room temperature. Slight magnetization increases are evident up to 300°C, but the 350°C cycle is reversible, which suggests that T_c for greigite must lie above 350°C. Thermal alteration is evident in the 400°C cycle. (c) Cycles up to maximum temperatures of 400°C, 450°C, 500°C, and 550°C, with progressive thermal alteration evident in each cycle. Note the expanded vertical scales in Figures 17b and 17c. (d) Cycles up to maximum temperatures of 550°C, 600°C, 650°C, and 700°C. Magnetite is the main magnetic alteration phase in each curve.

and the alteration products are pyrrhotite and magnetite. Some devices used for thermomagnetic analysis can consume oxygen during heating, and even if an air atmosphere is used, a reducing environment can develop during heating. It is therefore evident that the thermal breakdown products of greigite depend on a wide range of factors, not just the nature of the atmosphere used for heating. Perhaps the most systematic study of thermal decomposition of greigite is that of *Krs et al.* [1992]. Their XRD data, which were measured after heating a magnetic extract dominated by greigite at a succession of temperatures in air, are summarized in Figure 18. While variability in alteration products will depend on the sample and on the heating procedure, these data provide useful insights. The greigite reflections for this sample start to decrease between 250° and 300°C, and they completely disappear between 300°C and 320°C. This might seem surprising on the basis of studies of other samples, but thermal decay is much sharper for this sample compared to others (Figure 15b). Pyrrhotite starts to form in this sample at 320°C, but it disappears again above 400°C, where hematite becomes increasingly important. No magnetite is documented, which is surprising when one inspects the thermomagnetic curve in Figure 15b. The key observation from various studies of thermal decomposition of greigite is that a wide range of heating products is possible and that many of the products are not magnetic minerals (Figure 18).

6.4.2. Thermal Demagnetization of NRM

[55] As stated in section 6.2.2, thermal demagnetization is preferred for determining ChRM directions in paleomagnetic studies involving greigite. NRM intensity spectra for thermal demagnetization data provide clues about the presence of greigite, so it is worth considering these spectra in addition to paleomagnetic directional data. As expected

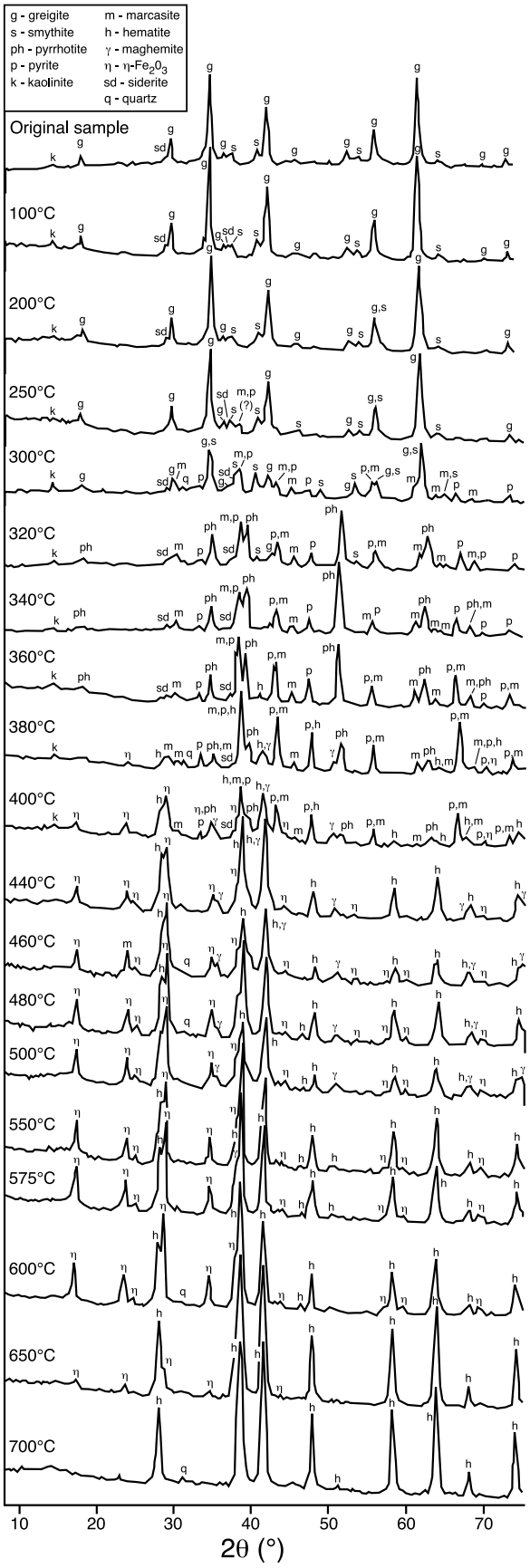

Figure 18. X-ray diffraction data (Cu-Kα radiation) for a greigite sample after heating at the indicated steps [after *Krs et al.*, 1992]. Greigite starts to break down between 250°C and 300°C, as indicated by the decreased intensity of greigite reflections, and it completely disappears due to thermal alteration by 320°C. This detailed study of the thermal alteration products of greigite demonstrates the complex range of magnetic and nonmagnetic minerals that result from progressive heating of a greigite-rich sample.

from thermomagnetic curves (Figure 15), NRM intensity spectra also usually undergo gradual unblocking from 150°C to about 300°C (Figure 19). An NRM can have both reversed and normal polarity components, so where there is a reversed polarity ChRM underlying a normal polarity overprint, the initial trend can involve an increase in NRM intensity (Figures 19a and 19e). Nevertheless, there is generally a major decrease in NRM intensity by about 350°C. Even though there appear to be some common trends, there is significant variability in the NRM intensity spectra (Figure 19), as was the case with thermomagnetic curves (Figure 15). The NRM for selected samples from southwestern Taiwan (Figure 19d) markedly decreases at ~350°C–360°C. Other samples are not significantly demagnetized at 350°C (Figure 19e); in this case, data are not shown above 350°C because thermal alteration obscured any trends at higher temperatures [*Roberts*, 1992]. The results shown in Figure 19 therefore indicate significant variability in thermal demagnetization spectra for greigite-bearing sediments.

6.4.3. Thermal Demagnetization of a Three-Axis M_r

[56] Thermal demagnetization of a composite M_r, where a stepwise decreasing DC field is successively applied to three mutually orthogonal sample axes, enables magnetic mineral identification by discrimination between unblocking characteristics of minerals with different coercivities [*Lowrie*, 1990]. For greigite-bearing samples (Figure 20), as would be expected from the M_r acquisition spectra shown in Figure 8, a high-coercivity component is either weak or is virtually absent, and M_r is dominantly carried by the intermediate- and low-coercivity components, which have similar thermal unblocking characteristics. Significant unblocking occurs between about 150°C and 300°C, although the spectra are variable, and remanences persist to 350°C–400°C in some cases (Figures 20a and 20c). *Sagnotti and Winkler* [1999] reported maximum unblocking temperatures up to 410°C in a wide range of greigite-bearing sediments, which is consistent with results in Figure 17. Data from Miocene sediments from the Ross Sea, Antarctica (Figure 20d), contain evidence of both greigite at lower unblocking temperatures and magnetite up to 580°C [*Sagnotti et al.*, 2005]. These data demonstrate that thermal demagnetization of a three-axis M_r can be effective for identifying greigite in mixed magnetic mineral assemblages. Nevertheless, thermal techniques alone are not completely diagnostic because several magnetic minerals with low to intermediate coercivities undergo thermal unblocking in the 300°C–400°C range [*Roberts and Pillans*, 1993].

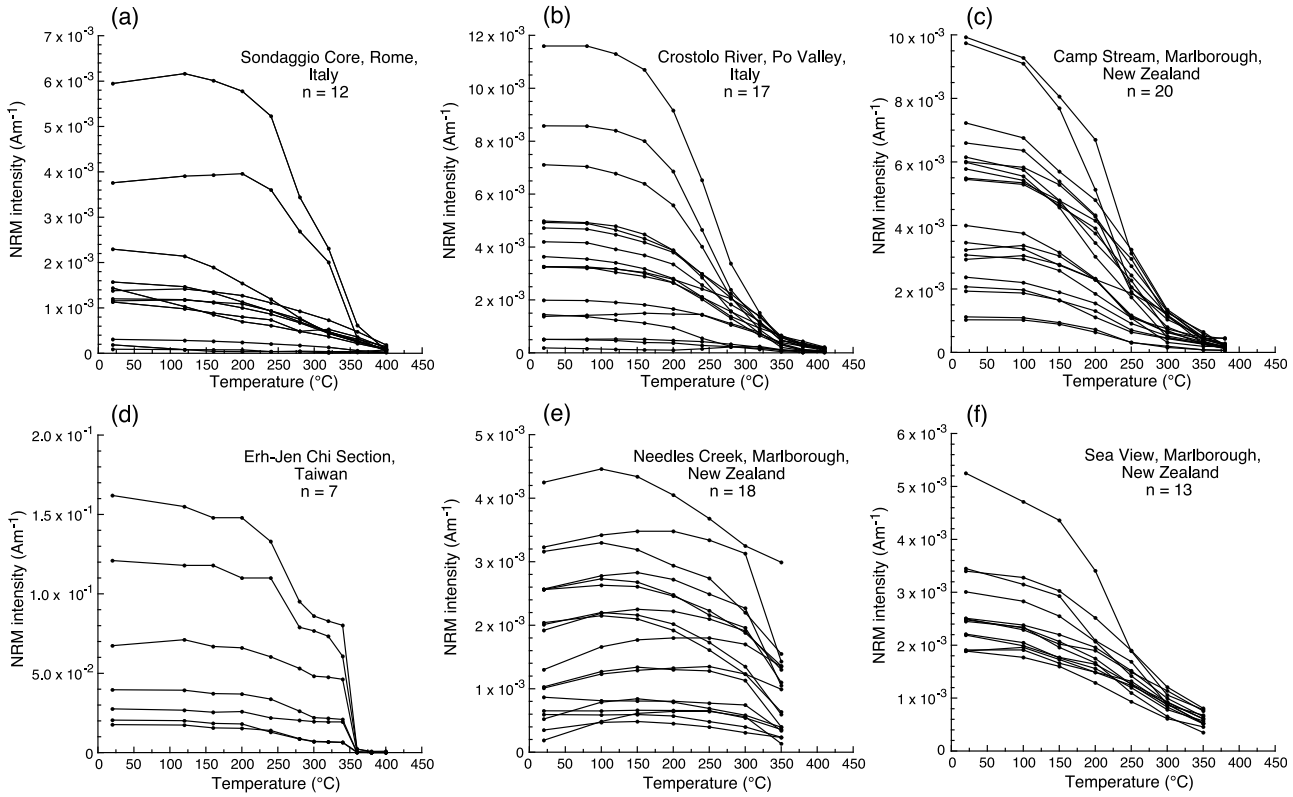

Figure 19. NRM intensity versus temperature spectra for greigite-bearing samples subjected to stepwise thermal demagnetization. The data are from (a) the paleo-Tiber Valley, Rome, Italy [*Florindo et al.*, 2007]; (b) Crostolo River, Po Valley, Italy [*Roberts et al.*, 2005]; (c) Camp Stream, Marlborough, New Zealand [*Roberts*, 1992]; (d) Erh-Jen Chi, southwestern Taiwan [*Horng et al.*, 1992a, 1992b]; (e) Needles Creek, Marlborough, New Zealand [*Roberts*, 1992]; and (f) Sea View, Marlborough, New Zealand [*Roberts*, 1992].

6.4.4. Temperature Dependence of Susceptibility

[57] Temperature dependence of magnetic susceptibility [*Hrouda*, 1994] is inherently more complicated than high-field magnetization measurements because paramagnetic matrix minerals can significantly contribute along with potentially weak ferrimagnetic contributions at low applied fields. Temperature-dependent susceptibility data for greigite-bearing samples (Figure 21) are therefore more variable than high-field thermomagnetic curves (Figure 15). Regardless, a probable *Hopkinson peak* is evident at 240°C–250°C during heating for some samples, along with a secondary peak at 320°C–340°C, after which susceptibility decreases sharply at ~400°C. Magnetite, which results from thermal alteration, is indicated by a susceptibility decrease at 580°C in all cases. Variable behavior occurs upon cooling, with magnetite usually evident at 580°C and monoclinic pyrrhotite often evident at 320°C. The Hopkinson peak at 240°C–250°C could indicate the upper end of the unblocking temperature spectrum for greigite within the respective samples. However, this peak is not present in all samples. In a sample largely comprising amorphous (SP) greigite produced extracellularly by sulfate-reducing bacteria [*Watson et al.*, 2000], a peak occurs at ~210°C (Figure 21c). Overall, however, while such behavior in temperature-dependent susceptibility measurements might provide evidence for the presence of greigite, intrinsic variability makes susceptibility measurements less diagnostic than high-field thermomagnetic measurements.

[58] Low-field magnetic susceptibility measurements are routinely made during stepwise thermal demagnetization in paleomagnetic studies. It is worth considering whether these data provide evidence about the presence of greigite. Magnetic susceptibility can decrease above ~250°C in greigite-bearing samples [e.g., *Roberts and Turner*, 1993] because of greigite breakdown during heating. As indicated in section 6.4.1, alteration products that accompany breakdown of greigite can be variable. Thus, while decreased susceptibilities are often observed in greigite-bearing samples (Figure 22) [cf. *Ariztegui and Dobson*, 1996; *Pósfai et al.*, 2001; *Babinszki et al.*, 2007], samples from the same localities often have increased susceptibilities at the same temperatures, probably due to formation of new magnetic minerals (pyrrhotite or magnetite) during heating. Decreased susceptibility should therefore not be routinely expected, but if observed, it could be an indicator for greigite because most other magnetic minerals do not decompose physically during heating.

6.5. Anisotropy of Magnetic Susceptibility

[59] *Rochette* [1988] argued that SD materials should have inverse magnetic fabrics, so it is worth considering whether such fabrics have been reported from greigite-

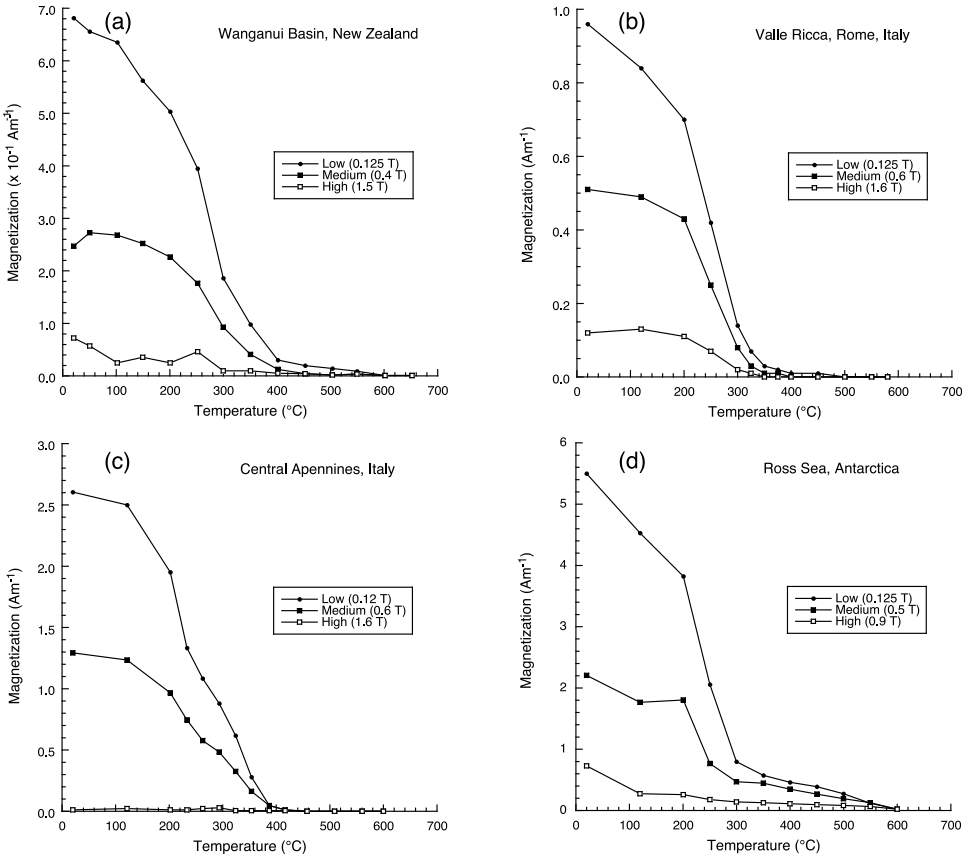

Figure 20. Representative published results of stepwise thermal demagnetization of a composite three-axis M_r [cf. *Lowrie*, 1990] for greigite-bearing samples. A high field was applied along one sample axis (ranging from 0.9 to 1.6 T), an intermediate field was applied along an orthogonal axis (ranging from 0.4 to 0.6 T), and a low field was applied along the third orthogonal axis (~0.12 T). Samples are from (a) Site 1, Whangaehu River, Wanganui Basin, New Zealand [*Roberts and Pillans*, 1993]; (b) Valle Ricca, Italy [*Florindo and Sagnotti*, 1995]; (c) sample MR3410 from the central Apennines, Italy [*Sagnotti and Winkler*, 1999]; and (d) a sample from 145.85 m below seafloor from the CRP-1 Hole, Ross Sea, Antarctica [*Sagnotti et al.*, 2005]. In each case, the low-coercivity component is dominant, with a smaller contribution from the intermediate-coercivity component and a small to negligible contribution from the high-coercivity component (which is consistent with Figures 8 and 9).

bearing sediments. The Italian greigite samples studied by *Sagnotti and Winkler* [1999] are dominated magnetically by SD greigite. It might therefore be surprising that inverse fabrics have not been reported in detailed AMS studies of greigite-bearing sediments from Italy [e.g., *Florindo and Marra*, 1995; *Sagnotti et al.*, 1998, 1999, 2010; *Mattei et al.*, 1999]. A normal magnetic fabric is also observed in fine-grained greigite-bearing sediments from southwestern Taiwan and New Zealand (Figure 23). This apparent paradox can be explained if the susceptibility is dominated by paramagnetic clay minerals rather than by ferrimagnetic greigite (which usually occurs in relatively small concentrations). This interpretation was used to explain the normal magnetic fabric of greigite-bearing sediments from the Ross Sea, Antarctica [*Sagnotti et al.*, 2005]. However, paramagnetic clays should only dominate when the bulk low-field magnetic susceptibility is $<300 \times 10^{-6}$ International System of Units (SI) [*Rochette*, 1987]. Some greigite-dominated sediments have magnetic susceptibility $>300 \times 10^{-6}$ SI but still have a normal AMS fabric. The normal magnetic fabric must therefore be due to greigite rather than clay (e.g., site MR30 of *Sagnotti et al.* [1998]).

[60] Hints of inverse magnetic fabrics have been reported, however, as exemplified by AMS analysis of greigite-enhanced organic-rich sapropel layers from the eastern Mediterranean Sea [*Roberts et al.*, 1999]. The studied sapropels contain ~15% less clay than the surrounding sediments [*Diester-Haass et al.*, 1998], and organic matter is not magnetic, so these sapropels provide an opportunity to test the relative effects of greigite and clay content on the magnetic fabric. *Roberts et al.* [1999] noted inverse magnetic fabrics in a few samples from a greigite-enriched sapropel, which is consistent with the expectation that SD materials should give rise to inverse magnetic fabrics (note that greigite enrichment is not typical of a much larger catalog of sapropels [*Larrasoaña et al.*, 2003]). *Aubourg and Robion* [2002] also reported inverse magnetic fabrics for a single greigite-bearing locality from Iran. The AMS results of *Roberts et al.* [1999] and *Aubourg and Robion* [2002] do not provide sufficient evidence to reach a statistically

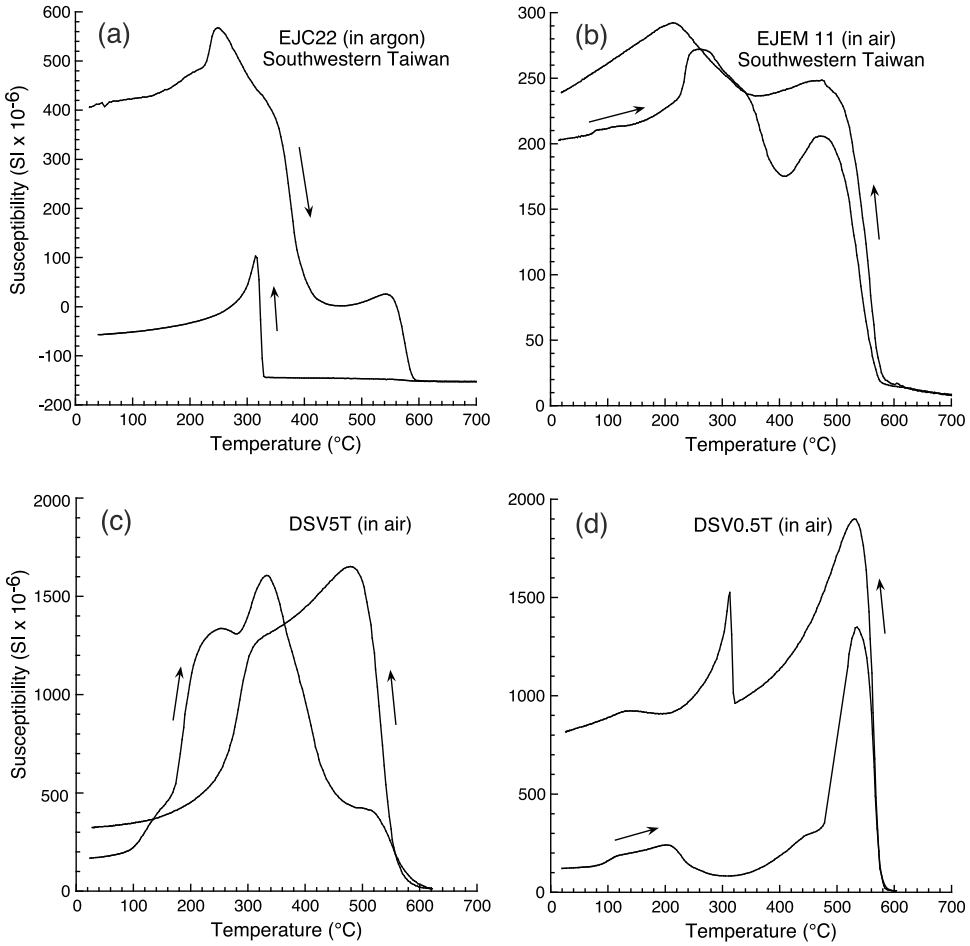

Figure 21. Temperature-dependent low-field magnetic susceptibility results for greigite-bearing samples (a and b) from southwestern Taiwan [*Horng et al.*, 1992a, 1992b], with measurements in argon atmosphere (Figure 21a) and air (Figure 21b), and (c and d) from extracellularly produced greigite from sulfate-reducing bacteria [*Watson et al.*, 2000]. Arrows indicate heating and cooling curves. See text for discussion.

robust conclusion. Regardless, as discussed above, there are greigite-bearing sites with normal magnetic fabrics and strong magnetic susceptibilities in which the fabric must be due to ferrimagnetic greigite rather than to paramagnetic clays [*Sagnotti et al.*, 1998]. *Sagnotti and Winkler* [1999] suggested that two factors might explain this apparent

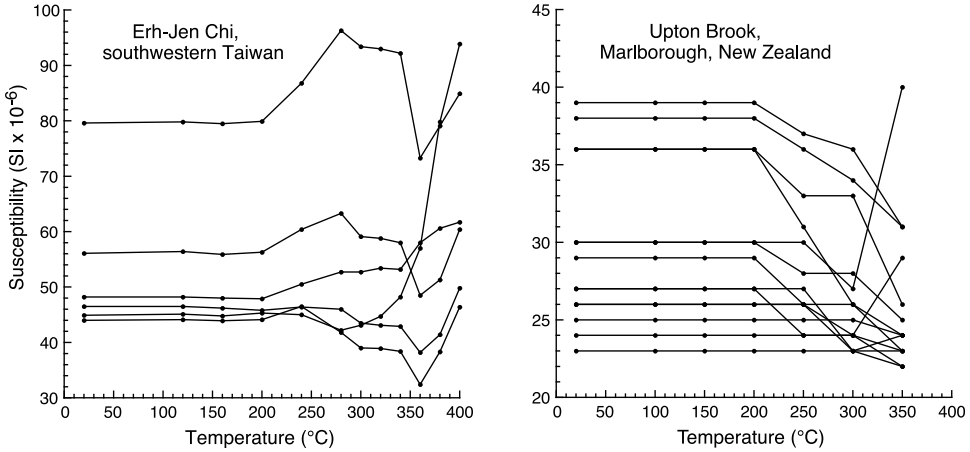

Figure 22. Low-field magnetic susceptibility data measured during stepwise thermal demagnetization experiments on greigite-bearing sediments from Erh-Jen Chi, southwestern Taiwan [cf. *Horng et al.*, 1992a, 1992b], and Upton Brook, Marlborough, New Zealand [*Roberts and Turner*, 1993].

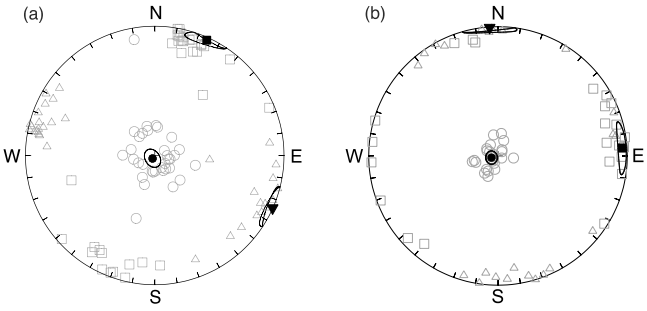

Figure 23. Equal-area stereographic projection of anisotropy of magnetic susceptibility (AMS) results for greigite-bearing samples from fine-grained marine sediments. (a) Southwestern Taiwan [cf. *Horng et al.*, 1992a, 1992b] and (b) Mahia Peninsula, eastern North Island, New Zealand [*Rowan and Roberts*, 2006, 2008]. Squares represent κ_{max}, triangles represent κ_{int}, and circles represent κ_{min}. Means for each parameter are represented by solid symbols with associated 95% confidence ellipses (plotted using the software of *Tauxe* [1998], to which the reader is directed for an explanation of AMS statistics). A normal sedimentary fabric is documented, with κ_{min} vertical (see text).

paradox. The fundamental magnetic and crystallographic differences between magnetite (dominant shape anisotropy and [111] easy axis of magnetization) and greigite (dominant magnetocrystalline anisotropy and [100] easy axis of magnetization) as well as the common occurrence of greigite in closely packed magnetically interacting aggregates are proposed as responsible for normal magnetic fabrics in greigite-bearing sediments instead of the inverse fabrics expected for SD magnetite. Further work is needed to test these interpretations.

7. WHAT IS THE BEST WAY TO IDENTIFY GREIGITE?

[61] The authors of this paper are regularly asked how best to identify greigite. It is therefore useful to consider this question now that its known magnetic properties have been surveyed. While greigite has a range of striking magnetic properties, these properties do not provide unique indicators of its presence. For example, several magnetic minerals, including titanomagnetites, maghemite, pyrrhotite, and greigite, magnetically unblock in the 270°C–350°C temperature range. Likewise, greigite commonly occurs in domain states other than the stable SD state, which means that use of parameters that are indicative of SD-like properties will underestimate its presence. Thus, while thermomagnetic measurements, hysteresis and FORC data, M_r/κ ratios, GRM acquisition, and other measurements often point to the presence of greigite, direct mineralogical identification using XRD or X-ray microanalysis coupled with SEM observation provides the most robust means of identifying greigite.

[62] For XRD analysis, a mineral must usually make up >5% of the sample, so it is necessary to analyze magnetic mineral separates or iron sulfide nodules in which greigite occurs well above trace levels. It can be difficult to separate enough greigite to get good results, but when adequate concentrations can be obtained, XRD enables definitive identification of greigite (Figure 24a). Likewise, SEM observations coupled with X-ray microanalysis of resin-impregnated polished sediment samples, when calibrated with an appropriate standard (e.g., pyrite), can enable identification of greigite (Figures 24b and 24c) [e.g., *Jiang et al.*, 2001; *Roberts and Weaver*, 2005]. Several pitfalls can affect analyses. For example, it can be difficult to obtain a uniform polish on the resin-impregnated surface of soft sediments, and X-rays will scatter from irregular surfaces. Likewise, the diameter of the electron beam (several micrometers) often exceeds the size of individual crystals of interest. In this case, it is desirable to analyze aggregates of grains with uniform mineralogy (i.e., uniform electron backscatter) in close contact with each other. The electron beam will also

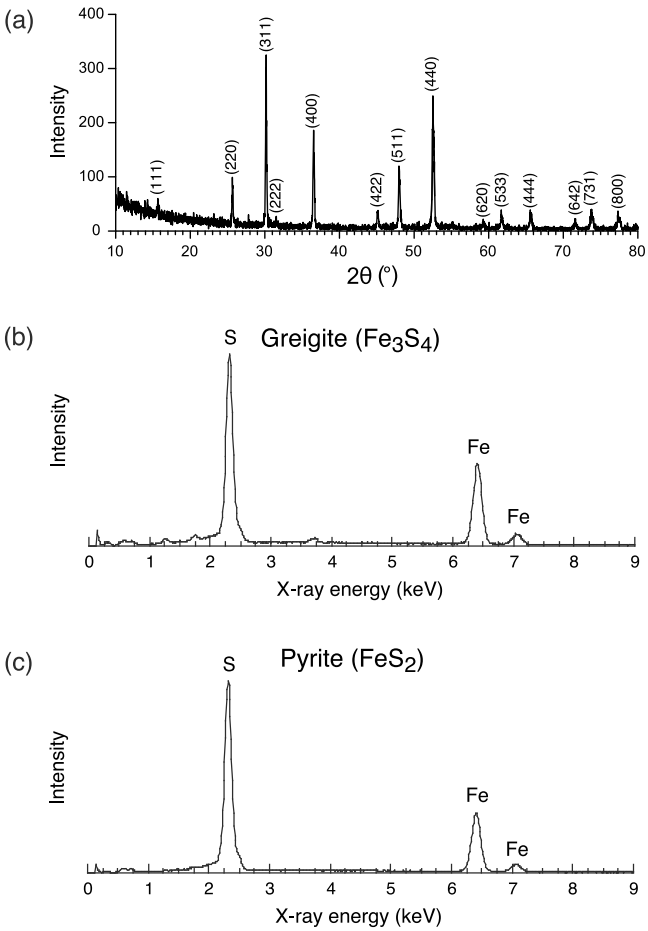

Figure 24. Mineralogical techniques for greigite identification. (a) Room temperature X-ray diffraction spectrum for pure synthetic greigite [after *Chang et al.*, 2008]. Miller indices of the main Bragg reflections are labeled. (b) Energy dispersive X-ray counts for Fe and S for a greigite particle aggregate such as in Figure 6 [from *Roberts and Weaver*, 2005]. Greigite is 43% Fe (atomic %) and 57% S, whereas (c) pyrite is 33% Fe and 67% S, and monoclinic pyrrhotite is 47% Fe and 53% S. Good analyses of well-polished surfaces of fresh, unoxidized samples enable clear identification of, and discrimination among, iron sulfide species.

penetrate below the polished surface; obtaining a good analysis therefore requires uniform mineralogy throughout the volume of material with which the X-rays interact. Even if the above conditions are satisfied, poor results will be obtained for oxidized samples. In this case, the Fe peak will have reduced intensity, a small oxygen peak will be recorded, and the Fe/S ratio will be lower than expected. Careful sample selection and preparation is therefore essential. Nevertheless, this method has proven to be highly effective for routine identification of greigite and discrimination from pyrite and other iron sulfides (Figures 24b and 24c). It is possible to use other techniques such as *Mössbauer spectroscopy* (see Table 1), but we have not used it to identify greigite in sediments, which typically contain Fe^{2+} and Fe^{3+} in multiple minerals.

8. COMPARISON OF THE MAGNETIC PROPERTIES OF GREIGITE AND MAGNETITE

[63] It has been widely assumed in the literature that because greigite and magnetite share an inverse spinel structure with a similar ferrimagnetic ionic structure ($[\uparrow Fe^{3+}]^A$ $[\downarrow Fe^{2+}$ $\downarrow Fe^{3+}]^B$ S_4^{2-} compared to $[\uparrow Fe^{3+}]^A$ $[\downarrow Fe^{2+}$ $\downarrow Fe^{3+}]^B$ O_4^{2-}), many magnetic properties will be analogous for the two minerals. We have found this to be a false assumption in a sufficient number of cases as to make it worth documenting here.

[64] 1. Room temperature M_s for greigite is 59 A m^2 kg^{-1} [*Chang et al.*, 2008] compared to 90–92 A m^2 kg^{-1} for magnetite [*Dunlop and Özdemir*, 1997]. This value is low even when considering the different atomic weight of O and S atoms (which converts to an equivalent M_s of ~70 A m^2 kg^{-1} for greigite [*Chang et al.*, 2008]).

[65] 2. In contrast to the well-known Verwey transition in magnetite [*Verwey*, 1939], no low-temperature magnetic discontinuity has been documented for greigite [*Coey et al.*, 1970; *Spender et al.*, 1972; *Vandenberghe et al.*, 1991; *Moskowitz et al.*, 1993; *Roberts*, 1995; *Torii et al.*, 1996; *Dekkers et al.*, 2000; *Chang et al.*, 2008, 2009b]. Recent ab initio calculations, which make use of the new M_s value of *Chang et al.* [2008], indicate that the electron correlation associated with the Fe atoms in greigite is insufficient to facilitate a Verwey-type transition, so that a monoclinic structure below a hypothetical low-temperature transition is not energetically favored for any meaningful range of relevant parameters [*Devey et al.*, 2009]. This provides the first theoretical confirmation that a Verwey-type transition should not be observed for greigite, which supports extensive experimental data. The Verwey transition remains poorly explained, so it is possible that magnetite is more anomalous than greigite by having a low-temperature magnetic transition.

[66] 3. The [111] crystallographic axis is the easy axis of magnetization at room temperature in magnetite [*Dunlop and Özdemir*, 1997], whereas in greigite it is the [100] axis [*Yamaguchi and Wada*, 1970; *Heywood et al.*, 1991; *Bazylinski et al.*, 1993].

[67] 4. The exchange energy estimated by *Chang et al.* [2008] is lower than that of magnetite. This could result from replacement of O by S in the crystal lattice in greigite, but this is unlikely to affect the superexchange coupling between Fe in octahedral and tetrahedral sites [*Chang et al.*, 2008].

[68] 5. K_1 for greigite is estimated to be 2.1×10^4 J m^{-3} from hysteresis properties of equidimensional SD greigite particles, while EPR measurements give a value of $(2.9 \pm 0.2) \times 10^4$ J m^{-3} (Chang et al., manuscript in preparation, 2011). These values are higher than for magnetite (1.35×10^4 J m^{-3} [*Dunlop and Özdemir*, 1997]). The slightly higher value of K_1 for greigite probably explains the fact that equidimensional SD greigite has coercivity of >60 mT, while this value is ~20 mT for magnetite [e.g., *Dunlop and Özdemir*, 1997].

[69] The contrast in the above properties for greigite and magnetite indicates intrinsic differences between these two ferrimagnetic inverse spinels. These differences could originate in the electronic structure, which highlights the need to develop a complete understanding of the electronic structure of greigite. Considerable caution should therefore be applied when comparing these two minerals. There is no substitute for making the appropriate experimental observations, with constraints from theory, to obtain robust estimates of any parameter of interest.

9. FUTURE WORK

[70] The magnetic properties of magnetite vary significantly depending on grain size and shape, stress, magnetostatic interactions, cation substitution, degree of oxidation, etc. [e.g., *Dunlop and Özdemir*, 1997]. It remains to be seen whether such variability also exists for greigite, but our current knowledge only scratches the surface in relation to this range of variables. Determining a more detailed grain size–dependent framework for the magnetic properties of greigite remains an important challenge for future studies. Likewise, grain shape has been poorly documented in most studies. Preliminary indications from acicular greigite nanorods suggest that coercivity increases significantly with grain elongation [e.g., *Chen et al.*, 2005; *He et al.*, 2006], but much more work is needed to understand the variation in magnetic properties with grain shape. Stoichiometric Fe_3S_4 is not unusual in synthetic samples [e.g., *Chang et al.*, 2008, 2009a], but sulfides are complex minerals, and many different cations can be substituted into the crystal lattice with almost complete solid solution between various end-members [e.g., *Vaughan and Craig*, 1985; *Pearce et al.*, 2006]. *van Velzen et al.* [1993] reported the possibility of Ni substitution in greigite in Plio-Pleistocene marine marls from Calabria, Italy. Such observations have neither been confirmed by follow-up studies at the same location [*Roberts et al.*, 2010] nor been widely made elsewhere. The importance of other ferrimagnetic cation-substituted inverse spinel sulfide minerals in nature therefore remains unknown. Nevertheless, cation substitution is a useful property for further understanding the magnetic properties of greigite. For

example, magnetic properties vary systematically with Ti substitution in titanomagnetite. Substitution of Ti or other cations into the greigite lattice could systematically reduce the Curie temperature of greigite to below its alteration temperature. This could be exploited to enable accurate determination of the Curie temperature of greigite by extrapolation. Greigite readily oxidizes in moist terrestrial weathering environments. Few systematic studies have been made of the changes in magnetic properties of greigite with progressive weathering [e.g., *Crockford and Willett*, 1995]. Such work will be important, as has been the case for surficially oxidized magnetite. Finally, determination of the fundamental magnetic constants for greigite means that we are now in a position to undertake micromagnetic modeling of greigite to investigate the grain size dependence of magnetic properties and magnetic recording fidelity of greigite.

10. CONCLUSIONS

[71] Much progress has been made in recent years to develop a more complete understanding of the magnetic properties of greigite and the range of grain sizes in which greigite occurs in nature. Greigite has an inverse spinel crystallographic structure, with a cubic unit cell with 8 Fe^{3+} ions in tetrahedral (*A* site) coordination and 16 Fe ions (both Fe^{2+} and Fe^{3+}) in octahedral (*B* site) coordination with 32 sulfur anions. Greigite has been demonstrated to be a collinear (R-type) ferrimagnet with antiferromagnetic coupling between octahedral and tetrahedral ions and no evidence for spin canting, so that the formula for greigite is $[\uparrow Fe^{3+}]^A\ [\downarrow Fe^{2+}\ \downarrow Fe^{3+}]^B\ S_4^{2-}$. Pure synthetic samples lack significant lattice vacancy concentrations and do not depart from Fe_3S_4 stoichiometry. Despite having an inverse spinel structure, most measured magnetic parameters are sufficiently different from those of magnetite that inferring magnetic properties on the basis of expectations from magnetite is unlikely to be robust. Empirically determined estimates of the fundamental magnetic constants for greigite have been recently obtained, including the saturation magnetization (59 A m^2 kg^{-1}; 3.13 μ_B formula $unit^{-1}$), anisotropy constant (2.1–3.1 $\times$ 10^{-4} J m^{-3}), and exchange constant (2 $\times$ 10^{-12} J m^{-1}). The low-field mass magnetic susceptibility of greigite is 3.2 $\times$ 10^{-4} m^3 kg^{-1}. The crystallographic *c* axis ([100]) is the easy axis of magnetization, and the magnetic properties of greigite are dominated by magnetocrystalline anisotropy. The Curie temperature of greigite remains unknown but must exceed 350°C. Greigite, unlike several other common magnetic minerals, lacks a low-temperature magnetic transition. A grain size–dependent framework for the magnetic properties of greigite is now also available for the first time. On the basis of bacterial greigite magnetosome and natural size distributions and preliminary micromagnetic modeling, the size range for stable SD behavior is estimated at ~20–200 nm for cubic grains and ~20–500 nm for octahedral grains. There is a sharp difference in magnetic properties of SD compared to PSD greigite. Gradual variation in magnetic properties is observed through the PSD size range from 3 ± 2 μm to >35 μm (a significant gap exists between the measured magnetic properties of stable SD samples and the smallest sieved sample at 3 ± 2 μm). We have systematically documented the known magnetic properties of greigite (at high, ambient, and low temperatures and with alternating and direct fields) and have illustrated how variations in greigite grain size affect these magnetic properties. Variable mixtures of greigite with different grain sizes produce a broad range of magnetic properties. When this broader range of properties is recognized in future studies, it is likely that greigite will be identified even more frequently in the geological record than is currently the case. Recognition of this range of magnetic properties will be crucial for constraining interpretation of the often complex magnetic signals carried by greigite.

GLOSSARY

Alternating field (AF) demagnetization: A technique for progressively demagnetizing a sample by exposing it to a sinusoidally alternating magnetic field of gradually decreasing magnitude in the presence of a zero direct field. AF demagnetization is used to identify different magnetization components in rocks and sediments in which low-coercivity phases like titanomagnetite or magnetite are the dominant ferrimagnetic minerals. It is less effective in demagnetizing samples in which the remanence is carried by high-coercivity phases such as hematite or goethite.

Anhysteretic remanent magnetization (ARM): A laboratory-induced remanent magnetization imparted by means of a strong alternating magnetic field in the presence of a direct current bias field. The bias field usually has comparable intensity to the geomagnetic field. ARM provides an indicator of magnetic mineral concentration; the efficiency of ARM acquisition also varies with grain size. It is therefore a widely used parameter in rock magnetism.

Anisotropy constant: The spontaneous magnetization M_s of a mineral will preferentially align along certain crystallographic "easy" axes where magnetocrystalline anisotropy is minimized. In a magnetic particle with one easy axis of magnetization (i.e., a uniaxial particle), the magnetocrystalline anisotropy energy density (i.e., energy per unit volume) is $E = K_1 \sin^2\theta$. K is the magnetic anisotropy constant, and θ is the angle between the easy axis and the magnetic moment of the particle. For minerals with cubic symmetry, $E = K_1(\alpha_1^2\alpha_2^2 + \alpha_2^2\alpha_3^2 + \alpha_1^2\alpha_3^2) + K_2(\alpha_1^2\alpha_2^2\alpha_3^2) + \ldots$, where ($\alpha_1$, α_2, α_3) are the direction cosines of the internal magnetization with respect to the cubic axes. K_1 and K_2 are the first and second magnetocrystalline anisotropy constants, respectively. K_2 and higher-order constants are usually small compared to K_1. The magnetic anisotropy constant is a fundamental parameter that controls the magnetic behavior of a magnetic material. Once a magnetization is aligned with an easy direction, work is needed to deflect it. The coercivity of a mineral is therefore related to K.

Anisotropy of magnetic susceptibility (AMS): A property of a material whereby identical magnetic fields applied in different directions produce different induced

magnetization intensities. AMS reflects the statistical alignment of crystallographic directions and/or shape in platy or elongate grains. The degree of anisotropy in bulk geological samples rarely exceeds 10%.

Authigenic: An authigenic mineral is one that formed in place, rather than being transported from another location.

Band structure: Also referred to as band scheme. The electronic band structure of a solid describes the allowable energy ranges for an electron. The electrons in an isolated atom occupy atomic orbitals with discrete energy levels. In a solid, the number of orbitals becomes exceedingly large, and energy differences between orbitals become small. Energy levels are then treated as continuous bands rather than as discrete energy levels as in isolated atoms. The band structure determines important characteristics of a material, including its electronic, magnetic, and optical properties.

Bitter pattern imaging: Bitter patterns enable imaging of magnetic domains and domain walls. A wet magnetic colloid is applied to a smooth, polished sample surface that is prepared to eliminate residual strain from grinding. Colloidal particles are attracted by magnetic field gradients around domain walls, which give rise to characteristic Bitter patterns. With liquid colloid, details as small as 1 μm can be resolved. Details as small as a few tenths of a micron can be investigated if the colloid is dried on the sample surface and the pattern is viewed with a scanning electron microscope. Named for the American physicist Francis Bitter (1902–1967).

Bloch spin wave: At absolute zero temperature, the array of spins in a ferromagnetic solid will be completely ordered. With increasing temperature, thermal excitations of the coupled spins will cause a wave-like motion through the system of spins, which is called a spin wave. The Swiss physicist Felix Bloch demonstrated from spin wave arguments that the spontaneous magnetization should decline from its saturated value at absolute zero (M_{s0}) as follows: $M_s = M_{s0}[1 - A(k_0T/J_{AB})^{3/2}]$, where $T \ll T_c$, A is a numerical constant that depends on crystal structure, k_0 is Boltzmann's constant, and J_{AB} is the exchange constant. Low-temperature M_s data can be fitted using this "Bloch $T^{3/2}$ law" to determine the exchange constant for a magnetic mineral.

Characteristic remanent magnetization (ChRM): The highest-stability NRM component isolated during progressive stepwise demagnetization. Unlike the term "primary remanence," ChRM does not imply a time for acquisition of the magnetic component.

Coercive force (B_c): The direct reversed magnetic field that must be applied to reduce to zero the saturation magnetization that was imparted in the opposite direction.

Coercivity of remanence (B_{cr}): The direct reversed magnetic field that must be applied and then removed to demagnetize to zero the saturation remanent magnetization that was imparted in the opposite direction.

Crystallographic axis: The crystallographic axes are three imaginary lines (four in the case of a hexagonal crystal) that pass through the center of an ideal crystal, that are chosen to have definite relation to the symmetry properties of a crystal, and that are used as a reference in describing crystal symmetry and structure.

Curie temperature (T_c): As temperature increases in a ferromagnetic material, interatomic distances increase, and the magnetic exchange interaction becomes weaker. At T_c, thermal energy overcomes the exchange energy, and magnetic moments become independent so that the material becomes paramagnetic. Named for the French scientist Pierre Curie (1859–1906).

Domain wall: The thin boundary region between adjacent magnetic domains with uniform magnetization. Magnetic moments usually change direction by 90°–180° across a domain wall, generally over distances of 100–150 atoms. The width of a domain wall depends on the balance between the magnetocrystalline anisotropy and the exchange energy, both of which seek minimization when nucleating a domain wall.

Exchange constant: The ability of materials to record magnetic information depends on the existence of strong exchange interactions between neighboring electron spins. Electrostatic interaction among electron orbitals and the fact that electrons in neighboring orbitals cannot have the same spin state (from quantum mechanical considerations following the Pauli exclusion principle) mean that neighboring spins interact with each other to produce long-range spin ordering. This exchange coupling results in minimization of exchange energy when spins align in either a parallel or antiparallel manner (where the alignment depends on crystal structure). The exchange constant is a fundamental magnetic property of magnetic materials and is a function of the difference in exchange energy between parallel and antiparallel spins, the spin vectors of neighboring atoms, and the interatomic distance.

Ferromagnetic resonance: A spectroscopic technique that is used to probe the magnetization of ferromagnetic materials. Ferromagnetic resonance is a form of electron paramagnetic resonance (EPR) that causes the energy of an electron with spin aligned with an applied magnetic field to be lower than that of an electron with spin aligned against the field. EPR spectroscopy has been used in rock magnetism to identify magnetite magnetofossil chains.

First-order reversal curve (FORC): Partial hysteresis loop measured by applying a positive saturation field, cycling back to a lower reversal field, and then measuring a magnetization curve with increasing field back to positive saturation. FORCs are measured for a series of reversal fields, and a FORC distribution is calculated as the mixed second derivative of magnetization with respect to field spacing. FORC diagrams provide information about the distribution of switching fields (i.e., coercivities) and interaction fields for all magnetic particles that contribute to a hysteresis loop. They are widely used to characterize samples in rock and mineral magnetism.

Fold test: A field test for paleomagnetic stability that provides information about the timing of acquisition of remanent magnetizations. Samples are collected from sites on opposing limbs of the same fold. The distributions of remanence directions before and after correcting for bedding tilt

are compared. If these directions become more closely grouped after untilting, the remanence was acquired before folding (producing a positive fold test). If the directions are more scattered after untilting, the magnetization postdates folding (negative fold test).

Gyroremanent magnetization (GRM): A laboratory remanence that is acquired by anisotropic magnetic samples in alternating fields. GRM acquisition is commonly observed in greigite, which impedes identification of the characteristic remanent magnetization.

Hopkinson peak: When measuring magnetic susceptibility as a function of temperature, a well-defined peak, known as a Hopkinson peak, is often observed just below the Curie temperature. Named for the English scientist John Hopkinson (1849–1898).

Inverse spinel structure: Spinels are a class of mineral with general formulation $A^{2+}B_2^{3+}O_4^{2-}$ that crystallize with oxide anions arranged in a cubic close-packed lattice and *A* and *B* cations occupying some or all octahedral and tetrahedral sites in the lattice. In a normal spinel, similar cations occupy the same sublattice. In the inverse spinel structure (e.g., greigite and magnetite), Fe^{3+} occupies tetrahedral (*A*) sites, and both Fe^{2+} and Fe^{3+} occupy octahedral (*B*) sites.

Low-temperature cycling (LTC): Experiments in which a saturation remanence is imparted at room temperature and then measured in zero field during cooling to low temperatures (usually below 20 K) and then during warming back to room temperature. Multidomain particles undergo partial demagnetization during cooling to low temperatures. This makes LTC measurements useful for probing the magnetic grain size distribution in samples, as well as for identifying low-temperature magnetic transitions.

Low-temperature magnetic properties: Mineral magnetism relies on electronic exchange interactions, which are strongly dependent on interatomic distances and therefore on temperature. Low-temperature magnetic measurements provide information about thermally controlled, dynamic energy barriers in magnetic materials. Below room temperature, magnetite, hematite, and monoclinic pyrrhotite all undergo magnetic transitions with various origins (e.g., crystallographic, electronic, magnetocrystalline, or unknown) at different temperatures. These transitions provide important information about crystal and magnetic structures, but they are also used widely to determine the presence of magnetic minerals within a sample.

Magnetocrystalline anisotropy: An intrinsic property of magnetic minerals, independent of grain size and shape. Magnetocrystalline anisotropy is the energy necessary to deflect the magnetic moment in a single crystal from the easy to the hard direction. The easy and hard directions arise from the interaction of the spin magnetic moment with the crystal lattice (spin-orbit coupling).

Magneto-optical Kerr effect: A magneto-optical effect is a phenomenon in which an electromagnetic wave propagates through a medium that has been altered by the presence of a quasi-static magnetic field. The magneto-optical Kerr effect describes changes of light reflected from magnetized media. The Kerr microscope is an optical light microscope with an additional polarizer and an analyzer to obtain different contrasts from different magnetic orientations. It is used to visualize magnetic domain structures in samples. Named for the Scottish physicist John Kerr (1824–1907).

Magnetosome: A magnetic nanoparticle produced by, and found in, magnetotactic bacteria. Magnetosomes are usually aligned in chains and are encased by a thin cellular membrane. These chains act like a compass needle to orient magnetotactic bacteria in the geomagnetic field. Magnetosomes commonly consist of magnetite or greigite.

Magnetostatic interactions: When magnetic particles are located close enough to each other, their respective magnetic fields will interact. The interaction field depends on the configuration of neighboring particles and will be stronger if more adjacent particles are magnetized in the same direction. Magnetostatic interactions can have an important influence on the magnetic properties of closely aggregated or intergrown particles in rocks and sediments.

Magnetotactic bacteria: A class of bacteria discovered in the 1960s that contain ferrimagnetic crystals within cell structures that enable the bacteria to navigate along geomagnetic field lines.

Morin transition: A magnetic phase transition that occurs at ~260 K in hematite where antiferromagnetic ordering is reorganized from having a perpendicular alignment to the crystallographic *c* axis to a parallel alignment. The weak antiferromagnetism of hematite is lost at this transition. Like the Verwey transition in magnetite, the temperature at which the Morin transition occurs is sensitive to impurities in the crystal lattice (e.g., Ti and Al).

Mössbauer spectroscopy: A spectroscopic technique based on recoil-free resonant absorption and emission of gamma rays in solids. Solid samples are exposed to a beam of gamma radiation, and the beam intensity transmitted through the sample is measured with a detector. Spectra of gamma ray intensity are plotted against velocity of the accelerated source (e.g., ^{57}Fe). At velocities corresponding to the resonant energy levels, a drop in gamma ray intensity will produce a dip in the Mössbauer spectrum. Mössbauer spectroscopy is used to probe subtle variations in the chemical environment of the nucleus, including oxidation state changes, the effects of different ligands on an atom, and the magnetic environment of a sample. Applying a magnetic field will cause interactions between nuclei and the field, which produces a measurable hyperfine splitting in the Mössbauer spectrum. Named for the German physicist Rudolf Mössbauer (1929–).

Multidomain (MD): As a magnetic particle increases in size, its magnetic energy increases. In order to minimize this energy, a particle will begin to nucleate domain walls at a critical grain size threshold. These walls divide the particle into two or more magnetic volumes or domains. The magnetization is uniform in each domain, but it differs in direction from domain to domain. MD grains are less effective paleomagnetic recorders than single-domain grains.

Natural remanent magnetization (NRM): The magnetic remanence of a geological sample prior to laboratory treatment. The NRM is typically composed of more than

one component acquired at different times during a sample's history. Magnetization components are usually identified in the laboratory using stepwise thermal or alternating field demagnetization.

Nonstoichiometric: A chemical compound with an elemental composition that cannot be represented by a ratio of integers. Nonstoichiometric materials often contain crystallographic point defects, such as atomic vacancies. Nonstoichiometry is common in transition metal oxides and sulfides and is therefore important in mineral magnetism (see vacancy concentration).

Pseudo-single-domain (PSD): A magnetic structure intermediate between the single-domain (SD) and multidomain states in which particles contain more than one domain but exhibit many of the stable magnetic properties typical of SD particles. PSD grains can have stable remanent magnetizations over geological time scales and can therefore be paleomagnetically important.

Rotational remanent magnetization (RRM): Another manifestation of the gyroremanent magnetization, which is acquired when a sample is tumbled during AF demagnetization.

Saturation magnetization (M_s): The maximum magnetization of a sample measured within a magnetizing field. Sometimes referred to as the spontaneous magnetization.

Saturation remanent magnetization (M_r): The maximum remanent magnetization of a sample measured within zero field after removal of a magnetizing field. Sometimes referred to as the saturation isothermal remanent magnetization.

Single-domain (SD): A uniformly magnetized magnetic particle with a single magnetic domain. Noninteracting SD grains are ideal recorders of paleomagnetic information. In most magnetic minerals, stable SD grains are extremely small (the SD size range in magnetite is ~30–80 nm).

Spin canting: Occurs when magnetic moments within the two crystal sublattices are deflected away from an antiparallel alignment. Spin canting results in a weak net magnetic moment. Hematite is a canted antiferromagnet.

Sublattice magnetization: Ferrimagnetic materials have atomic magnetic moments on two magnetic sublattices that oppose each other in an unequal manner. The unequal magnetization of the two sublattices gives rise to a net spontaneous magnetization. Neutron diffraction techniques can be used to probe the microscopic magnetic structure of a material and enable determination of the magnetization of the two sublattices.

Superparamagnetism (SP): Class of magnetic behavior exhibited by very small particles (<30 nm in magnetite) that have relaxation times on laboratory time scales (typically <100 s). For these particles, atomic magnetic moments align in a magnetic field to produce a strong induced magnetization that can be rapidly destroyed by thermal vibration soon after removing the field (seconds to minutes).

Switching field distribution: When a magnetic field is applied opposite to the magnetization vector and becomes large enough to overcome the magnetic anisotropy energy of a particle, its magnetic moment will jump over the energy barrier. The field required to achieve this flip is called the switching field. The switching field is also referred to as the microscopic coercivity. Most geological materials have a distribution of magnetic grain sizes, so the resulting coercivity distribution is often referred to as the switching field distribution.

Thermal demagnetization: Demagnetization carried out by heating a specimen to an elevated temperature below the Curie temperature of constituent magnetic minerals, then cooling to room temperature in zero magnetic field. The remanence of all magnetic grains with unblocking temperature less than or equal to the demagnetization temperature is randomized upon heating. Stepwise increases in temperature up to the Curie temperature enable progressive removal of the total remanent magnetization. Heating can thermally alter constituent minerals and obscure results. Nevertheless, thermal treatment can effectively demagnetize minerals and is particularly useful for high-coercivity minerals such as hematite and goethite, which usually cannot be effectively demagnetized using AF treatment.

Unblocking temperature: The temperature during warming at which thermal energy overcomes the magnetic exchange energy and the magnetization "unblocks." At this unblocking temperature, the magnetic relaxation time decreases so that the particle has superparamagnetic behavior rather than stable single-domain behavior.

Vacancy concentration: Solids can contain crystallographic point defects, such as vacancies, which result in deficiency of an element within the crystal. Such vacancies occur naturally in crystalline materials and are important for mineral magnetism because they can produce local changes in atomic spin coupling that can give rise to, or alter, a net magnetic moment.

Verwey transition: A crystallographic change in magnetite that occurs at ~120 K and that involves a redistribution of Fe ions such that the cubic spinel crystal lattice is slightly distorted to monoclinic symmetry. Surface oxidation and substitution of other cations into the crystal lattice affect the temperature at which the transition occurs. Named after E. J. W. Verwey (1905–1981).

Zero-field-cooled (ZFC) and field-cooled (FC) low-temperature magnetic measurements: In the ZFC magnetic measurement, a sample is first cooled without an applied magnetic field from a temperature well above the blocking temperature (T_b), down to a temperature well below T_b. Then a magnetic field is applied, and the magnetization is measured during warming to a temperature well above T_b. In the FC magnetization measurement, a sample is cooled in a small constant applied field while recording the magnetization. ZFC and FC magnetization curves are widely used in rock magnetism; differences between the curves have been used to indicate the presence of fossil magnetosome chains in sediments.

[72] **ACKNOWLEDGMENTS.** We have benefited from discussions with many colleagues about sedimentary greigite over the years, particularly Rich Reynolds, Ian Snowball, Leonardo Sagnotti, Mark Dekkers, Liane Benning, Shuh-Ji Kao, Wei-Teh Jiang, and Masayuki Torii. Kate Davis redrafted Figures 2d and 18 from the originals. Review comments from Leonardo Sagnotti,

Masayuki Torii, Joe Stoner, and Eelco Rohling improved the paper. We gratefully acknowledge funding from the Leverhulme Trust, the U.K. Natural Environment Research Council (NERC), the Royal Society, the European Commission, and the National Science Council (NSC) of Taiwan that supported different parts of this work. This work contributes to the objectives of NERC grant NE/G003319/1 and NSC91-2911-I-001-001.

[73] The Editor for this paper was Eelco Rohling. He thanks reviewers Masayuki Torii, Leonardo Sagnotti, and Joseph S. Stoner.

REFERENCES

Arató, B., Z. Szányi, C. Flies, D. Schüler, R. B. Frankel, P. R. Buseck, and M. Pósfai (2005), Crystal-size and shape distributions of magnetite from uncultured magnetotactic bacteria as a potential biomarker, *Am. Mineral.*, *90*, 1233–1241, doi:10.2138/am.2005.1778.

Ariztegui, D., and J. Dobson (1996), Magnetic investigations of framboidal greigite formation: A record of anthropogenic environmental changes in eutrophic Lake St Moritz, Switzerland, *Holocene*, *6*, 235–241, doi:10.1177/095968369600600209.

Aubourg, C., and P. Robion (2002), Composite ferromagnetic fabrics (magnetite, greigite) measured by AMS and partial AARM in weakly strained sandstones from western Makran, Iran, *Geophys. J. Int.*, *151*, 729–737, doi:10.1046/j.1365-246X.2002.01800.x.

Babinszki, E., E. Marton, P. Marton, and L. F. Kiss (2007), Widespread occurrence of greigite in the sediments of Lake Pannon: Implications for environment and magnetostratigraphy, *Palaeogeogr. Palaeoclimatol. Palaeoecol.*, *252*, 626–636, doi:10.1016/j.palaeo.2007.06.001.

Banerjee, S. K., J. King, and J. Marvin (1981), A rapid method for magnetic granulometry with applications to environmental studies, *Geophys. Res. Lett.*, *8*, 333–336, doi:10.1029/GL008i004p00333.

Bazylinski, D. A., and R. B. Frankel (2004), Magnetosome formation in prokaryotes, *Nat. Rev. Microbiol.*, *2*, 217–230, doi:10.1038/nrmicro842.

Bazylinski, D. A., R. B. Frankel, A. J. Garratt-Reed, and S. Mann (1990), Biomineralization of iron sulfides in magnetotactic bacteria from sulfidic environments, in *Iron Biominerals*, edited by R. B. Frankel and R. P. Blakemore, pp. 239–255, Plenum, New York.

Bazylinski, D. A., B. R. Heywood, S. Mann, and R. B. Frankel (1993), Fe_3O_4 and Fe_3S_4 in a bacterium, *Nature*, *366*, 218, doi:10.1038/366218a0.

Bazylinski, D. A., R. B. Frankel, B. R. Heywood, S. Mann, J. W. King, P. L. Donaghay, and A. K. Hanson (1995), Controlled biomineralization of magnetite (Fe_3O_4) and greigite (Fe_3S_4) in a magnetotactic bacterium, *Appl. Environ. Microbiol.*, *61*, 3232–3239.

Benning, L. G., R. T. Wilkin, and H. L. Barnes (2000), Reaction pathways in the Fe-S system below 100°C, *Chem. Geol.*, *167*, 25–51, doi:10.1016/S0009-2541(99)00198-9.

Berner, R. A. (1970), Sedimentary pyrite formation, *Am. J. Sci.*, *268*, 1–23, doi:10.2475/ajs.268.1.1.

Berner, R. A. (1984), Sedimentary pyrite formation: An update, *Geochim. Cosmochim. Acta*, *48*, 605–615, doi:10.1016/0016-7037(84)90089-9.

Blanchet, C. L., N. Thouveny, and L. Vidal (2009), Formation and preservation of greigite (Fe_3S_4) in sediments from the Santa Barbara basin: Implications for paleoenvironmental changes during the past 35 ka, *Paleoceanography*, *24*, PA2224, doi:10.1029/2008PA001719.

Borradaile, G. J., and M. Jackson (2004), Anisotropy of magnetic susceptibility (AMS): Magnetic petrofabrics of deformed rocks, in *Magnetic Fabric: Methods and Applications*, edited by F. Martin-Hernandez et al., *Geol. Soc. Spec. Publ.*, *238*, 299–360.

Bracci, G., D. Dalena, and P. Orlandi (1985), La greigite di Mentana, Lazio, *Rend. Soc. Ital. Mineral. Petrol.*, *40*, 295–298.

Braga, M., S. K. Lie, C. A. Taft, and W. A. Lester Jr. (1988), Electronic structure, hyperfine interactions, and magnetic properties for iron octahedral sulfides, *Phys. Rev.*, *38*, 10,837–10,851, doi:10.1103/PhysRevB.38.10837.

Carvallo, C., and A. R. Muxworthy (2006), Low-temperature first-order reversal curve (FORC) diagrams for synthetic and natural samples, *Geochem. Geophys. Geosyst.*, *7*, Q09003, doi:10.1029/2006GC001299.

Carvallo, C., A. R. Muxworthy, D. J. Dunlop, and W. Williams (2003), Micromagnetic modeling of first-order reversal curve (FORC) diagrams for single-domain and pseudo-single-domain magnetite, *Earth Planet. Sci. Lett.*, *213*, 375–390, doi:10.1016/S0012-821X(03)00320-0.

Chang, L., A. P. Roberts, A. R. Muxworthy, Y. Tang, Q. Chen, C. J. Rowan, Q. Liu, and P. Pruner (2007), Magnetic characteristics of synthetic pseudo-single-domain and multi-domain greigite (Fe_3S_4), *Geophys. Res. Lett.*, *34*, L24304, doi:10.1029/2007GL032114.

Chang, L., A. P. Roberts, Y. Tang, B. D. Rainford, A. R. Muxworthy, and Q. Chen (2008), Fundamental magnetic parameters from pure synthetic greigite (Fe_3S_4), *J. Geophys. Res.*, *113*, B06104, doi:10.1029/2007JB005502.

Chang, L., B. D. Rainford, J. R. Stewart, C. Ritter, A. P. Roberts, Y. Tang, and Q. Chen (2009a), Magnetic structure of greigite (Fe_3S_4) probed by neutron powder diffraction and polarized neutron diffraction, *J. Geophys. Res.*, *114*, B07101, doi:10.1029/2008JB006260.

Chang, L., A. P. Roberts, C. J. Rowan, Y. Tang, P. Pruner, Q. Chen, and C. S. Horng (2009b), Low-temperature magnetic properties of greigite (Fe_3S_4), *Geochem. Geophys. Geosyst.*, *10*, Q01Y04, doi:10.1029/2008GC002276.

Chen, X. Y., X. F. Zhang, J. X. Wan, Z. H. Wang, and Y. T. Qian (2005), Selective fabrication of metastable greigite (Fe_3S_4) nanocrystallites and its magnetic properties through a simple solution-based route, *Chem. Phys. Lett.*, *403*, 396–399, doi:10.1016/j.cplett.2005.01.050.

Chikazumi, S. (1964), *Physics of Magnetism*, 554 pp., John Wiley, New York.

Coey, J. M. D., M. R. Spender, and A. H. Morrish (1970), The magnetic structure of the spinel, Fe_3S_4, *Solid State Commun.*, *8*, 1605–1608, doi:10.1016/0038-1098(70)90473-4.

Crockford, R. H., and I. R. Willett (1995), Drying and oxidation effects on the magnetic properties of sulfidic material during oxidation, *Aust. J. Soil Res.*, *33*, 19–29, doi:10.1071/SR9950019.

Cutter, G. A., and R. S. Kluckhohn (1999), The cycling of particulate carbon, nitrogen, sulfur, and sulfur species (iron monosulfide, greigite, pyrite, and organic sulfur) in the water columns of Framvaren Fjord and the Black Sea, *Mar. Chem.*, *67*, 149–160, doi:10.1016/S0304-4203(99)00056-0.

Day, R., M. Fuller, and V. A. Schmidt (1977), Magnetic hysteresis properties of synthetic titanomagnetites, *Phys. Earth Planet. Inter.*, *13*, 260–267, doi:10.1016/0031-9201(77)90108-X.

de Boer, C. B., and M. J. Dekkers (1998), Thermomagnetic behaviour of haematite and goethite as a function of grain size in various non-saturating magnetic fields, *Geophys. J. Int.*, *133*, 541–552, doi:10.1046/j.1365-246X.1998.00522.x.

Dekkers, M. J. (1989), Magnetic properties of natural pyrrhotite. II. High- and low-temperature behaviour of J_{rs} and TRM as function of grain size, *Phys. Earth Planet. Inter.*, *57*, 266–283, doi:10.1016/0031-9201(89)90116-7.

Dekkers, M. J., and M. A. A. Schoonen (1996), Magnetic properties of hydrothermally synthesised greigite (Fe_3S_4)—I. Rock magnetic parameters at room temperature, *Geophys. J. Int.*, *126*, 360–368, doi:10.1111/j.1365-246X.1996.tb05296.x.

Dekkers, M. J., J.-L. Mattéi, G. Fillion, and P. Rochette (1989), Grain-size dependence of the magnetic behavior of pyrrhotite

during its low-temperature transition at 34 K, *Geophys. Res. Lett.*, *16*, 855–858, doi:10.1029/GL016i008p00855.

Dekkers, M. J., H. F. Passier, and M. A. A. Schoonen (2000), Magnetic properties of hydrothermally synthesised greigite (Fe_3S_4)—II. High- and low-temperature characteristics, *Geophys. J. Int.*, *141*, 809–819, doi:10.1046/j.1365-246x.2000.00129.x.

Devey, A. J., R. Grau-Crespo, and N. H. de Leeuw (2009), Electronic and magnetic structure of Fe_3S_4: GGA + U investigation, *Phys. Rev. B*, *79*, 195126, doi:10.1103/PhysRevB.79.195126.

Diaz Ricci, J. C., and J. L. Kirschvink (1992), Magnetic domain state and coercivity predictions for biogenic greigite (Fe_3S_4): A comparison of theory with magnetosome observations, *J. Geophys. Res.*, *97*, 17,309–17,315, doi:10.1029/92JB01290.

Dickens, G. R., M. M. Castillo, and J. C. G. Walker (1997), A blast of gas in the latest Paleocene: Simulating first-order effects of massive dissociation of oceanic methane hydrate, *Geology*, *25*, 259–262, doi:10.1130/0091-7613(1997)025<0259:ABOGIT>2.3.CO;2.

Diester-Haass, L., C. Robert, and H. Chamley (1998), Paleoproductivity and climate variations during sapropel deposition in the eastern Mediterranean Sea, *Proc. Ocean Drill. Program Sci. Results*, *160*, 227–248.

Doss, B. N. (1912a), Über die natur und zusammensetzung des Miocänen tonen der gouvernements Samara auftretenden Schwefeleisens, *Neues Jahrb. Mineral.*, *A33*, 662–713.

Doss, B. N. (1912b), Melnikowit, ein neues eisenbisulfid, und seine bedeutung für genesis der Kieslagerstätten, *Z. Prakt. Geol.*, *20*, 453–483.

Dunlop, D. J. (2002), Theory and application of the Day plot (M_{rs}/M_s versus H_{cr}/H_c): 1. Theoretical curves and tests using titanomagnetite data, *J. Geophys. Res.*, *107*(B3), 2056, doi:10.1029/2001JB000486.

Dunlop, D. J., and Ö. Özdemir (1997), *Rock Magnetism: Fundamentals and Frontiers*, 573 pp., Cambridge Univ. Press, Cambridge, U. K.

Egli, R., A. P. Chen, M. Winklhofer, K. P. Kodama, and C. S. Horng (2010), Detection of noninteracting single domain particles using first-order reversal curve diagrams, *Geochem. Geophys. Geosyst.*, *11*, Q01Z11, doi:10.1029/2009GC002916.

Enkin, R. J., J. Baker, D. Nourgaliev, P. Iassonov, and T. S. Hamilton (2007), Magnetic hysteresis parameters and Day plot analysis to characterize diagenetic alteration in gas-hydrate-bearing sediments, *J. Geophys. Res.*, *112*, B06S90, doi:10.1029/2006JB004638.

Farina, M., D. M. S. Esquivel, and H. G. P. Lins de Barros (1990), Magnetic iron-sulphur crystals from a magnetotactic microorganism, *Nature*, *343*, 256–258, doi:10.1038/343256a0.

Fassbinder, J. W. E., and H. Stanjek (1994), Magnetic properties of biogenic soil greigite (Fe_3S_4), *Geophys. Res. Lett.*, *21*, 2349–2352, doi:10.1029/94GL02506.

Fell, V., and M. Ward (1998), Iron sulphides: Corrosion products on artifacts from waterlogged deposits, in *Metal 98: Proceedings of the International Conference on Metals Conservation*, edited by W. Mourey and L. Robbiola, pp. 111–115, James and James, Newbury, U. K.

Florindo, F., and F. Marra (1995), A revision of the stratigraphy for the Middle Pleistocene continental deposits of Rome (central Italy): Palaeomagnetic data, *Ann. Geofis.*, *38*, 177–188.

Florindo, F., and L. Sagnotti (1995), Palaeomagnetism and rock magnetism at the upper Pliocene Valle Ricca (Rome, Italy) section, *Geophys. J. Int.*, *123*, 340–354, doi:10.1111/j.1365-246X.1995.tb06858.x.

Florindo, F., S. M. Bohaty, P. S. Erwin, C. Richter, A. P. Roberts, P. A. Whalen, and J. M. Whitehead (2003), Magnetobiostratigraphic chronology and palaeoenvironmental history of Cenozoic sequences from ODP sites 1165 and 1166, Prydz Bay, Antarctica, *Palaeogeogr. Palaeoclimatol. Palaeoecol.*, *198*, 69–100, doi:10.1016/S0031-0182(03)00395-X.

Florindo, F., D. B. Karner, F. Marra, P. R. Renne, A. P. Roberts, and R. Weaver (2007), Radioisotopic age constraints for Glacial Terminations IX and VII from aggradational sections of the Tiber River delta in Rome, Italy, *Earth Planet. Sci. Lett.*, *256*, 61–80, doi:10.1016/j.epsl.2007.01.014.

Frank, U., N. R. Nowaczyk, and J. F. W. Negendank (2007a), Palaeomagnetism of greigite bearing sediments from the Dead Sea, Israel, *Geophys. J. Int.*, *168*, 904–920, doi:10.1111/j.1365-246X.2006.03263.x.

Frank, U., N. R. Nowaczyk, and J. F. W. Negendank (2007b), Rock magnetism of greigite bearing sediments from the Dead Sea, Israel, *Geophys. J. Int.*, *168*, 921–934, doi:10.1111/j.1365-246X.2006.03273.x.

Fu, Y., T. von Dobeneck, C. Franke, D. Heslop, and S. Kasten (2008), Rock magnetic identification and geochemical process models of greigite formation in Quaternary marine sediments from the Gulf of Mexico (IODP Hole U1319A), *Earth Planet. Sci. Lett.*, *275*, 233–245, doi:10.1016/j.epsl.2008.07.034.

García, J., and G. Subías (2004), The Verwey transition—A new perspective, *J. Phys. Condens. Matter*, *16*, R145–R178, doi:10.1088/0953-8984/16/7/R01.

Giovanoli, F. (1979), A comparison of the magnetization of detrital and chemical sediments from Lake Zurich, *Geophys. Res. Lett.*, *6*, 233–235, doi:10.1029/GL006i004p00233.

Goffredi, S. K., A. Wáren, V. C. Orphan, C. L. Van Dover, and R. C. Vrijenhoek (2004), Novel forms of structural integration between microbes and a hydrothermal vent gastropod from the Indian Ocean, *Appl. Environ. Microbiol.*, *70*, 3082–3090, doi:10.1128/AEM.70.5.3082-3090.2004.

Goodenough, J. B., and G. A. Fatseas (1982), Mössbauer ^{57}Fe isomer shift as a measure of valence in mixed-valence iron sulfides, *J. Solid State Chem.*, *41*, 1–22, doi:10.1016/0022-4596(82)90028-7.

Hall, F. R., S. Cisowski, and J. W. King (1997), Magnetic hysteresis properties of fine-grained magnetic iron sulfide nodules and crusts on the Amazon Fan, *Proc. Ocean Drill. Program Sci. Results*, *155*, 245–249.

Hallam, D. F., and B. A. Maher (1994), A record of reversed polarity carried by the iron sulphide greigite in British early Pleistocene sediments, *Earth Planet. Sci. Lett.*, *121*, 71–80, doi:10.1016/0012-821X(94)90032-9.

Han, W., and M. Y. Gao (2008), Investigations on iron sulfide nanosheets prepared via a single-source precursor approach, *Cryst. Growth Des.*, *8*, 1023–1030, doi:10.1021/cg701075u.

He, Z. B., S. H. Yu, X. Y. Zhou, X. G. Li, and J. F. Qu (2006), Magnetic-field-induced phase-selective synthesis of ferrosulfide microrods by a hydrothermal process: Microstructure control and magnetic properties, *Adv. Funct. Mater.*, *16*, 1105–1111, doi:10.1002/adfm.200500580.

Heslop, D., M. J. Dekkers, P. P. Kruiver, and I. H. M. van Oorschot (2002), Analysis of isothermal remanent magnetization acquisition curves using the expectation-maximization algorithm, *Geophys. J. Int.*, *148*, 58–64, doi:10.1046/j.0956-540x.2001.01558.x.

Heslop, D., G. McIntosh, and M. J. Dekkers (2004), Using time- and temperature-dependent Preisach models to investigate the limitations of modelling isothermal remanent magnetization acquisition curves with cumulative log Gaussian functions, *Geophys. J. Int.*, *157*, 55–63, doi:10.1111/j.1365-246X.2004.02155.x.

Heywood, B. R., D. A. Bazylinski, A. Garratt-Reed, S. Mann, and R. B. Frankel (1990), Controlled biosynthesis of greigite (Fe_3S_4) in magnetotactic bacteria, *Naturwissenschaften*, *77*, 536–538, doi:10.1007/BF01139266.

Heywood, B. R., S. Mann, and R. B. Frankel (1991), Structure, morphology and growth of biogenic greigite (Fe_3S_4), *Mater. Res. Soc. Symp. Proc.*, *218*, 93–108.

Hilton, J. (1990), Greigite and the magnetic properties of sediments, *Limnol. Oceanogr.*, *35*, 509–520, doi:10.4319/lo.1990.35.2.0509.

Hoffmann, V. (1992), Greigite (Fe_3S_4): Magnetic properties and first domain observations, *Phys. Earth Planet. Inter.*, *70*, 288–301, doi:10.1016/0031-9201(92)90195-2.

Horng, C. S., and K. H. Chen (2006), Complicated magnetic mineral assemblages in marine sediments offshore of southwestern Taiwan: Possible influence of methane flux on the early diagenetic process, *Terr. Atmos. Oceanic Sci.*, *17*, 1009–1026.

Horng, C. S., J. C. Chen, and T. Q. Lee (1992a), Variations in magnetic minerals from two Plio-Pleistocene marine-deposited sections, southwestern Taiwan, *J. Geol. Soc. China*, *35*, 323–335.

Horng, C. S., C. Laj, T. Q. Lee, and J. C. Chen (1992b), Magnetic characteristics of sedimentary rocks from the Tsengwen-chi and Erhjen-chi sections in southwestern Taiwan, *Terr. Atmos. Oceanic Sci.*, *3*, 519–532.

Horng, C. S., M. Torii, K. S. Shea, and S. J. Kao (1998), Inconsistent magnetic polarities between greigite- and pyrrhotite/magnetite-bearing marine sediments from the Tsailiao-chi section, southwestern Taiwan, *Earth Planet. Sci. Lett.*, *164*, 467–481, doi:10.1016/S0012-821X(98)00239-8.

Housen, B. A., and R. J. Musgrave (1996), Rock-magnetic signature of gas hydrates in accretionary prism sediments, *Earth Planet. Sci. Lett.*, *139*, 509–519, doi:10.1016/0012-821X(95)00245-8.

Hrouda, F. (1994), A technique for the measurement of thermal changes of magnetic susceptibility of weakly magnetic rocks by the CS-2 apparatus and KLY-2 Kappabridge, *Geophys. J. Int.*, *118*, 604–612, doi:10.1111/j.1365-246X.1994.tb03987.x.

Hu, S., E. Appel, V. Hoffmann, W. W. Schmahl, and S. Wang (1998), Gyromagnetic remanence acquired by greigite (Fe_3S_4) during static three-axis alternating field demagnetization, *Geophys. J. Int.*, *134*, 831–842, doi:10.1046/j.1365-246x.1998. 00627.x.

Hu, S., A. Stephenson, and E. Appel (2002), A study of gyroremanent magnetisation (GRM) and rotational remanent magnetisation (RRM) carried by greigite from lake sediments, *Geophys. J. Int.*, *151*, 469–474, doi:10.1046/j.1365-246X.2002.01793.x.

Hunger, S., and L. G. Benning (2007), Greigite: A true intermediate on the polysulfide pathway to pyrite, *Geochem. Trans.*, *8*, article 1, doi:10.1186/1467-4866-8-1.

Hunt, C. P., B. M. Moskowitz, and S. K. Banerjee (1995), Magnetic properties of rocks and minerals, in *Rock Physics and Phase Relations: A Handbook of Physical Constants*, edited by T. J. Ahrens, pp. 189–204, AGU, Washington, D. C.

Hüsing, S. K., M. J. Dekkers, C. Franke, and W. Krijgsman (2009), The Tortonian reference section at Monte dei Corvi (Italy): Evidence for early remanence acquisition in greigite-bearing sediments, *Geophys. J. Int.*, *179*, 125–143, doi:10.1111/j.1365-246X.2009.04301.x.

Jelinowska, A., P. Tucholka, F. Guichard, I. Lefèvre, D. Badaut-Trauth, F. Chalié, F. Gasse, N. Tribovillard, and A. Desprairies (1998), Mineral magnetic study of Late Quaternary south Caspian Sea sediments: Palaeoenvironmental implications, *Geophys. J. Int.*, *133*, 499–509, doi:10.1046/j.1365-246X.1998.00536.x.

Jiang, W. T., C. S. Horng, A. P. Roberts, and D. R. Peacor (2001), Contradictory magnetic polarities in sediments and variable timing of neoformation of authigenic greigite, *Earth Planet. Sci. Lett.*, *193*, 1–12, doi:10.1016/S0012-821X(01)00497-6.

Kao, S. J., C. S. Horng, A. P. Roberts, and K. K. Liu (2004), Carbon-sulfur-iron relationships in sedimentary rocks from southwestern Taiwan: Influence of geochemical environment on greigite and pyrrhotite formation, *Chem. Geol.*, *203*, 153–168, doi:10.1016/j.chemgeo.2003.09.007.

Kasama, T., M. Pósfai, R. K. K. Chong, A. P. Finlayson, P. R. Buseck, R. B. Frankel, and R. E. Dunin-Borkowski (2006), Magnetic properties, microstructure, composition, and morphology of greigite nanocrystals in magnetotactic bacteria from electron holography and tomography, *Am. Mineral.*, *91*, 1216–1229, doi:10.2138/am.2006.2227.

Kasten, S., T. Freudenthal, F. X. Gingele, and H. D. Schulz (1998), Simultaneous formation of iron-rich layers at different redox boundaries in sediments of the Amazon deep-sea fan, *Geochim. Cosmochim. Acta*, *62*, 2253–2264, doi:10.1016/S0016-7037(98)00093-3.

Kennett, J. P., K. G. Cannariato, I. L. Hendy, and R. J. Behl (2000), Carbon isotopic evidence for methane hydrate instability during Quaternary interstadials, *Science*, *288*, 128–133, doi:10.1126/science.288.5463.128.

Kopp, R. E., C. Z. Nash, A. Kobayashi, B. P. Weiss, D. A. Bazylinski, and J. L. Kirschvink (2006), Ferromagnetic resonance spectroscopy for assessment of magnetic anisotropy and magnetostatic interactions: A case study of mutant magnetotactic bacteria, *J. Geophys. Res.*, *111*, B12S25, doi:10.1029/2006JB004529.

Krs, M., M. Krsová, P. Pruner, A. Zeman, F. Novák, and J. Jansa (1990), A petromagnetic study of Miocene rocks bearing micro-organic material and the magnetic mineral greigite (Sokolov and Cheb basins, Czechoslovakia), *Phys. Earth Planet. Inter.*, *63*, 98–112, doi:10.1016/0031-9201(90)90064-5.

Krs, M., M. Krsová, L. Koulíková, P. Pruner, and F. Valín (1992), On the applicability of oil shale to paleomagnetic investigations, *Phys. Earth Planet. Inter.*, *70*, 178–186, doi:10.1016/0031-9201(92)90180-4.

Kruiver, P. P., M. J. Dekkers, and D. Heslop (2001), Quantification of magnetic coercivity components by the analysis of acquisition curves of isothermal remanent magnetization, *Earth Planet. Sci. Lett.*, *189*, 269–276, doi:10.1016/S0012-821X(01)00367-3.

Krupp, R. E. (1991), Smythite, greigite, and mackinawite: New observations on natural low-temperature iron sulfides, in *Source, Transport and Deposition of Metals*, edited by M. Pagel and J. L. Leroy, pp. 193–195, Balkema, Rotterdam, Netherlands.

Krupp, R. E. (1994), Phase relations and phase transformations between the low-temperature iron sulfides mackinawite, greigite, and smythite, *Eur. J. Mineral.*, *6*, 265–278.

Larrasoaña, J. C., A. P. Roberts, J. S. Stoner, C. Richter, and R. Wehausen (2003), A new proxy for bottom-water ventilation based on diagenetically controlled magnetic properties of eastern Mediterranean sapropel-bearing sediments, *Palaeogeogr. Palaeoclimatol. Palaeoecol.*, *190*, 221–242, doi:10.1016/S0031-0182(02)00607-7.

Larrasoaña, J. C., A. P. Roberts, R. J. Musgrave, E. Gràcia, E. Piñero, M. Vega, and F. Martínez-Ruiz (2007), Diagenetic formation of greigite and pyrrhotite in marine sedimentary systems containing gas hydrates, *Earth Planet. Sci. Lett.*, *261*, 350–366, doi:10.1016/j.epsl.2007.06.032.

Letard, I., P. Sainctavit, N. Menguy, J.-P. Valet, A. Isambert, M. Dekkers, and A. Gloter (2005), Mineralogy of greigite Fe_3S_4, *Phys. Scr.*, *T115*, 489–491, doi:10.1238/Physica.Topical.115a00489.

Liu, J., R. X. Zhu, A. P. Roberts, S. Q. Li, and J. H. Chang (2004), High-resolution analysis of early diagenetic effects on magnetic minerals in post-middle-Holocene continental shelf sediments from the Korea Strait, *J. Geophys. Res.*, *109*, B03103, doi:10.1029/2003JB002813.

Liu, Q., Y. J. Yu, J. Torrent, A. P. Roberts, Y. Pan, and R. Zhu (2006), The characteristic low-temperature magnetic properties of aluminous goethite [α-(Fe, Al)OOH] explained, *J. Geophys. Res.*, *111*, B12S34, doi:10.1029/2006JB004560.

Lowrie, W. (1990), Identification of ferromagnetic minerals in a rock by coercivity and unblocking temperature properties, *Geophys. Res. Lett.*, *17*, 159–162, doi:10.1029/GL017i002p00159.

Lowrie, W., and M. Fuller (1971), On the alternating field demagnetization characteristics of multidomain thermoremanent magnetization in magnetite, *J. Geophys. Res.*, *76*, 6339–6349, doi:10.1029/JB076i026p06339.

Mann, S., N. H. C. Sparks, R. B. Frankel, D. A. Bazylinski, and H. W. Jannasch (1990), Biomineralization of ferrimagnetic grei-

gite (Fe_3S_4) and iron pyrite (FeS_2) in a magnetotactic bacterium, *Nature*, *343*, 258–261, doi:10.1038/343258a0.

Mattei, M., C. Kissel, and R. Funiciello (1996), No tectonic rotation of the Tuscan Tyrrhenian margin (Italy) since late Messinian, *J. Geophys. Res.*, *101*, 2835–2845, doi:10.1029/95JB02398.

Mattei, M., F. Speranza, A. Argentieri, F. Rossetti, L. Sagnotti, and R. Funiciello (1999), Extensional tectonics in the Amantea basin (Calabria, Italy): A comparison between structural and magnetic anisotropy data, *Tectonophysics*, *307*, 33–49, doi:10.1016/S0040-1951(99)00117-1.

McKay, D. S., E. K. Gibson Jr., K. L. Thomas-Keprta, H. Vali, C. S. Romanek, S. J. Clemett, X. D. F. Chillier, C. R. Maechling, and R. N. Zare (1996), Search for past life on Mars: Possible relic biogenic activity in Martian meteorite ALH84001, *Science*, *273*, 924–930, doi:10.1126/science.273.5277.924.

Mohamed, K. J., D. Rey, B. Rubio, M. J. Dekkers, A. P. Roberts, and F. Vilas (2011), Onshore-offshore gradient in reductive early diagenesis in coastal marine sediments of the Ria de Vigo, northwest Iberian Peninsula, *Continent. Shelf Res.*, doi:10.1016/j.csr.2010.06.006, in press.

Morin, F. J. (1950), Magnetic susceptibility of αFe_2O_3 and αFe_2O_3 with added titanium, *Phys. Rev.*, *78*, 819–820, doi:10.1103/PhysRev.78.819.2.

Moskowitz, B. M. (1995), Biomineralization of magnetic minerals, *U.S. Natl. Rep. Int. Union Geod. Geophys. 1991–1994*, *Rev. Geophys.*, *33*, 123–128, doi:10.1029/95RG00443.

Moskowitz, B. M., R. B. Frankel, and D. A. Bazylinski (1993), Rock magnetic criteria for the detection of biogenic magnetite, *Earth Planet. Sci. Lett.*, *120*, 283–300, doi:10.1016/0012-821X(93)90245-5.

Moskowitz, B. M., M. Jackson, and C. Kissel (1998), Low-temperature magnetic behavior of titanomagnetites, *Earth Planet. Sci. Lett.*, *157*, 141–149, doi:10.1016/S0012-821X(98)00033-8.

Moskowitz, B. M., D. A. Bazylinski, R. Egli, R. B. Frankel, and K. J. Edwards (2008), Magnetic properties of marine magnetotactic bacteria in a seasonally stratified coastal pond (Salt Pond, MA, USA), *Geophys. J. Int.*, *174*, 75–92, doi:10.1111/j.1365-246X.2008.03789.x.

Musgrave, R. J., N. L. Bangs, J. C. Larrasoaña, E. Gràcia, J. A. Hollamby, and M. E. Vega (2006), Rise of the base of the gas hydrate zone since the last glacial recorded by rock magnetism, *Geology*, *34*, 117–120, doi:10.1130/G22008.1.

Muxworthy, A. R., and A. P. Roberts (2007), First-order reversal curve (FORC) diagrams, in *Encyclopedia of Geomagnetism and Paleomagnetism*, edited by D. Gubbins and E. Herrero-Bervera, pp. 266–272, Springer, Dordrecht, Netherlands.

Muxworthy, A. R., and W. Williams (2006), Critical single-domain/multi-domain grain sizes in noninteracting and interacting elongated magnetite particles: Implications for magnetosomes, *J. Geophys. Res.*, *111*, B12S12, doi:10.1029/2006JB004588.

Muxworthy, A. R., and W. Williams (2009), Critical superparamagnetic/single domain grain sizes in interacting magnetite particles: Implications for magnetosome crystals, *J. R. Soc. Interface*, *6*, 1207–1212.

Muxworthy, A. R., D. Heslop, and W. Williams (2004), Influence of magnetostatic interactions on first-order-reversal-curve (FORC) diagrams: A micromagnetic approach, *Geophys. J. Int.*, *158*, 888–897, doi:10.1111/j.1365-246X.2004.02358.x.

Neretin, L. N., M. E. Böttcher, B. B. Jørgensen, I. I. Volkov, H. Lüschen, and K. Kilgenfeldt (2004), Pyritization processes and greigite formation in the advancing sulphidization front in the Upper Pleistocene sediments of the Black Sea, *Geochim. Cosmochim. Acta*, *68*, 2081–2093, doi:10.1016/S0016-7037(03)00450-2.

Newell, A. J. (2005), A high-precision model of first-order reversal curve (FORC) functions for single-domain ferromagnets with uniaxial anisotropy, *Geochem. Geophys. Geosyst.*, *6*, Q05010, doi:10.1029/2004GC000877.

Oda, H., and M. Torii (2004), Sea-level change and remagnetization of continental shelf sediments off New Jersey (ODP Leg 174A): Magnetite and greigite diagenesis, *Geophys. J. Int.*, *156*, 443–458, doi:10.1111/j.1365-246X.2004.02162.x.

Oldfield, F., I. Darnley, G. Yates, D. E. France, and J. Hilton (1992), Storage diagenesis versus sulphide authigenesis: Possible implications in environmental magnetism, *J. Paleolimnol.*, *7*, 179–189, doi:10.1007/BF00181713.

Oles, D., and G. Houben (1998), Greigite (Fe_3S_4) in an acid mudpool at Makiling volcano, the Philippines, *J. Asian Earth Sci.*, *16*, 513–517, doi:10.1016/S0743-9547(98)00029-4.

Opdyke, N. D., and J. E. T. Channell (1996), *Magnetic Stratigraphy*, 346 pp., Academic, San Diego, Calif.

Özdemir, Ö., D. J. Dunlop, and B. M. Moskowitz (1993), The effect of oxidation on the Verwey transition in magnetite, *Geophys. Res. Lett.*, *20*, 1671–1674, doi:10.1029/93GL01483.

Ozima, M., M. Ozima, and S. Akimoto (1964), Low temperature characteristics of remanent magnetization of magnetite–self-reversal and recovery phenomena of remanent magnetization, *J. Geomagn. Geoelectr.*, *16*, 165–177.

Pearce, C. I., R. A. D. Pattrick, and D. J. Vaughan (2006), Electrical and magnetic properties of sulfides, *Rev. Mineral. Geochem.*, *61*, 127–180, doi:10.2138/rmg.2006.61.3.

Peters, C., and M. J. Dekkers (2003), Selected room temperature magnetic parameters as a function of mineralogy, concentration and grain size, *Phys. Chem. Earth*, *28*, 659–667.

Peters, C., and R. Thompson (1998), Magnetic identification of selected natural iron oxides and sulphides, *J. Magn. Magn. Mater.*, *183*, 365–374, doi:10.1016/S0304-8853(97)01097-4.

Pike, C. R., A. P. Roberts, and K. L. Verosub (1999), Characterizing interactions in fine magnetic particle systems using first order reversal curves, *J. Appl. Phys.*, *85*, 6660–6667, doi:10.1063/1.370176.

Pike, C. R., A. P. Roberts, and K. L. Verosub (2001), First-order reversal curve diagrams and thermal relaxation effects in magnetic particles, *Geophys. J. Int.*, *145*, 721–730, doi:10.1046/j.0956-540x.2001.01419.x.

Pillans, B. J., A. P. Roberts, G. S. Wilson, S. T. Abbott, and B. V. Alloway (1994), Magnetostratigraphic, lithostratigraphic and tephrostratigraphic constraints on Middle/Lower Pleistocene sea level changes, Wanganui Basin, New Zealand, *Earth Planet. Sci. Lett.*, *121*, 81–98, doi:10.1016/0012-821X(94)90033-7.

Porreca, M., and M. Mattei (2010), Tectonic and environmental evolution of Quaternary intramontane basins in southern Apennines (Italy): Insights from palaeomagnetic and rock magnetic investigations, *Geophys. J. Int.*, *182*, 682–698, doi:10.1111/j.1365-246X.2010.04661.x.

Porreca, M., M. Mattei, and G. Di Vincenzo (2009), Post-deformational growth of late diagenetic greigite in lacustrine sediments from southern Italy, *Geophys. Res. Lett.*, *36*, L09307, doi:10.1029/2009GL037350.

Pósfai, M., P. R. Buseck, D. A. Bazylinski, and R. B. Frankel (1998), Reaction sequence of iron sulfide minerals in bacteria and their use as biomarkers, *Science*, *280*, 880–883, doi:10.1126/science.280.5365.880.

Pósfai, M., K. Cziner, E. Márton, P. Márton, P. R. Buseck, R. B. Frankel, and D. A. Bazylinski (2001), Crystal-size distributions and possible biogenic origin of Fe sulfides, *Eur. J. Mineral.*, *13*, 691–703, doi:10.1127/0935-1221/2001/0013-0691.

Pye, K. (1981), Marshrock formed by iron sulphide and siderite cementation in saltmarsh sediments, *Nature*, *294*, 650–652, doi:10.1038/294650a0.

Qian, X. F., X. M. Zhang, C. Wang, Y. Xie, W. Z. Wang, and Y. T. Qian (1999), The preparation and phase transition of nanocrystalline iron sulfides via toluene-thermal process, *Mater. Sci. Eng.*, *64*, 170–173, doi:10.1016/S0921-5107(99)00145-2.

Radusinovic, D. R. (1966), Greigite from the Lojane chromium deposit, Macedonia, *Am. Mineral.*, *51*, 209–215.

Rey, D., K. J. Mohamed, A. Bernabeu, B. Rubio, and F. Vilas (2005), Early diagenesis of magnetic minerals in marine transitional environments: Geochemical signatures of hydrodynamic forcing, *Mar. Geol.*, *215*, 215–236, doi:10.1016/j.margeo.2004.12.001.

Reynolds, R. L., M. L. Tuttle, C. A. Rice, N. S. Fishman, J. A. Karachewski, and D. M. Sherman (1994), Magnetization and geochemistry of greigite-bearing Cretaceous strata, North Slope basin, Alaska, *Am. J. Sci.*, *294*, 485–528, doi:10.2475/ajs.294.4.485.

Reynolds, R. L., J. G. Rosenbaum, P. van Metre, M. Tuttle, E. Callender, and A. Goldin (1999), Greigite as an indicator of drought—The 1912–1994 sediment magnetic record from White Rock Lake, Dallas, Texas, USA, *J. Paleolimnol.*, *21*, 193–206, doi:10.1023/A:1008027815203.

Rickard, D., and G. W. Luther III (2007), Chemistry of iron sulfides, *Chem. Rev.*, *107*, 514–562, doi:10.1021/cr0503658.

Roberts, A. P. (1992), Paleomagnetic constraints on the tectonic rotation of the southern Hikurangi margin, *N. Z. J. Geol. Geophys.*, *35*, 311–323, doi:10.1080/00288306.1992.9514524.

Roberts, A. P. (1995), Magnetic characteristics of sedimentary greigite (Fe_3S_4), *Earth Planet. Sci. Lett.*, *134*, 227–236, doi:10.1016/0012-821X(95)00131-U.

Roberts, A. P., and B. J. Pillans (1993), Rock magnetism of Lower/Middle Pleistocene marine sediments, Wanganui Basin, New Zealand, *Geophys. Res. Lett.*, *20*, 839–842, doi:10.1029/93GL00802.

Roberts, A. P., and G. M. Turner (1993), Diagenetic formation of ferrimagnetic iron sulphide minerals in rapidly deposited marine sediments, South Island, New Zealand, *Earth Planet. Sci. Lett.*, *115*, 257–273, doi:10.1016/0012-821X(93)90226-Y.

Roberts, A. P., and R. Weaver (2005), Multiple mechanisms of remagnetization involving sedimentary greigite (Fe_3S_4), *Earth Planet. Sci. Lett.*, *231*, 263–277, doi:10.1016/j.epsl.2004.11.024.

Roberts, A. P., G. M. Turner, and P. P. Vella (1994), Magnetostratigraphic chronology of Late Miocene to Early Pliocene biostratigraphic and oceanographic events in New Zealand, *Geol. Soc. Am. Bull.*, *106*, 665–683, doi:10.1130/0016-7606(1994)106<0665:MCOLMT>2.3.CO;2.

Roberts, A. P., R. L. Reynolds, K. L. Verosub, and D. P. Adam (1996), Environmental magnetic implications of greigite (Fe_3S_4) formation in a 3 million year lake sediment record from Butte Valley, Northern California, *Geophys. Res. Lett.*, *23*, 2859–2862, doi:10.1029/96GL02831.

Roberts, A. P., G. S. Wilson, F. Florindo, L. Sagnotti, K. L. Verosub, and D. M. Harwood (1998), Magnetostratigraphy of lower Miocene strata from the CRP-1 core, McMurdo Sound, Ross Sea, Antarctica, *Terra Antart.*, *5*, 703–713.

Roberts, A. P., J. S. Stoner, and C. Richter (1999), Diagenetic magnetic enhancement of sapropels from the eastern Mediterranean Sea, *Mar. Geol.*, *153*, 103–116, doi:10.1016/S0025-3227(98)00087-5.

Roberts, A. P., C. R. Pike, and K. L. Verosub (2000), First-order reversal curve diagrams: A new tool for characterizing the magnetic properties of natural samples, *J. Geophys. Res.*, *105*, 28,461–28,475, doi:10.1029/2000JB900326.

Roberts, A. P., W. T. Jiang, F. Florindo, C. S. Horng, and C. Laj (2005), Assessing the timing of greigite formation and the reliability of the Upper Olduvai polarity transition record from the Crostolo River, Italy, *Geophys. Res. Lett.*, *32*, L05307, doi:10.1029/2004GL022137.

Roberts, A. P., Q. Liu, C. J. Rowan, L. Chang, C. Carvallo, J. Torrent, and C. S. Horng (2006), Characterization of hematite (α-Fe_2O_3), goethite (α-FeOOH), greigite (Fe_3S_4), and pyrrhotite (Fe_7S_8) using first-order reversal curve diagrams, *J. Geophys. Res.*, *111*, B12S35, doi:10.1029/2006JB004715.

Roberts, A. P., F. Florindo, J. C. Larrasoaña, M. A. O'Regan, and X. Zhao (2010), Complex polarity pattern at the (former) Plio-Pleistocene global stratotype section at Vrica (Italy): Remagnetization by magnetic iron sulphides, *Earth Planet. Sci. Lett.*, *292*, 98–111, doi:10.1016/j.epsl.2010.01.025.

Rochette, P. (1987), Magnetic susceptibility of the rock matrix related to magnetic fabric studies, *J. Struct. Geol.*, *9*, 1015–1020, doi:10.1016/0191-8141(87)90009-5.

Rochette, P. (1988), Inverse magnetic fabric in carbonate-bearing rocks, *Earth Planet. Sci. Lett.*, *90*, 229–237, doi:10.1016/0012-821X(88)90103-3.

Rochette, P., G. Fillion, J.-L. Mattéi, and M. J. Dekkers (1990), Magnetic transition at 30–34 Kelvin in pyrrhotite: Insight into a widespread occurrence of this mineral in rocks, *Earth Planet. Sci. Lett.*, *98*, 319–328, doi:10.1016/0012-821X(90)90034-U.

Ron, H., N. R. Nowaczyk, U. Frank, M. J. Schwab, R. Naumann, B. Striewski, and A. Agnon (2007), Greigite detected as dominating remanence carrier in late Pleistocene sediments, Lisan Formation, from Lake Kinneret (Sea of Galilee), Israel, *Geophys. J. Int.*, *170*, 117–131, doi:10.1111/j.1365-246X.2007.03425.x.

Rowan, C. J., and A. P. Roberts (2005), Tectonic and geochronological implications of variably timed remagnetizations carried by authigenic greigite in fine-grained sediments from New Zealand, *Geology*, *33*, 553–556, doi:10.1130/G21382.1.

Rowan, C. J., and A. P. Roberts (2006), Magnetite dissolution, diachronous greigite formation, and secondary magnetizations from pyrite oxidation: Unravelling complex magnetizations in Neogene marine sediments from New Zealand, *Earth Planet. Sci. Lett.*, *241*, 119–137, doi:10.1016/j.epsl.2005.10.017.

Rowan, C. J., and A. P. Roberts (2008), Widespread remagnetizations and a new view of Neogene tectonic rotations within the Australia-Pacific plate boundary zone, New Zealand, *J. Geophys. Res.*, *113*, B03103, doi:10.1029/2006JB004594.

Rowan, C. J., A. P. Roberts, and T. Broadbent (2009), Paleomagnetic smoothing and magnetic enhancement in marine sediments due to prolonged early diagenetic growth of greigite, *Earth Planet. Sci. Lett.*, *277*, 223–235, doi:10.1016/j.epsl.2008.10.016.

Russell, M. J., and A. J. Hall (1997), The emergence of life from iron monosulphide bubbles at a submarine hydrothermal redox and pH front, *J. Geol. Soc.*, *154*, 377–402, doi:10.1144/gsjgs.154.3.0377.

Russell, M. J., R. M. Daniel, A. J. Hall, and J. A. Sherringham (1994), A hydrothermally precipitated catalytic iron sulphide membrane as a first step toward life, *J. Mol. Evol.*, *39*, 231–243, doi:10.1007/BF00160147.

Sagnotti, L., and A. Winkler (1999), Rock magnetism and palaeomagnetism of greigite-bearing mudstones in the Italian peninsula, *Earth Planet. Sci. Lett.*, *165*, 67–80, doi:10.1016/S0012-821X(98)00248-9.

Sagnotti, L., F. Speranza, A. Winkler, M. Mattei, and R. Funiciello (1998), Magnetic fabric of clay sediments from the external northern Apennines (Italy), *Phys. Earth Planet. Inter.*, *105*, 73–93, doi:10.1016/S0031-9201(97)00071-X.

Sagnotti, L., A. Winkler, P. Montone, L. Di Bella, F. Florindo, M. T. Mariucci, F. Marra, L. Alfonsi, and A. Frepoli (1999), Magnetic anisotropy of Plio-Pleistocene sediments from the Adriatic margin of the northern Apennines (Italy): Implications for the time-space evolution of the stress-field, *Tectonophysics*, *311*, 139–153, doi:10.1016/S0040-1951(99)00159-6.

Sagnotti, L., A. Winkler, L. Alfonsi, F. Florindo, and F. Marra (2000), Paleomagnetic constraints on the Plio-Pleistocene geodynamic evolution of the external central-northern Apennines (Italy), *Earth Planet. Sci. Lett.*, *180*, 243–257, doi:10.1016/S0012-821X(00)00172-2.

Sagnotti, L., P. Rochette, M. Jackson, F. Vadeboin, J. Dinarès-Turell, A. Winkler, and "Mag-Net" Science Team (2003), Inter-laboratory calibration of low-field magnetic and anhysteretic susceptibility measurements, *Phys. Earth Planet. Inter.*, *138*, 25–38, doi:10.1016/S0031-9201(03)00063-3.

Sagnotti, L., A. P. Roberts, R. Weaver, K. L. Verosub, F. Florindo, C. R. Pike, T. Clayton, and G. S. Wilson (2005), Apparent magnetic polarity reversals due to remagnetization resulting from late

diagenetic growth of greigite from siderite, *Geophys. J. Int.*, *160*, 89–100, doi:10.1111/j.1365-246X.2005.02485.x.

Sagnotti, L., A. Cascella, N. Ciaranfi, P. Macrì, P. Maiorano, M. Marino, and J. Taddeucci (2010), Rock magnetism and palaeomagnetism of the Montalbano Jonico section (Italy): Evidence for late diagenetic growth of greigite and implications for magnetostratigraphy, *Geophys. J. Int.*, *180*, 1049–1066, doi:10.1111/j.1365-246X.2009.04480.x.

Schoonen, M. A. A., and H. L. Barnes (1991), Reactions forming pyrite and marcasite from solution: II. Via FeS precursors below 100°C, *Geochim. Cosmochim. Acta*, *55*, 1505–1514, doi:10.1016/0016-7037(91)90123-M.

Schwarz, E. J., and D. J. Vaughan (1972), Magnetic phase relations of pyrrhotite, *J. Geomagn. Geoelectr.*, *24*, 441–458.

Sherman, D. M. (1990), Mössbauer spectra, crystal chemistry, and electronic structure of greigite, Fe_3S_4, *Eos Trans. AGU*, *71*, 1649.

Skinner, B. J., R. C. Erd, and F. S. Grimaldi (1964), Greigite, the thio-spinel of iron: A new mineral, *Am. Mineral.*, *49*, 543–555.

Smirnov, A. V. (2006), Low-temperature magnetic properties of magnetite using first-order reversal curve analysis: Implications for the pseudo-single domain state, *Geochem. Geophys. Geosyst.*, *7*, Q11011, doi:10.1029/2006GC001397.

Snowball, I. F. (1991), Magnetic hysteresis properties of greigite (Fe_3S_4) and a new occurrence in Holocene sediments from Swedish Lappland, *Phys. Earth Planet. Inter.*, *68*, 32–40, doi:10.1016/0031-9201(91)90004-2.

Snowball, I. F. (1997a), Gyroremanent magnetization and the magnetic properties of greigite-bearing clays in southern Sweden, *Geophys. J. Int.*, *129*, 624–636, doi:10.1111/j.1365-246X.1997.tb04498.x.

Snowball, I. F. (1997b), The detection of single-domain greigite (Fe_3S_4) using rotational remanent magnetization (RRM) and the effective gyro field (B_g): Mineral magnetic and palaeomagnetic applications, *Geophys. J. Int.*, *130*, 704–716, doi:10.1111/j.1365-246X.1997.tb01865.x.

Snowball, I. F., and R. Thompson (1988), The occurrence of greigite in sediments from Loch Lomond, *J. Quat. Sci.*, *3*, 121–125, doi:10.1002/jqs.3390030203.

Snowball, I. F., and R. Thompson (1990a), A stable chemical remanence in Holocene sediments, *J. Geophys. Res.*, *95*, 4471–4479, doi:10.1029/JB095iB04p04471.

Snowball, I. F., and R. Thompson (1990b), A mineral magnetic study of Holocene sedimentation in Lough Catherine, Northern Ireland, *Boreas*, *19*, 127–146, doi:10.1111/j.1502-3885.1990.tb00574.x.

Snowball, I. F., and M. Torii (1999), Incidence and significance of magnetic iron sulphides in Quaternary sediments and soils, in *Quaternary Climates, Environments and Magnetism*, edited by B. A. Maher and R. Thompson, pp. 199–230, Cambridge Univ. Press, Cambridge, U. K., doi:10.1017/CBO9780511535635.007.

Spender, M. R., J. M. D. Coey, and A. H. Morrish (1972), The magnetic properties and Mössbauer spectra of synthetic samples of Fe_3S_4, *Can. J. Phys.*, *50*, 2313–2326.

Stanjek, H., and E. Murad (1994), Comparison of pedogenic and sedimentary greigite by X-ray diffraction and Mössbauer spectroscopy, *Clays Clay Mineral.*, *42*, 451–454.

Stanjek, H., J. W. E. Fassbinder, H. Vali, H. Wägele, and W. Graf (1994), Evidence of biogenic greigite (ferrimagnetic Fe_3S_4) in soil, *Eur. J. Soil Sci.*, *45*, 97–103, doi:10.1111/j.1365-2389.1994.tb00490.x.

Stephenson, A. (1980), Gyromagnetism and the remanence acquired by a rotating rock in an alternating-field, *Nature*, *284*, 48–49, doi:10.1038/284048a0.

Stephenson, A., and I. F. Snowball (2001), A large gyromagnetic effect in greigite, *Geophys. J. Int.*, *145*, 570–575, doi:10.1046/j.0956-540x.2001.01434.x.

Suzuki, Y., et al. (2006), Sclerite formation in the hydrothermal-vent "scaly-foot" gastropod—Possible control of iron sulfide biomineralization by the animal, *Earth Planet. Sci. Lett.*, *242*, 39–50, doi:10.1016/j.epsl.2005.11.029.

Sweeney, R. E., and I. R. Kaplan (1973), Pyrite framboid formation: Laboratory synthesis and marine sediments, *Econ. Geol.*, *68*, 618–634, doi:10.2113/gsecongeo.68.5.618.

Tang, Y., Q. W. Chen, Y. Xiong, and Y. Li (2007), Magnetic field-induced increase in conversion rate of Fe_3S_4 to FeS_2, *Chin. J. Inorg. Chem.*, *23*, 941–947.

Tarduno, J. A. (1995), Superparamagnetism and reduction diagenesis in pelagic sediments: Enhancement or depletion?, *Geophys. Res. Lett.*, *22*, 1337–1340, doi:10.1029/95GL00888.

Tauxe, L. (1998), *Paleomagnetic Principles and Practice*, 309 pp., Kluwer Acad., Dordrecht, Netherlands.

Tauxe, L., T. A. T. Mullender, and T. Pick (1996), Potbellies, wasp-waists, and superparamagnetism in magnetic hysteresis, *J. Geophys. Res.*, *101*, 571–583, doi:10.1029/95JB03041.

Thompson, R., and T. D. J. Cameron (1995), Palaeomagnetic study of Cenozoic sediments in North Sea boreholes: An example of a magnetostratigraphic conundrum in a hydrocarbon-producing area, in *Palaeomagnetic Applications in Hydrocarbon Exploration*, edited by P. Turner and A. Turner, *Geol. Soc. Spec. Publ.*, *98*, 223–236.

Torii, M., K. Fukuma, C. S. Horng, and T. Q. Lee (1996), Magnetic discrimination of pyrrhotite- and greigite-bearing sediment samples, *Geophys. Res. Lett.*, *23*, 1813–1816, doi:10.1029/96GL01626.

Tric, E., C. Laj, C. Jehanno, J.-P. Valet, C. Kissel, A. Mazaud, and S. Iaccarino (1991), High-resolution record of the Upper Olduvai transition from Po Valley (Italy) sediments: Support for dipolar transition geometry?, *Phys. Earth Planet. Inter.*, *65*, 319–336, doi:10.1016/0031-9201(91)90138-8.

Turner, G. M. (2001), Toward an understanding of the multicomponent magnetization of uplifted marine sediments in New Zealand, *J. Geophys. Res.*, *106*, 6385–6397, doi:10.1029/2000JB900406.

Turner, G. M., and P. J. J. Kamp (1990), Paleomagnetic location of the Jaramillo Subchron and the Matuyama-Brunhes transition in the Castlecliffian stratotype section, Wanganui Basin, New Zealand, *Earth Planet. Sci. Lett.*, *100*, 42–50, doi:10.1016/0012-821X(90)90174-V.

Turner, G. M., A. P. Roberts, C. Laj, C. Kissel, A. Mazaud, S. Guitton, and D. A. Christoffel (1989), New paleomagnetic results from Blind River: Revised magnetostratigraphy and tectonic rotation of the Marlborough region, South Island, New Zealand, *N. Z. J. Geol. Geophys.*, *32*, 191–196.

Uda, M. (1965), On the synthesis of greigite, *Am. Mineral.*, *50*, 1487–1489.

Vandenberghe, R. E., E. De Grave, P. M. A. De Bakker, M. Krs, and J. J. Hus (1991), Mössbauer effect study of natural greigite, *Hyperfine Interact.*, *68*, 319–322, doi:10.1007/BF02396500.

van Dongen, B. E., A. P. Roberts, S. Schouten, W. T. Jiang, F. Florindo, and R. D. Pancost (2007), Formation of iron sulfide nodules during anaerobic oxidation of methane, *Geochim. Cosmochim. Acta*, *71*, 5155–5167, doi:10.1016/j.gca.2007.08.019.

van Velzen, A. J., M. J. Dekkers, and J. D. A. Zijderveld (1993), Magnetic iron-nickel sulphides in the Pliocene and Pleistocene marine marls from the Vrica section (Calabria, Italy), *Earth Planet. Sci. Lett.*, *115*, 43–55, doi:10.1016/0012-821X(93)90211-Q.

Vasiliev, I., M. J. Dekkers, W. Krijgsman, C. Franke, C. G. Langereis, and T. A. T. Mullender (2007), Early diagenetic greigite as a recorder of the palaeomagnetic signal in Miocene-Pliocene sedimentary rocks of the Carpathian foredeep (Romania), *Geophys. J. Int.*, *171*, 613–629, doi:10.1111/j.1365-246X. 2007.03560.x.

Vasiliev, I., C. Franke, J. D. Meeldijk, M. J. Dekkers, C. G. Langereis, and W. Krijgsman (2008), Putative greigite magnetofossils from the Pliocene Epoch, *Nat. Geosci.*, *1*, 782–786, doi:10.1038/ngeo335.

Vaughan, D. J., and J. R. Craig (1985), The crystal chemistry of iron-nickel thiospinels, *Am. Mineral.*, *70*, 1036–1043.

Verwey, E. J. W. (1939), Electronic conduction of magnetite (Fe_3O_4) and its transition point at low temperatures, *Nature*, *144*, 327–328, doi:10.1038/144327b0.

Walker, R., A. D. Steele, and D. T. B. Morgan (1996), Pyrophoric nature of iron sulfides, *Ind. Eng. Chem. Res.*, *35*, 1747–1752, doi:10.1021/ie950397t.

Walker, R., A. D. Steele, and D. T. B. Morgan (1997), Deactivation of pyrophoric iron sulfides, *Ind. Eng. Chem. Res.*, *36*, 3662–3667, doi:10.1021/ie960575y.

Wáren, A., S. Bengtson, S. K. Goffredi, and C. L. Van Dover (2003), A hot-vent gastropod with iron sulfide dermal schlerites, *Science*, *302*, 1007, doi:10.1126/science.1087696.

Watson, J. H. P., D. C. Ellwood, Q. X. Deng, S. Mikhalovsky, C. E. Hayter, and J. Evans (1995), Heavy-metal adsorption on bacterially produced FeS, *Miner. Eng.*, *8*, 1097–1108, doi:10.1016/0892-6875(95)00075-2.

Watson, J. H. P., B. A. Cressey, A. P. Roberts, D. C. Ellwood, J. M. Charnock, and A. K. Soper (2000), Structural and magnetic studies on heavy-metal-adsorbing iron sulphide nanoparticles produced by sulphate-reducing bacteria, *J. Magn. Magn. Mater.*, *214*, 13–30, doi:10.1016/S0304-8853(00)00025-1.

Watson, J. H. P., I. W. Croudace, P. E. Warwick, P. A. B. James, J. M. Charnock, and D. C. Ellwood (2001), Adsorption of radioactive metals by strongly magnetic iron sulfide nanoparticles produced by sulfate-reducing bacteria, *Sep. Sci. Technol.*, *36*, 2571–2607, doi:10.1081/SS-100107214.

Weiss, B. P., S. S. Kim, J. L. Kirschvink, R. E. Kopp, M. Sankaran, A. Kobayashi, and A. Komeili (2004), Ferromagnetic resonance and low-temperature magnetic test for biogenic magnetite, *Earth Planet. Sci. Lett.*, *224*, 73–89, doi:10.1016/j.epsl.2004.04.024.

Wilkin, R. T., and H. L. Barnes (1996), Pyrite by reactions of iron monosulfides with dissolved inorganic and organic sulfur species, *Geochim. Cosmochim. Acta*, *60*, 4167–4179, doi:10.1016/S0016-7037(97)81466-4.

Williams, S. A. (1968), More data on greigite, *Am. Mineral.*, *53*, 2087–2088.

Wolf, S. A., D. D. Awschalom, R. A. Buhrman, J. M. Daughton, S. von Molnár, M. L. Roukes, A. Y. Chtchelkanova, and D. M. Treger (2001), Spintronics: A spin-based electronics vision for the future, *Science*, *294*, 1488–1495, doi:10.1126/science.1065389.

Yamaguchi, S., and H. Wada (1970), Magnetic anisotropy of Fe_3S_4 as revealed by electron diffraction, *J. Appl. Phys.*, *41*, 1873–1874, doi:10.1063/1.1659128.

Zapponi, M., T. Pérez, C. Ramos, and C. Saragovi (2005), Prohesion and outdoors tests on corrosion products developed over painted galvanized steel sheets with and without Cr(VI) species, *Corros. Sci.*, *47*, 923–936, doi:10.1016/j.corsci.2004.06.007.

L. Chang, National Oceanography Centre, Southampton, University of Southampton, European Way, Southampton SO14 3ZH, UK.

F. Florindo, Istituto Nazionale di Geofisica e Vulcanologia, Via di Vigna Murata, 605, I-00143 Rome, Italy.

C.-S. Horng, Institute of Earth Sciences, Academia Sinica, PO Box 1-55, Taipei 11529, Taiwan.

A. P. Roberts, Research School of Earth Sciences, Australian National University, Canberra, ACT 0200, Australia. (andrew.roberts@anu.edu.au)

C. J. Rowan, School of GeoSciences, University of Edinburgh, Grant Institute, King's Buildings, West Mains Road, Edinburgh EH9 3JW, UK.